Semiclassical Study of the Optimal Control of Molecular Rotors in Tilted Fields

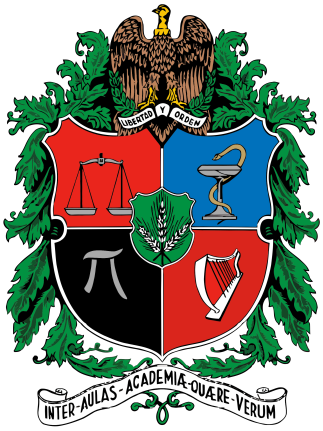

A thesis submitted in conformity with the requirements
for the degree of Doctor en Ciencias-Física
Sciences Faculty
Universidad Nacional de Colombia

presented by:

Rubén Darío Guerrero

Advisor:	Andres Reyes, PhD	Universidad Nacional de Colombia, Colombia
Co-Advisor:	Carlos Arango, PhD	Universidad ICESI, Colombia

Dedication

This thesis is dedicated to:
My mother, for her faith in my strength and competence.
My sons Jacobo, Salomé and Silvana, for their support and understanding.
My wife, for her endless love.

Rubén Darío Guerrero

Declaration of Authorship

I, Rubén Darío Guerrero, declare that this thesis titled, "Semiclassical Study of the Optimal Control of Molecular Rotors in Tilted Fields" and the work presented in it are my own. I confirm that:

- This work was done wholly or mainly while in candidature for a research degree at this University.
- Where any part of this thesis has previously been submitted for a degree or any other qualification at this University or any other institution, this has been clearly stated.
- Where I have consulted the published work of others, this is always clearly attributed.
- Where I have quoted from the work of others, the source is always given. With the exception of such quotations, this thesis is entirely my own work.
- I have acknowledged all main sources of help.
- Where the thesis is based on work done by myself jointly with others, I have made clear exactly what was done by others and what I have contributed myself.

Signed:

Date:

Abstract

Advances towards the active manipulation of the quantum state of material system using laser pulses is offering the opportunity for progress towards a quantum information age.

A broad set of powerful iterative numerical procedures has being developed within the framework of the Mathematical quantum control (QOC) theory having as a common goal of design, producing optimal pulse shapes capable of steer the quantum dynamics of an initial state towards a predetermined target state within a time of propagation that is predetermined too. All the formerly mentioned QOC procedures have in common that the convergence of the iterative procedure is conditioned to have non-zero overlap between the evolution of the initial state and the target at some point during the prescribed propagation time. Therefore, in order to guarantee the convergence of the optimization of the pulse, the initial guess for the optimal field should be chosen as a constant field of very high optical intensity. In summary all the iterative procedures for QOC have the following flaws: 1) The iterative procedure produces a discretization of the optimal pulse, therefore the resulting pulse shapes have the character of being proof of principle experiments that not necessarily have an experimental realm. 2) The results of the theorems regarding the existence of optimal controllers are limited to systems of low dimensionality. 3) Achieve convergence depends on using initial guesses of high optical intensity that can ionize the system that we are attempting to control.

The issues listed above makes traditional procedures for QOC unsuitable in order to attempt controlling the dynamics of molecular systems. This thesis is aimed to design a pseudo-spectral approach to the QOC, in which the

optimization of the pulse is performed using a genetic algorithm (GA) and is constrained to employ linear combination of analytic sub-pulses having the advantages of: 1) The methodology produces pulse shapes that are stressed to have experimental realm and at the same time avoid damaging the molecule along the optimization process 2) The pulse shapes have to be optimized only once per molecule and/or molecular process offering the opportunity of collecting a data-base of optimal pulses for broad set of molecules (or molecular processes) systematically 3) It is possible to employ the information collected along the GA optimization in order to infer the control mechanism induced by the pulse. As a consequnce of the set of improvements listed formerly, the methodology proposed in this thesis is a promising progress towards formulations of QOC suitable for the study and analysis of the QOC of molecular quantum dynamics determined on-the-fly.

Contents

Acknowledgments

Firstly, I would like to express my sincere gratitude to my adviser Prof. Andrés Reyes for the continuous support of my PhD studies and related research, for his patience, motivation and mentorship. His guidance helped me in all the time of research and writing of this thesis. I also would like to express my gratitude to Prof. Carlos Arango for the guidance on the semiclassical and quantum dynamics regards of the thesis. I also would like to express my gratitude to my wife Paola Méndez for her continuous support and encouragement. This research would have been impossible without support of this people in every respect.

Secondly, I would like to express my sincere gratitude to Prof. Todd Martínez for his mentorship during my stay at Stanford and beyond it, for his valuable guidance in many of the computational implementations for the thesis, and for his generosity. I also would like to express my gratitude to Prof. Jiri Vanicek for his guidance on quantum dynamics and the spectroscopic applications of it during my stay at EPFL.

Finally, I would like to express my gratitude to the National Program for Doctoral Formation and to the DIB-UNAL for their economic support.

List of Symbols

Symbol	Description
t	Time coordinate.
$\tau, \delta t$	Time-step.
K	Propagator.
$\mathbf{x} = \{x_1, x_2, x_3\}$	Cartessian coordinates for one particle.
$\mathbf{p} = \{p_1, p_2, p_3\}$	Momentum for one particle.
$\hat{\mathbf{x}} = \{\hat{x}_1, \hat{x}_2, \hat{x}_3\}$	Position operator for one particle.
$\hat{\mathbf{p}} = \{\hat{p}_1, \hat{p}_2, \hat{p}_3\}$	Momentum operator for one particle.
$\mathbf{z} = \{\mathbf{q}, \mathbf{p}\}$	Canonical coordinates for one particle.
$\|\cdot\|$	Eucidean distance or L_2-norm.
$\|G(\boldsymbol{\gamma}, \mathbf{z})\rangle$	Klauder coherent state with centroid $\mathbf{z}$.
$\mathbf{r} = \{r_1, r_2, r_3\}$	Cartessian coordinates for one electron.
$\mathbf{R} = \{R_1, R_2, R_3\}$	Cartessian coordinates for nuclei.
$\eta(\mathbf{R}, \alpha, l, m, n)$	Gaussian type function (GTF).
$\boldsymbol{\varepsilon}(t)$	Pulse shape.
$\hat{e}$	Polarization vector of the light.
$\hat{\mu}$	Electric dipole moment operator.
$\mathcal{C}_{JK}$	Nonadiabatic Coupling.
μ_{ab}	Transition dipole moment.
$\|\Psi(t)\rangle$	State of the system at current time.
$J[\Psi, \hat{O}, \boldsymbol{\varepsilon}, T]$	Cost functional.
$\mathcal{F}[f]$	Fourier transform of the function f.
$\mathcal{F}^{-1}[f]$	Inverse Fourier transform of the function f.
$\mathcal{L}[f]$	Laplace transform of the function f.
$\mathcal{L}^{-1}[f]$	Inverse Laplace transform of the function f.

Chapter 1

INTRODUCTION

The first generation of technologies based on the passive manipulation of quantum phenomena that took place during the last six decades have promoted the development of low-dimensionality semiconductor transistors, laser diodes and other devices. The development of these devices have boosted the development of microprocessors of high computational power and have a significant impact on the development of optical fiber communications, high fidelity digital information processing, photometry, and linear and nonlinear spectroscopies. It is believed that these technological developments brought about the transition from the industrial to the information age[1].

Current and future developments in the active control of quantum phenomena at the molecular scale are expected to promote the transition towards a second generation of quantum technology also known as the quantum information age.

Along these lines, this dissertation proposes reliable and modular algebraic methodologies [1] for the simulation of sequences of events in polyatomic molecules and their application in the design of strategies for the optical control of such events within the high and moderate optical intensity regimes.

Many of the sequences of events that we will attempt to control using laser pulses occur in time scales below 100 fs. To achieve this short time scale,

[1] Algebraic in the sense that the original integro-differential equation for the evolution and/or the optimal pulse are reformulated in terms of linear algebra equations by the inclusion of basis sets.

the first step before producing complex pulse shapes is to generate a Gaussian pulse with a carrier frequency in the region of the spectrum of interest. Gaussian pulses at these short time scales are readily generated since the invention of the colliding pulse mode-locked(CPM) ring dye laser in 1981.[2] The next step is the compression, or so called chirping, of CPM pulses to obtain even shorter pulses.[3, 4, 5, 6, 7] The record stands in a 6 fs pulse since 1987,[7] this pulse duration with carrier frequencies in the visible will be close to the single optical cycle limit, $\omega T \approx 2\pi$. [8, 9, 10, 11, 12, 13] Femtosecond laser technologies based on solid state have made such important progress in the last decade that pulses below 6 fs can be generated directly from the laser.

Pulse shaping is analogous to the electronic waveform synthesis often employed in electronic instrumentation but operates in a smaller time scale. Here, an input signal (often a Gaussian pulse) undergoes a series of filtering processes by its convolution with the response function of a material medium. The spatial light modulator (SLM).[2] technique for pulse shaping is one of the most versatile and broadly employed setups as a result of two advantageous features: first, the synthesis of the wave form is achieved by parallel modulation in the frequency domain and therefore an effective bandwidth of terahertz can be achieved; second, SLM using as hardware liquid crystal modulator (LCM) arrays (as an example) accomplishes a versatile computer programmable light pulse-shaping technique.[14] Pulse shapes simulated in this dissertation will be constrained to those that can be generated by employing state of the art SLM+LCM techniques.

Photoinduced processes can be classified as photophysical, if the chemical identity of the molecule is conserved along the process, and as photochemical if chemical changes occur during the interaction with the light. Examples of photophysical processes are: the radiative (fluorescence, phosphorescence) and radiationless (internal conversion, intersystem crossing) electronic transitions. Examples of photochemical processes are: photodissociation and photoisomerization. Either radiationless electronic transitions or photochemical processes involve transitions between Born-Oppenheimer (BO) adiabatic potential energy surfaces (PESs) induced by diabatic effects.

[2] *Here the waveform synthesis is achieved by spatial masking of the spatially dispersed optical frequency spectrum.[14]*

We cannot obtain an exact solution of the electronic Schrödinger equation for polyatomic molecules. However, reliable electronic structure methods of increasing accuracy are being developed to describe either the PESs or the mechanical[3] and electric responses[4] of the molecules for the ground and excited PESs.[15, 16, 17] It is nowadays possible to have an *ab-initio* description of the nuclear dynamics of the molecule coupled to a pulse of light. An accurate description of the PESs is achieved by the compromise between the completeness of the Hilbert space on which the spin orbitals are described and the truncation in the level of excitation of the Fock space that is employed to describe the excited PESs in the molecule.[18]

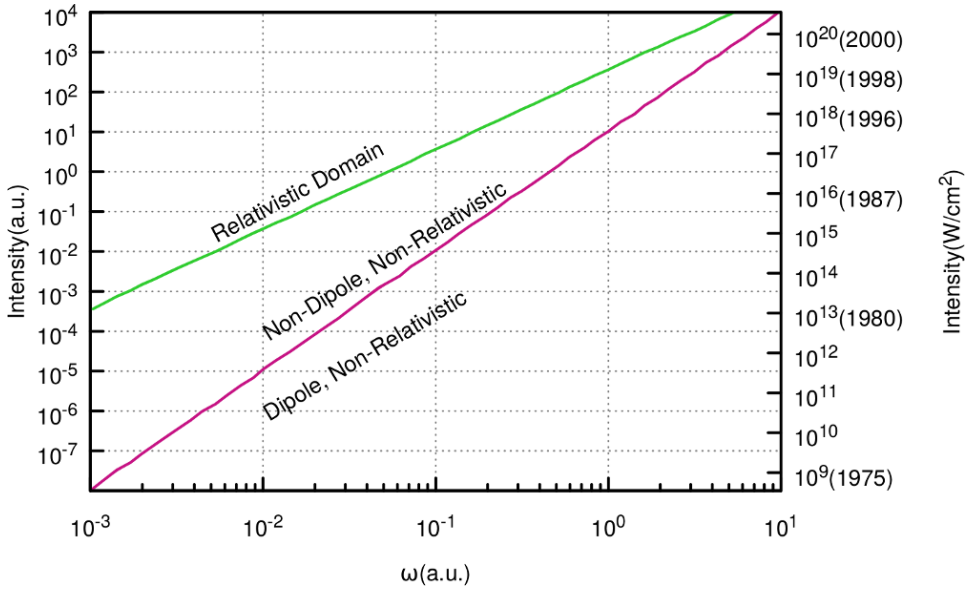

Figure 1.1: *Frequency versus intensity diagram, in the figure the purple line is the boundary between the linear and the non-linear domains of the molecule-light coupling strengths, while the green line separates between the non-linear and the relativistic domains molecule-light coupling strengths.*

The comparison between the ponderomotive energy[5] and the rest energy stands out as the most appropriate criteria to judge if the dipolar interaction is enough to describe the interaction between light and molecule.

[3] It is gradient and Hessian of the PESs

[4] It is polarizability and hyperpolarizability tensors of the molecule.

[5] It is the amount of energy gained by a free electron due to its interaction with a pulse of light per each optical cycle.

[6] This comparison also allows judging if relativistic effects can be induced by the interaction between light and molecule. In the case of an electron, the ponderomotive energy and the rest mass energy are defined as follows:

$$U_P = \frac{q_e^2}{2m_e\varepsilon_0 c\omega^2}\mathrm{I}, \tag{1.1}$$

$$U_0 = m_e c^2, \tag{1.2}$$

where q_e is the charge and m_e the mass of the electron, I is the optical intensity and ω the carrier frequency of the radiation, ε_0 is the permittivity of the electromagnetic vacuum and c is the speed of light. Experimentalist use these quantities to partitioning the frequency *versus* intensity diagram, in fig. 1.1, as follows: If $U_P < 0.1U_0$, the interaction between light and molecule does not induce relativistic effects and the dipolar approximation for the light-molecule coupling term works properly. Under these circumstances the time-dependent perturbation theory (TDPT) works properly too. If $0.1U_0 \leqslant U_P < U_0$, neither the use of the dipolar approximation nor the neglect of relativistic effects for the light-molecule interaction work properly. Therefore, higher multipolar terms must be considered to build up the molecule-light interaction term and also relativistic corrections[19] must be included. Finally, if $U_0 \leqslant U_P$, the light-molecule interaction becomes essentially a relativistic phenomenon and quantum electrodynamics theory must be employed. [20] In the figure, the quantities in parentheses accompanying some intensities corresponds to the years in which such intensities orders were reached experimentally.[21]

The radiation-molecule coupling can play two prominent roles: In the first place, it can be associated to a measurement mechanism as in ultrafast nonlinear spectroscopy, and in this regime, it is often modeled employing perturbation theory level (within the dipole, non-relativistic region in fig. 1.1). In the second place, it can be associated to an active control mechanism where a perturbation theory treatment is controversial (within the non-dipole, non-relativistic region in fig. 1.1) for both physically and chemically induced processes.[21] In contrast, as it usually happens beyond the Born-Oppenheimer and adiabatic approximations, the inter-electronic state couplings are considered to be strong, implying that the diabatic corrections should be included as accurately as possible in the computations, originating conical intersection (ConI) as regions of exact degeneracy between two

[6] Comparison between the wavelength of the radiation and the molecular size as criteria to determine the validity of the dipole approximation. It is misleading as it is established in many text books.

or more electronic states. The interplay between the inter-electronic state and the molecule-light coupling strengths must be described properly in order to perform a reliable simulation of sequences of events at the molecular scale.

Most of the available procedures to obtain a model representing the dynamics of a molecular phenomenon involve some approximations to perform a reduction of dimensionality. An approach that is broadly used employs regular electronic structure methods to perform a frequency computation and use the results to separate the normal modes between fast and slow modes, and or between coupled and decoupled modes.[22, 23, 24] However, in order to obtain theoretical predictions that are in good agreement with the experimental observations, the full dimensionality of the molecule must be considered.

In particular, we are interested in designing a methodology for the quantum optimal control (QOC) of molecules compatible with the on-the-fly molecular quantum dynamics that takes into account the full dimensionality of the molecule. In order to reach this goal, two key aspects must be tackled: In the first place, the existing algorithms to solve QOC problems run forward and backward propagations while upgrading the optimal pulse shape until self-consistency is reached. One severe caveat of such algorithms is that in the few first iterations the field strengths become extremely high so that they can induce undesirable photochemical processes that cannot be described properly with the employed electronic structure level of theory. In the second place, it is still unknown how to perform the existing controllability result [7] for high dimensionality systems, therefore a methodology with robust global convergence properties is highly desirable.

Overview of quantum optimal control

Thirty years after the development of optical control of photochemical processes [25, 26, 27, 28] it is reasonable to ask whether this idea can be applied to a broader variety of molecules and if the answer is no, what is needed to put it in practice These concerns becomes even worth if we consider that, as established in the previous section, the basic ingredients to put this goal

[7] Mainly based in local properties like gradient and Hessian of the cost function.

within reach have all been developed. It seems that the challenge that remains to overcome, is carry out an optimal control setup and apply it to a specific photochemical process. [29]

Nowadays it is broadly accepted that the mathematical control theory plays a key role in the design and development of strategies to accomplish the active control of molecular events, [30] since the establishment of its foundations, [31, 32, 33] optimal control theory have been a potential source of enlightenment regarding the solution of technological problems. The quantum version it, the so called quantum optimal control, [34, 35, 36] is based on a version of the Pontryagin theorem that involves finding the conditions on the pulse shape that makes stationary a Lagrangian function. The Lagrangian depends on the evolution of the initial state and its overlap with the (desired) final state and other unphysical quantities originated by the addition of constraints. Often, optimality conditions are derived in the form of a closed set of coupled Euler-Lagrange equations. The collection of methods developed to solve optimal control problems formulated in this way are grouped in the subfield of numerical optimal control. The algorithms within this subfield are classified as (i) gradient ascent and (ii) Krotov type methods.

In (i) starting from an initial guess for the pulse shape discretized on a time-grid for the entire propagation time, those field strengths are updated simultaneously, in the steepest descent direction of the Lagrangian,[37, 38, 39] from the current iteration to the next. The evaluation of the performance of the pulse shape to achieving the target for each iteration requires the propagation of the initial state, and despite its robust convergence, normally this family of algorithms requires thousandths of iterations to converge. Because these algorithms are gradient-based methods, the early iterations need to produce a large field strength in order to reach the neighborhood of the Lagrangian manifold where the optimal pulse shape lies, making these methods potentially unsuitable for on-the-fly dynamics.

In the algorithms type (ii) starting from the initial guess for the field strength at the initial time of propagation, the remaining points of the pulse shape are upgraded sequentially, employing the numerical solutions of the set of Euler-Lagrange equations for each iteration. One iteration is accomplished by a full forward-backward sequence of upgrades.[40, 41, 42, 36] Again in order to evaluate the performance of the pulse shape to achieving the target at each iteration, requires the propagation of the initial state. The conver-

gence of this family of algorithms[8] is in general faster than for type (i). The algorithm generally stuck if the guess for the field at the initial time of propagation for the first iteration is not large enough, [43] this a symptom of the local convergence properties of this family of methods. The dependence on very strong fields to achieve convergence, [9] makes these methods unsuitable for on-the-fly molecular quantum dynamics.

Nowadays, it is broadly recognized in the QOC community [29] that one of the important remaining issues that hampers the realization of QOC of photochemical processes in polyatomic molecules is: *The need for accurate ground and excited potential energy surfaces to design optimal pulses a priory, as well as to interpret the mechanism of pulses that are found by experimental optimization.*

An appealing approach to the former issue consist on the determination of the portions of the ground and excites PES as needed during the molecular dynamics. One of the first methods for on-the-fly propagation of a nuclear-electronic wave packet can be attributed to Öhrn *et al.*,[44, 45] but the applicability of such methods was limited to mostly diatomic molecules because this method was not based on regular electronic structure. Since the appearance of the frozen Gaussian method for semiclassical dynamics promoted by Heller, [46] on-the-fly molecular quantum dynamics have become in a very active field of research, between the methods based in Heller's approach to the dynamics, The Full Multiple Spawning (FMS) method of Martinez and co-workers [47, 48, 49, 50] stands out as the most successful and efficient method that is available. The efficiency of the method roots on its adaptability, avoiding expenditure of computational resources when diabatic events[10] are not occurring, making FMS the method of choice for the study of nonadibatic molecular dynamics.

The interpretation of the control mechanisms induced by the optimal pulses remains as an open question for research. Therefore, part of the developments in this dissertation will be focused to attempting to develop a methodology capable of put in quantitative grounds the interpretations of arbitrarily complex control mechanisms.

[8] Particularly the rapidly convergent versions of it.[36]

[9] Potentially conflicting with the preservation of the chemical identity of the system that we are attempting to control.

[10] Also called rare events

OUR APPROACH TO THE QUANTUM OPTIMAL CONTROL

The advances in the pulse shaping technology exposed previously, would make possible the measurement and active manipulation of events at the molecular scale in the near future. But to achieve the active manipulation of molecular events is imperative to develop computational methodologies capable of producing reliable simulations making possible the quantitative analysis of complex sequences of events at the nuclear and electronic scales of time, because within a quantum mechanical description, the adsorption of photons triggers a complex sequence of dynamical processes that in the case of polyatomic molecules involves transitions towards (and between) excited electronic states, and also radiationless relaxations via conical intersections.[11] [23, 51, 52, 53, 54] Our aim is to propose a methodology for the simulation and analysis of the nuclear-electronic dynamics in which the accuracy in the description of the dynamics can be adapted to the computational resources at hand. In order to limit the scope of the thesis, the methodology that will be propose has been designed to perform well for the *ab-initio* study of photoinduced processes in isolated polyatomic molecules containing up to twenty atoms.

Electronic structure theory has mature and well established methodologies capable of describe the ground and excited PESs [15, 17] and the ConIs between them.[23, 51, 52, 53, 55] However most of the state-of-the-art computer codes for electronic structure computations, use the transition dipole moment to describe the interaction between the molecule and the electric field component of light. Unfortunately, such approximation have a very limited zone of validity in the frequency *versus* intensity diagram in fig. 1.1. The former issue exposes the need of implementations of the electronic structure codes, capable of model properly the interaction light-molecule for broader regions of fig. 1.1 and allows the possibility of manage the time-dependence of the field. The work in this dissertation regarding electronic structure is aimed to work on this issue by doing the implementations allowing to add a coupling term between the electrons and a time-dependent external field at various levels of theory going from Hartree-Fock to configurations interaction singles and doubles.

Aiming to avoid the dependence of the convergence of the algorithms of type (i) and (ii), on strong fields, as it was exposed in the previous sec-

[11] A conical intersection is a true degeneracy region between two or more electronic states.

tion, we will develop the proposal for a pseudospectral optimization of the Lagrangian of the corresponding traditional QOC problem, where the optimal solution is constrained to be a linear combination of a basis set of experimentally attainable pulse functions. The topology of the Lagrangian manifold close to the optimal QOC solution [12] is unknown for systems of high dimensionality as polyatomic molecules. [13] Therefore, is highly desirable to employ an optimization method that, without using gradient information, offers strong convergence towards global optimal solutions. Heuristic optimization strategies has been proposed to fulfill these needs in high dimensionality search spaces, [56] and because of their versatility and robustness, nowadays genetic algorithms have become the method of choice and the method of optimization to be used to find our solution to QOC problems.

A bonus feature of the use of GA in the optimization, is that it allowed us to use machine learning methods in order to perform a quantitative analysis identifying the most relevant sequences of events taking place in the molecule along the optimal path from the initial to the target state.

Outline of the dissertation

The thesis is organized as follows: in chapter 2 the theoretical background for electronic structure and quantum control is reviewed, in chapter 3 we expose the developments of new theory and implementations, covering: a new pseudospectral methodology for the solution of QOC in section 3.1, the proposal for a modular approach to the approximated solution to TDSE accounting for nonadianbatic effects in section 3.2, its extension to the on-the-fly molecular nonadianbatic dynamics in section 3.2, and an extension to the Hartree-Fock theory in order to take into account the interaction between electrons and time-dependent electric fields. Finally, in chapter 4 the concluding remarks and perspectives are highlighted.

[12] Presumably exist many possible solutions

[13] As an example consider an $n-$atom nonlinear molecule that have $3n-6$ independent normal coordinates.

Chapter 2

Theoretical Background

In this chapter we present a review of the main ideas and concepts of semiclassical dynamics, quantum dynamics and regular electronic structure theory employed in this dissertation. For a detailed description of the topics regarding semiclassical and quantum dynamics we invite the reader to check references [57, 58] and references there in that will be cited accordingly. The topics regarding regular electronic structure are covered in references [15, 59, 16, 17] and references there in.

QUANTUM AND SEMICLASSICAL DYNAMICS

Pseudospectral solution of the time-dependent Schrödinger equation(TDSE)

In this methodology the continuous solution to the TDSE is represented in terms of a discrete set of time-evolving complex amplitudes that are located at the nodes of a predetermined and fixed set of grid points. We will call it wavepacket here after. Introducing an abstract Hilbert space accomplished by basis functions that are localized on the grid points, such a basis set if often called a pseudospectral basis, the set of complex and time-dependent coefficients of the wavepacket can be interpreted as a linear combination of the pseudospectral basis.

Consider that our Hilbert space is accomplished by a set of delta functions localized on the grid points, such a basis offers a good compromise be-

tween simplicity and accuracy, originating the following representation of the wavepacket:

$$c_n(t) = \int \delta(x - x_n)\psi(x,t)dx \tag{2.1}$$

$$\psi(x,t) \approx \sum_n c_n(t)\delta(x - x_n) = \psi_N(x_n,t), \tag{2.2}$$

this is an approximate representation of the wavepacket because although the chosen basis is orthogonal, it becomes complete only in the limit of a infinitely dense grid. The motion of the wavepacket is governed by the TDSE,

$$\frac{\partial\psi}{\partial t} = -\frac{i}{\hbar}\hat{H}\psi(x,t), \tag{2.3}$$

and have as formal solution:

$$\psi(x, t + \Delta t) = \hat{U}(t + \Delta t, t)\psi(x,t). \tag{2.4}$$

The operator $\hat{U}$ is the so called real-time propagator and is given by the solutions of the analogous to the TDSE for the propagator:

$$i\hbar\frac{\partial}{\partial t_f}\hat{U}(t_f,t_i) = \hat{H}(t_f)\hat{U}(t_f,t_i) \tag{2.5}$$

$$i\hbar\frac{\partial}{\partial t_i}\hat{U}(t_f,t_i) = -\hat{U}(t_f,t_i)\hat{H}(t_f) \tag{2.6}$$

$$\hat{U}(t,t) = \mathbb{1}. \tag{2.7}$$

where t_i and t_f are dummy variables that has being introduced to represent arbitrary initial an final times of propagation. In general, this set of equations are satisfied by the operator:

$$\hat{U}(t_f,t_i) = \hat{T}\exp\left(-\frac{i}{\hbar}\int_{t_i}^{t_f} dt\hat{H}(t)\right) \tag{2.8}$$

where $\hat{T}$ is the time-ordering operator. In the case of a time-independent Hamiltonian and shifting $t_i \longrightarrow 0$ and $t_f \longrightarrow t$, the propagator simplifies to:

$$\hat{U}(t,0) = \exp\left(-\frac{i}{\hbar}\hat{H}t\right). \tag{2.9}$$

Thus, we are seeking for a numerical implementation to compute the action of the propagator upon the wavepacket $e^{-\frac{i}{\hbar}\hat{H}t}\psi_N(x_n,0)$. The first step to achieve this goal consist in represent the propagator in the global interval of time $[0,t]$ as a product of short-time propagators Δt in such a way that $N\Delta t = t$.

$$\hat{U}(t,0) = \exp\left(-\frac{i}{\hbar}\hat{H}t\right) = \exp\left(-\frac{i}{\hbar}\hat{H}\Delta t\right)\exp\left(-\frac{i}{\hbar}\hat{H}\Delta t\right)\cdots\exp\left(-\frac{i}{\hbar}\hat{H}\Delta t\right). \tag{2.10}$$

Each short-time propagator can be approximate as the product of a symmetric Strang splitting of the potential and kinetic operators in the Hamiltonian: [1]

$$\exp\left(-\frac{i}{\hbar}\hat{H}\Delta t\right) = \exp\left(-\frac{i}{\hbar}(\hat{T}+\hat{V})\Delta t\right) \tag{2.11}$$

$$\approx \exp\left(-\frac{i}{\hbar}\hat{T}\frac{\Delta t}{2}\right)\exp\left(-\frac{i}{\hbar}\hat{V}\Delta t\right)\exp\left(-\frac{i}{\hbar}\hat{T}\frac{\Delta t}{2}\right) \tag{2.12}$$

$$+\mathcal{O}(\Delta t^3), \tag{2.13}$$

an intuitive picture of the former splitting can be achieved as follows: imagine that each Δt is partitioned in three subinterval, for the first interval the system evolves by one half of its kinetic energy only then, for the next subinterval, the system evolves by its potential energy only and finally for the last subinterval the system evolves by the remaining one half of its kinetic energy only; but, roughly speaking such a splited picture of the evolution represents properly the true propagation only if $E_{min}\Delta t/\hbar \ll 1$, being E_{min} the minimum energy of the process whose dynamics we are interested to simulate with accuracy $\mathcal{O}(\Delta t^3)$. Noticing that the $\hat{V}$ operator is diagonal in the position representation whereas the operator $\hat{T}$ is diagonal in the momentum representation, and recalling that:

$$\psi_N(p,t) = \mathcal{F}[\psi_N(x,t)], \tag{2.14}$$

$$\psi_N(x,t) = \mathcal{F}^{-1}[\psi_N(p,t)]; \tag{2.15}$$

the numerical approximation to the evolution of the wavepacket can be computed concatenating a series of short-time propagations accomplished by following the steps in algorithm 1.

[1] Just to keep in mind the idea of the on-the-fly evaluation of the PES, this form of the splitting is convenient because evaluates the expensive electronic structure only once per step.

Algorithm 1 Symmetric split-operator algorithm of accuracy $\mathcal{O}(\Delta t^3)$.

1: **for** each time step Δt **do**
2: Perform a fast Fourier transform (FFT) to the momentum representation
3: Multiply by the complex number corresponding to $\exp\left(-\frac{i}{\hbar}\hat{T}\frac{\Delta t}{2}\right)$.
4: Perform an inverse fast Fourier transform (IFFT) to the position representation
5: Multiply by the complex number corresponding to $\exp\left(-\frac{i}{\hbar}\hat{V}\Delta t\right)$.
6: Perform a FFT to the momentum representation
7: Multiply by the complex number corresponding to $\exp\left(-\frac{i}{\hbar}\hat{T}\frac{\Delta t}{2}\right)$.
8: Perform an IFFT to the position representation
9: **end for**

The maximum wavenumber that is possible to describe given a grid spacing along the corresponding direction is given by the following equation:

$$k^{x_i}_{max/min} = \pm\frac{2\pi}{\delta x_i} \tag{2.16}$$

Defining $k_{range} = 2|k^{x_i}_{max/min}|$, $p_{range} = \hbar k_{range}$ and considering N grid points along the direction i, the maximum phase space volume available to be covered by a wavepacket simulation in the direction i is :

$$volume_i = x_{range} \times p_{range} = \frac{L_i\hbar}{\Delta x_i} = N\hbar. \tag{2.17}$$

being L_i the size of the simulation box along the direction i.

Time-dependent perturbation theory (TDPT)

We will write the propagator in the interaction picture (IP) where $\hat{H}_0$ stands for a part of the Hamiltonian whose spectrum is known and $\hat{H}_I$ is a perturbation, The Hamiltonian can be written as:

$$\hat{H}(t) = \hat{H}_0(t) + \hat{H}_I(t). \tag{2.18}$$

For concretenes $\hat{H}_0(t)$ stands for the molecular Hamiltonian and $\hat{H}_I(t)$ stands for the molecule-light interaction. The concrete form of those terms can

be determined by using the electronic structure methods reviewed in sections 2.2.1 and 2.2.2. The propagator relative to $\hat{H}_0(t)$, $\hat{U}_0(t)$ satisfies the equation:

$$i\hbar\frac{\partial}{\partial t}\hat{U}_0(t,t_0) = \hat{H}_0(t)\hat{U}_0(t,t_0), \tag{2.19}$$

and its formal solution is:

$$\hat{U}_0(t,t_0) = \hat{T}\exp\left(-\frac{i}{\hbar}\int_{t_0}^{t} d\tau \hat{H}(\tau)\right). \tag{2.20}$$

The wavepacket in the interaction picture, relative to the wavepacket in the Schrödinger picture, is defined as follows:

$$|\psi_S(t)\rangle = \hat{U}_0(t,t_0)\,|\psi_I(t)\rangle\,. \tag{2.21}$$

replacing the former relation into the TDSE the equation of motion satisfied by the wavepacket in the interaction picture can be obtained:

$$\begin{aligned}
\hat{U}_0(t,t_0)\frac{\partial}{\partial t}|\psi_I(t)\rangle &= -\frac{i}{\hbar}\hat{H}_I(t)\hat{U}_0(t,t_0)\,|\psi_I(t)\rangle \\
\frac{\partial}{\partial t}|\psi_I(t)\rangle &= -\frac{i}{\hbar}\hat{U}_0^{\dagger}(t,t_0)\hat{H}_I(t)\hat{U}_0(t,t_0)\,|\psi_I(t)\rangle \\
\frac{\partial}{\partial t}|\psi_I(t)\rangle &= -\frac{i}{\hbar}\hat{H}'_I(t)\,|\psi_I(t)\rangle
\end{aligned} \tag{2.22}$$

Thus, from the TDSE in the IP the propagator in the IP can be computed as follows:

$$i\hbar\frac{\partial}{\partial t}\hat{U}_I(t,t_0) = \hat{H}'_I(t)\hat{U}_I(t,t_0), \tag{2.23}$$

and the propagator in IP is given by the formal solution of eq. (2.23):

$$\hat{U}_I(t,t_0) = \hat{T}\exp\left(-\frac{i}{\hbar}\int_{t_0}^{t} d\tau \hat{H}'_I(\tau)\right). \tag{2.24}$$

The evolution of the wavepacket in the Schrödinger picture can be obtained combining eqs. (2.20), (2.21) and (2.24) as follows:

$$\begin{aligned}
|\psi_S(t)\rangle &= \hat{U}_0(t,t_0)\,|\psi_I(t)\rangle \\
&= \hat{U}_0(t,t_0)\hat{U}_I(t,t_0)\,|\psi_I(t_0)\rangle \\
&= \hat{U}_0(t,t_0)\hat{U}_I(t,t_0)\,|\psi_S(t_0)\rangle\,.
\end{aligned} \tag{2.25}$$

Thus, the perturbed evolution is given by a composition of propagators as follows:

$$\begin{aligned}\hat{U}(t,t_0) =&\hat{U}_0(t,t_0)\hat{U}_I(t,t_0)\\ =&\hat{U}_0(t,t_0)\hat{T}\exp\left(-\frac{i}{\hbar}\int_{t_0}^{t}d\tau\hat{H}'_I(\tau)\right)\\ =&\hat{U}_0(t,t_0)+\sum_{n=1}^{\infty}\left(-\frac{i}{\hbar}\right)^n\int_{t_0}^{t}d\tau_n\int_{t_0}^{\tau_n}d\tau_{n-1}\cdots\int_{t_0}^{\tau_2}d\tau_1\\ =&\hat{U}_0(t,\tau_n)\hat{H}'_I(\tau_n)\hat{U}_0(\tau_n,\tau_{n-1})\hat{H}'_I(\tau_{n-1})\cdots\hat{U}_0(\tau_2,\tau_1)\hat{H}'_I(\tau_1)\hat{U}_0(\tau_1,\tau_0)\end{aligned} \tag{2.26}$$

where has been used the integral identity:

$$\hat{U}(t,t_0)=1-\frac{i}{\hbar}\int_{t_0}^{t}d\tau\hat{H}(\tau)\hat{U}(\tau,t_0). \tag{2.27}$$

It can be seen from eq. (2.26) that in n-th order TDPT, the solution to the TDSE is approximated by splitting the evolution in such a way that the unperturbed evolution of the molecular wavepacket is measured or perturbed n times by $\hat{H}'_I$ at times $\tau_1,\cdots\tau_n$. First order TDPT works properly for light whose frequencies and intensities are within the Dipole and non-relativistic region of fig. 1.1. But hihger orders of TDPT should be included in order to take into account interactions within the non-dipole and non-relativistic region of fig. 1.1.

Quantum optimal control(QOC)

From a mathematical point of view, for concretenes we will think that our goal is maximize the projection of the state of the molecule over an excited state $|\tilde{\phi}_b\rangle$ at the final propagation time T, what means maximize the projection operator $\hat{O}_b=|\tilde{\phi}_b\rangle\langle\tilde{\phi}_b|$.

The dynamics of the state of the molecule is steered permanently by it interaction with an electric field $\varepsilon(t)$. Therefore, the state of the molecule at the final propagation time is a functional of the history of its interaction with the field, in such a way that the optimization problem at hand is to

optimize:

$$J_{\hat{O}_b} = J^{(1)}_{\hat{O}_b}[\Psi] + J^{(2)}[\varepsilon(t)], \tag{2.28}$$

$$J^{(1)}_{\hat{O}_b}[\Psi] = \left\langle \Psi(T) \right| \hat{O}_b \left| \Psi(T) \right\rangle, \tag{2.29}$$

$$J^{(2)}[\varepsilon(t)] = -\lambda \int_0^T \|\varepsilon(t)\|^2 dt \tag{2.30}$$

where the constraint 2.30 should be added to penalize fields of high intensity that otherwise will drag the optimization procedure towards unphysical pulse shapes.

Using the notation $\hat{H}_a$ for the electronic Hamiltonian of the initial state, and $\hat{H}_b$ for the electronic Hamiltonian of the target one. For low enough field intensities TDPT applies, and first order TDPT let us approximate the evolution of the state of the molecule as:

$$\psi(T) = \frac{1}{i\hbar} \int_0^T e^{-\frac{i}{\hbar} H_b (T-t)} \{-\mu_{ab} \varepsilon(t)\} e^{-\frac{i}{\hbar} H_a(t)} \psi_i dt. \tag{2.31}$$

The combination of eq. (2.31), and the cost function eq. (3.21), allows to get the following result:

$$J_{\hat{O}_b} = \left| \frac{1}{i\hbar} \int_0^T \left\langle \tilde{\phi}_b \right| e^{-\frac{i}{\hbar} H_b (T-t)} \{-\mu_{ab} \varepsilon(t)\} e^{-\frac{i}{\hbar} H_a(t)} \left| \psi_i \right\rangle \right|^2 - \lambda \int_0^T \|\varepsilon(t)\|^2 dt \tag{2.32}$$

Typically, the initial state, ψ_i, is a proper function of the corresponding electronic Hamiltonian, H_a, supossing that the proper value is E_i. In that case, the operator $e^{-\frac{i}{\hbar} H_a(t)}$ becomes a complex number of norm one under the absolute value. Defining:

$$\phi_i = \mu_{ab} \psi_i \tag{2.33}$$

$$C(t) = \left\langle \tilde{\phi}_b \right| e^{-\frac{i}{\hbar} H_b (T-t)} \left| \phi_i \right\rangle, \tag{2.34}$$

allows to rewrite our target in a more informative way:

$$J_{\hat{O}_b} \approx_{TDPT} \frac{1}{\hbar^2} \int_0^T \int_0^T \left(C(t)\varepsilon(t) \right)^\star \left(C(t')\varepsilon(t') \right) dt dt' - \lambda \int_0^T \varepsilon(t)\varepsilon^\star(t) dt \tag{2.35}$$

For the optimal pulse shape, $\tilde{\varepsilon}(t)$, the following optimality conditions are satisfied:

$$\frac{\delta J_{\hat{O}_b}}{\delta \tilde{\varepsilon}(t)} = 0 \qquad\qquad \frac{\delta J_{\hat{O}_b}}{\delta \tilde{\varepsilon}^\star(t)} = 0. \tag{2.36}$$

The two conditions are redundant, so focusing on the variation respect to $\tilde{\varepsilon}^\star(t)$ tha following equations are obtained:

$$\delta J_{\hat{O}_b} = \frac{1}{\hbar^2}\int_0^T \int_0^T \left(C(t)\delta\varepsilon(t)\right)^\star \left(C(t')\varepsilon(t')\right) dtdt' - \lambda \int_0^T \varepsilon(t)\delta\varepsilon^\star(t)dt \tag{2.37}$$

$$\frac{\delta J_{\hat{O}_b}}{\delta \tilde{\varepsilon}^\star(t)} = \int_0^T \left(\frac{1}{\hbar^2}\int_0^T C(t)^\star \left(C(t')\varepsilon(t')\right) dt' - \lambda\varepsilon(t)\right) dt = 0 \tag{2.38}$$

Since eqs. (2.37) and (2.38) should be satisfied for any time:

$$\frac{1}{\hbar^2}\int_0^T C(t)^\star \left(C(t')\varepsilon(t')\right) dt' - \lambda\varepsilon(t) = 0. \tag{2.39}$$

The solution of the former equation gives the following solution for the optimal pulse shape within TDPT:

$$\varepsilon(t) = \alpha C^\star(t') = \alpha \left\langle \phi_i \right| e^{-\frac{i}{\hbar}H_b(t-T)} \left| \tilde{\phi}_b \right\rangle \tag{2.40}$$

where α is a complex constant and is related with the penalization factor, λ, as follows:

$$\lambda = \frac{1}{\hbar^2}\int_0^T |C(t)|^2 dt = \frac{1}{\hbar^2|\alpha|}\int_0^T |\varepsilon(t)|^2 dt. \tag{2.41}$$

The equation eq. (2.40) exposes the physical meaning of the computation of the optimal pulse shape that steers the molecule towards a target within first order TDPT: the optimal pulse shape in first order TDPT, within the Dipole and non-relativistic region of fig. 1.1, is given by the autocorrelation function obtained by the backward propagation of the target state.

Within the non-dipole and non-relativistic region of fig. 1.1, eq. (2.31) is not valid anymore and the strength of the light-molecule interaction triggers nonlinear effects leading to a dependence of the wavepacket at time t on the whole history of the light-molecule interaction. Within this regime,

the pulse shape optimization is accomplished employing the standard version of the QOC that deconstraining the optimization problem in eq. (2.30) by the addition of the Lagrange multiplier:

$$J_3[\varepsilon,\psi,\chi] = -2\Im\int_0^T dt \left\langle \chi(t)\right| i\hbar\frac{\partial}{\partial t} - \hat{H}(t) \left|\psi(t)\right\rangle, \tag{2.42}$$

where $\chi(t)$ is a Lagrange multiplier that was included in order to guarantee that, although the nonlinearity, the evolution of the wavepacket satisfies the Schrödinger equation. Now the Lagrangian takes the form:

$$J_{\hat{O}_b} = J^{(1)}_{\hat{O}_b}[\Psi] + J^{(2)}[\varepsilon(t)] + J_3[\varepsilon,\psi,\chi], \tag{2.43}$$

Since ψ, χ and ε in eq. (2.43) are independent variables, the total variation of $J_{\hat{O}_b}$ can be written as follows:

$$\delta J_{\hat{O}_b} = \delta_\psi J_{\hat{O}_b} + \delta_\chi J_{\hat{O}_b} + \sum_{k=x,y,z} \delta_{\varepsilon_k} J_{\hat{O}_b}. \tag{2.44}$$

The necessary optimality conditions should be:

$$\delta J_{\hat{O}_b} = \delta_\psi J_{\hat{O}_b} + \delta_\chi J_{\hat{O}_b} + \sum_{k=x,y,z} \delta_{\varepsilon_k} J_{\hat{O}_b} = 0 \tag{2.45}$$

from which the following set of Euler-Lagrange equations are obtained:

$$\lambda_k \varepsilon_k(t) = -\Im\left\langle\chi(t)\right| \mu_k \left|\psi(t)\right\rangle \tag{2.46}$$

$$\frac{\partial}{\partial t}\left|\psi(\mathbf{R},t)\right\rangle = -\frac{i}{\hbar}\hat{H}(t)\left|\psi(\mathbf{R},t)\right\rangle, \qquad \left|\psi(\mathbf{R},0)\right\rangle = \phi_i(\mathbf{R}) \tag{2.47}$$

$$\frac{\partial}{\partial t}\left|\chi(\mathbf{R},t)\right\rangle = +\frac{i}{\hbar}\hat{H}(t)\left|\chi(\mathbf{R},t)\right\rangle, \qquad \left|\chi(\mathbf{R},T)\right\rangle = \hat{O}\psi(\mathbf{R},T) \tag{2.48}$$

Semiclassical propagators

For an one dimensional harmonic oscillator, the bosonic creation and anihilation operators can be defined as follows:[60]

$$\sigma = \frac{\hbar}{m\omega} = \gamma^{-1/2} \tag{2.49}$$

$$\hat{a}^\dagger = \frac{1}{\sqrt{2}}\left(\frac{\hat{q}}{\sigma} - i\frac{\sigma}{\hbar}\hat{p}\right) \tag{2.50}$$

$$\hat{a} = \frac{1}{\sqrt{2}}\left(\frac{\hat{q}}{\sigma} + i\frac{\sigma}{\hbar}\hat{p}\right) \tag{2.51}$$

where the constant σ has dimensions of length. The operators $\hat{a}$ and $\hat{a}^\dagger$ are non-hermitian, has complex spectrum, and a left- and right-side sets of eigenfunctions. In the position representation, the right-side eigenfunctions are given by the equation:

$$\langle q|\overrightarrow{a}|\alpha\rangle_R = \alpha \langle q|\alpha\rangle_R \tag{2.52}$$

$$\frac{1}{\sqrt{2}}\left(\frac{q}{\sigma} + \sigma\frac{\partial}{\partial q}\right)\langle q|\alpha\rangle_R = \alpha \langle q|\alpha\rangle_R \tag{2.53}$$

whose solution gives the following eigenvalue and normalized right-side eigenfunction:

$$\alpha = \frac{1}{\sqrt{2}}\left(\frac{q_c}{\sigma} + i\frac{\sigma}{\hbar}p_c\right) \tag{2.54}$$

$$\langle q|\alpha\rangle_R = \left(\frac{\gamma}{\pi}\right)^{1/4}\exp\left(-\frac{1}{2}(q-q_c)\gamma(q-q_c) + \frac{i}{\hbar}\left(qp_c - \frac{q_c p_c}{2}\right)\right). \tag{2.55}$$

The right-side eigenfunction[2], in eq. (2.55), is known as a Klauder coherent state (KCS), KCS will be used in the theoretical development of the thesis as a pseudospectral basis in order to build a modular algebraic approach to the solution of the TDSE, allowing us to find approxiamted solutions to the TDSE for nonadiabatic high-dimensional multi-state problems.

The usage of KCS as basis set, in combinations with the harmonic approximation to linearize the dynamics, is the typical approach of most semiclassical methods. Semiclassical methods allows to study efficiently high-dimensionality systems, but the methods available currently are unable to describe efficiently coherent effects and diabatic population transfer between PESs.

For completeness, the left eigenfunction of $\hat{a}^\dagger$ can be computed by taking the hermitian conjugate of the eq. (2.52), giving the complex conjugate of eq. (2.55) and the corresponding complex conjugate eigenvalue. The corresponding eigenfunction in position representation takes the form:

$$\langle p|\alpha\rangle_R = \left(-\frac{1}{\pi\gamma\hbar^2}\right)^{-1/4}\exp\left(-\frac{1}{2\hbar^2}(p-p_c)\gamma^{-1}(p-p_c) - \frac{i}{\hbar}\left(qp_c - \frac{q_c p_c}{2}\right)\right) \tag{2.56}$$

[2] The left-side eigenfunctions are not normalizable therefore are not physically allowed solutions

The set of all the right-side eigenfunctions, $|\alpha\rangle_R$ ($|\alpha\rangle$ from here on), form an overcomplete basis for the Hilbert space of any one-dimensional system and satisfy the completeness relation:

$$\int \frac{d^2\alpha}{\pi} |\alpha\rangle \langle\alpha| = \int \frac{dq_c dp_c}{2\pi\hbar} |\alpha\rangle \langle\alpha| = 1. \tag{2.57}$$

Transformation theory of classical mechanics utilizes four generating functions in separated, or combined ways, in order to produce any meaningful canonical transformation [61]. Canonical transformations are understood as the change from old coordinates and/or momenta to new ones which remains as canonical conjugates. In the derivation of the van-Vleck semiclassical formula, the generating function $F_2(q, P, t)$ plays a fundamental role. It is a function of the old coordinates q, the new momenta P and time. The relation between F_2 and the old momenta and the new coordinates is as follows

$$p_i = \frac{\partial F_2}{\partial q_i} \tag{2.58}$$

$$Q_i = \frac{\partial F_2}{\partial P_i} \tag{2.59}$$

The transformed Hamiltonian depends on new variables Q, P that are constant in time. Then, the generating function F_2 in one dimension should satisfy

$$H(q, p, t) + \frac{\partial F_2}{\partial t} = 0 \tag{2.60a}$$

$$H\left(q, \frac{\partial F_2}{\partial q}, t\right) + \frac{\partial F_2}{\partial t} = 0. \tag{2.60b}$$

Eq. (2.60) is the Hamilton-Jacobi equation. It has a close resemblance to the time dependent Schrödinger equation

$$i\hbar \frac{\partial}{\partial t} \Psi(q, t) = H\Psi(q, t). \tag{2.61}$$

van-Vleck [62] showed that in the limit $\hbar \to 0$ the wave function

$$\Psi(q, t) = A\Delta^{\frac{1}{2}} \exp\left(\frac{F_2(q, P, t)}{i\hbar}\right) \tag{2.62}$$

[3]where A is a constant, satisfies equation

$$H\left(q, i\hbar\frac{\partial}{\partial q}\right)\Psi(q, t) = \Psi(q, t)H\left(q, \frac{\partial F_2}{\partial q}\right) + \mathcal{O}O(\hbar). \tag{2.63}$$

[3]that is often called the van-Vleck approximation to the wave function

For conservative systems, $F_2(q,P,t) = F_2(q,P) - Et$, (here E is the energy of the system). Thus, the energy of the system can be obtained as

$$E = -\frac{\partial F_2}{\partial t}, \tag{2.64}$$

where the determinant Δ in Eq. 2.62 is given by

$$\Delta = \left| \frac{\partial^2 F_2}{\partial q \partial P} \right|. \tag{2.65}$$

Therefore, in the van-Vleck (or semiclassical) approximation the system is evolved in time using both, the classical action $F_2(q,P,t)$ and its derivatives with respect to the canonical variables. A similar procedure can be used for the asymptotic ($\hbar \to 0$) solution of the time-dependent Schrödinger equation for the propagator $K(q,t;q_0,t_0)$

$$\left(H(q) - i\hbar \frac{\partial}{\partial t} \right) K(q,t;q_0,t_0) = 0 \tag{2.66}$$

where

$$\lim_{t \to t_0} K(q,t;q_0,t_0) = \delta(q - q_0). \tag{2.67}$$

Solving the Schrödinger equation using eq. (2.62), we derive the initial position to final momentum van-Vleck's semiclassical amplitude formula

$$K(P_f,t;q_0,t_0) = (2\pi i\hbar)^{-\frac{1}{2}} \left| \frac{\partial^2 F_2}{\partial q_0 \partial P_f} \right|^{\frac{1}{2}} \exp\left(\frac{F_2(q_0,P_f,t)}{i\hbar} \right). \tag{2.68}$$

Taking into account the relation between the F_1 and F_2 generators: $F_1(q_0,q_f) = F_2(q_0,P_f) - P_f q_f$, the van-Vleck formula for the initial position to final position semiclassical amplitude is obtained

$$K(q_f,t;q_0,t_0) = (2\pi i\hbar)^{-\frac{1}{2}} \left| \frac{\partial^2 F_1}{\partial q_0 \partial q_f} \right|^{\frac{1}{2}} \exp\left(\frac{F_1(q_0,q_f,t)}{i\hbar} \right), \tag{2.69}$$

for a dynamical transformation this formula should be evaluated along a classical trajectory $z_t(z_i)$ in phase space going from $z_i = (q_0,p_0)$ at $t = t_0$ to $z_f = (q_f,p_f)$ at time t. The generating function F_1 is

$$F_1(q_0,q_f,t) = \int_{t_0}^{t} dt' \left(p_x(t')\dot{q}(t') - H(q,p) \right), \tag{2.70}$$

it is often known as the classical action. Noticing that

$$-p(t_0) = \frac{\partial F_1}{\partial q_0} \tag{2.71}$$

$$p(t_f) = \frac{\partial F_1}{\partial q_f}, \tag{2.72}$$

The canonical transformation is identified as:

$$\left| \frac{\partial^2 F_1}{\partial q_0 \partial q_f} \right|^{\frac{1}{2}} = \left| \frac{\partial q_f}{\partial p_i} \right|^{-\frac{1}{2}}. \tag{2.73}$$

An alternative expression for the semiclassical amplitude van-Vleck formula is obtained as

$$K(q_f, t; q_0, t_0) = (2\pi i\hbar)^{-\frac{1}{2}} \left| \frac{\partial q_f}{\partial p_i} \right|^{-\frac{1}{2}} \exp\left(\frac{F_1(q_0, q_f, t)}{i\hbar} \right). \tag{2.74}$$

This expression can be extended to n dimensions and more than one path in phase space

$$K(\mathbf{q}_f, t; \mathbf{q}_0, t_0) = (2\pi i\hbar)^{-\frac{n}{2}} \sum_{paths} \left| \frac{\partial \mathbf{q}_f}{\partial \mathbf{p}_0} \right|^{-\frac{1}{2}} \exp\left(\frac{F_1(\mathbf{q}_0, \mathbf{q}_f, t)}{i\hbar} - i\frac{\pi}{2}\nu \right). \tag{2.75}$$

A caveat of this formula is that along a classical path in phase space $\mathbf{z}_t(\mathbf{x}_i)$ when $\frac{\partial \mathbf{q}_f}{\partial \mathbf{p}_0} = 0$ the path encounters a caustic and the van-Vleck formula diverges; in order to take into account the right sign for the prefactor, the parameter ν in eq. (2.75) is an integer counting the number of caustics, (often called the Maslov index) and the sum runs over all the classical paths starting at $\mathbf{q}_0$ for $t = t_0$ and ending at $\mathbf{q}_f$ for $t = t_f$. Although the above semiclassical amplitude formula is apparently easy to evaluate, its practical application runs into serious difficulties listed below

(a) It is necessary to search for all the paths satisfying the boundary conditions (often called the root search problem).

(b) The semiclassical amplitude diverges at caustics (limiting the semiclassical amplitude derived from the van-Vleck formula, to times prior a caustic).

(c) Numerical problems will occur for chaotic trajectories.

(d) A large number of trajectories are needed to obtain accurate results.

The initial momentum to final position quantum amplitude is given in terms of the coordinate representation as follows:

$$\langle \mathbf{q}_f | \exp\left(-\frac{i}{\hbar}Ht\right) |\mathbf{p}_0\rangle = \int \mathbf{q}_i \langle \mathbf{q}_f | \exp\left(-\frac{i}{\hbar}Ht\right) |\mathbf{q}_i\rangle \langle \mathbf{q}_i | \mathbf{p}_0\rangle \tag{2.76}$$

where,

$$\langle \mathbf{q}_i | \mathbf{p}_0\rangle = (2\pi i\hbar)^{-\frac{n}{2}} \exp\left(\frac{i\mathbf{q}_i\mathbf{p}_0}{\hbar}\right). \tag{2.77}$$

Inserting Eq. 2.75 in the integral, and employing the stationary phase approximation gives

$$K(\boldsymbol{q}_f, t; \boldsymbol{p}_0, t_0) = (2\pi i\hbar)^{-\frac{n}{2}} \left|\frac{\partial \boldsymbol{q}_f}{\partial \boldsymbol{q}_0}\right|^{-\frac{1}{2}} \exp\left(\frac{i}{\hbar}F_2(\boldsymbol{q}_f, \boldsymbol{p}_0, t)\right) \tag{2.78}$$

where the F_2 generator is

$$F_2(\mathbf{q}_f, \mathbf{p}_0, t) = F_1(\mathbf{q}_f, \mathbf{q}_0, t) + \mathbf{p}_0\mathbf{q}_0. \tag{2.79}$$

Finally, the initial to final momentum amplitude is

$$\langle \mathbf{p}_f | \exp\left(-\frac{i}{\hbar}Ht\right) |\mathbf{p}_0\rangle \approx (2\pi\hbar)^{-1} \int d\mathbf{q}_0 \left|\frac{\partial \mathbf{q}_t}{\partial \mathbf{q}_0}\right|^{\frac{1}{2}} \exp\left(\frac{i}{\hbar}(F_2(\mathbf{q}_f, \mathbf{p}_0, t) - \mathbf{q}_t\mathbf{p}_f)\right). \tag{2.80}$$

Solving the integral in the stationary phase approximation gives[63]

$$\begin{aligned}\langle \mathbf{p}_f | \exp\left(-\frac{i}{\hbar}Ht\right) |\mathbf{p}_0\rangle \approx & (2\pi\hbar)^{-1} \sum_{\text{paths}} \left|\frac{\partial \mathbf{p}_t}{\partial \mathbf{q}_0}\right|^{\frac{1}{2}} \\ & \exp\left(\frac{i}{\hbar}\left(F_4(\mathbf{p}_f, \mathbf{p}_0, t) + i\frac{\pi}{4}\text{sgn}\left(\frac{\partial \mathbf{p}(0^+)}{\partial \mathbf{q}_0}\right)\right)\right).\end{aligned} \tag{2.81}$$

Eq. 2.81 is the van-Vleck formula (VVF) in an initial value integral representation (IVR) for the semiclassical amplitude in the momentum representation. Here, the sum involves all the root trajectories with $\mathbf{p} = \mathbf{p}_0$ at $t = t_0$ and $\mathbf{p} = \mathbf{p}_f$ at $t = t_t$. The validity of this semiclassical formula is limited to times prior any of the trajectories crosses a momentum space caustic $\frac{\partial \mathbf{p}_t}{\partial \mathbf{q}_0} = 0$. The F_4 generator in this case is given by

$$F_4(\mathbf{p}_f, \mathbf{p}_0, t) = \int_{t_0}^{t_f} dt' \left(\mathbf{q}_{t'}\frac{d\mathbf{p}_{t'}}{dt'} - H_{t'}\right). \tag{2.82}$$

In the last term of the exponent, the limit $\|t_f - t_0\| \to 0$ has been taken.

Herman-Kluk propagator

Here is obtained the expression for the Herman-Kluk propagator by the process of modified Filinov filtering of the van-Vleck one. This procedure modifies a multidimensional integral of the form

$$I = \int \mathbf{dx} \exp\left(\frac{i}{\hbar} S(\mathbf{x})\right), \tag{2.83}$$

by multiplying the integrand by the following damping factor,

$$\left|\mathbf{1} + i\mathbf{c} \cdot \frac{\partial^2 S}{\partial \mathbf{x} \partial \mathbf{x}}\right| \exp\left(-\frac{1}{2\hbar} \frac{\partial S}{\partial \mathbf{x}} \cdot \mathbf{c} \cdot \frac{\partial S}{\partial \mathbf{x}}\right) \tag{2.84}$$

where $\mathbf{c}$ is a matrix that vary slowly or is constant respect to $\mathbf{x}$. If the matrix $\mathbf{c}$ is large enough, then this procedure converts the original integral into the stationary phase approximation to it,

$$I_{SPA} = \sum_n \left(\frac{(2\pi i\hbar)^F}{\left|\frac{\partial^2 S}{\partial \mathbf{x} \partial \mathbf{x}}\right|}\right)^{\frac{1}{2}} \exp\left(\frac{i}{\hbar} S(\mathbf{x})\right)\Bigg|_{\mathbf{x}=\mathbf{x}_n} \tag{2.85}$$

where F is the dimensionality of the integration space and $\mathbf{x}_n$ are the roots of the stationary phase condition

$$\frac{\partial S}{\partial \mathbf{x}} = 0. \tag{2.86}$$

If the matrix $\mathbf{c} \to 0$, then the damping factor in Eq. (2.84) becomes the unity and the original integral still unchanged.

Deriving the Herman-Kluk propagator from the van-Vleck one

Consider (in 1D) a probability amplitude from an initial state $|\psi_i\rangle$ to a final state $|\psi_f\rangle$ using the van-Vleck semiclassical formula:

$$K_{f,i} = \langle \psi_f | \exp\left(-\frac{i}{\hbar}\hat{H}t\right) |\psi_i\rangle \approx \int dq_f \int dq_i (2\pi i\hbar M_{qp})^{-\frac{1}{2}} \psi_f^*(q_f)\psi_i(q_i) \times \exp\left(\frac{i}{\hbar} S_t(q_f, r_i)\right); \tag{2.87}$$

where the sum over all the possible classical trajectories connecting the initial and final coordinates is implyed. If $|\psi_i\rangle$ and $|\psi_f\rangle$ are taken to be coherent states

$$|\psi_i\rangle = |p_i, q_i\rangle \tag{2.88a}$$

$$|\psi_f\rangle = |p_f, q_f\rangle \tag{2.88b}$$

with the wave function

$$\langle q|p', q'\rangle = \left(\frac{\gamma}{\pi}\right)^{\frac{1}{4}} \exp\left(-\frac{\gamma}{2}(q-q')^2 + \frac{i}{\hbar}p'(q-q')\right), \tag{2.89}$$

the transition probability becomes

$$K_{f,i} = \left(\frac{\gamma}{\pi}\right)^{\frac{1}{2}} \int dq_f \int dq_i (2\pi i M_{qp})^{-\frac{1}{2}} \exp\left(\frac{i}{\hbar}\phi(q_f, q_i)\right) \tag{2.90}$$

where

$$\phi(q_f, q_i) = S_t(q_f, q_i) + p_i(q_0 - q_i) - p_f(q_1 - q_f) + i\frac{\hbar\gamma}{2}\left[(q_1 - q_f)^2 + (q_0 - q_f)^2\right]. \tag{2.91}$$

To apply the Filinov filtering procedure, one requires the gradient of ϕ respect to the initial conditions

$$\frac{\partial\phi}{\partial q_1} = p_1 - p_f + i\hbar\gamma(q_1 - q_f), \tag{2.92a}$$

$$\frac{\partial\phi}{\partial q_0} = p_i - p_0 + i\hbar\gamma(q_0 - q_i), \tag{2.92b}$$

here has been taken into account that

$$\frac{\partial S_t(q_1.q_0)}{\partial q_1} = p_1(q_1, q_0), \tag{2.93a}$$

$$\frac{\partial S_t(q_1.q_0)}{\partial q_0} = -p_0(q_1, q_0). \tag{2.93b}$$

One also needs the Hessian of ϕ

$$\begin{pmatrix} \frac{\partial^2\phi}{\partial q_1^2} & \frac{\partial^2\phi}{\partial q_1 \partial q_0} \\ \frac{\partial^2\phi}{\partial q_0 \partial q_1} & \frac{\partial^2\phi}{\partial q_0^2} \end{pmatrix} = \begin{pmatrix} \frac{\partial p_1}{\partial q_1} + i\hbar\gamma & \frac{\partial p_1}{\partial q_0} \\ -\frac{\partial p_0}{\partial q_1} & -\frac{\partial p_0}{\partial q_0} + i\hbar\gamma \end{pmatrix}. \tag{2.94}$$

The simpler option is choose the 2D matrix $\mathbf{c}$ to be diagonal

$$\mathbf{c} = \begin{pmatrix} c_1 & 0 \\ 0 & c_0 \end{pmatrix}. \tag{2.95}$$

Inserting eqs. (2.92)(2.93)(2.94)(2.95) into eq. (2.84) we find for the Filinov factor

$$\left|\begin{pmatrix}1 & 0\\ 0 & 1\end{pmatrix} + i\begin{pmatrix}c_1 & 0\\ 0 & c_0\end{pmatrix}\begin{pmatrix}\frac{\partial^2\phi}{\partial q_1^2} & \frac{\partial^2\phi}{\partial q_1\partial q_0}\\ \frac{\partial^2\phi}{\partial q_0\partial q_1} & \frac{\partial^2\phi}{\partial q_0^2}\end{pmatrix}\right| \times \exp\left(\left[-\frac{c_1}{2\hbar}\left(\frac{\partial\phi}{\partial q_1}\right)^2 - \frac{c_0}{2\hbar}\left(\frac{\partial\phi}{\partial q_0}\right)^2\right]\right). \tag{2.96}$$

Multiplying by the former Filinov factor the transition amplitude in eq. (2.90) and simplifying the resulting expression we find

$$K_{f,i} = (2\pi\hbar)^{-1}\int dq_1 \int dq_0 \left(\frac{2\hbar\gamma}{iM_{qp}}\right)^{\frac{1}{2}} \mathcal{A}^{\frac{1}{2}} \exp\left(\Phi\right) \tag{2.97a}$$

$$\mathcal{A} = (1-c_0\hbar\gamma)(1-c_1\hbar\gamma) + ic_1(1-c_0\hbar\gamma)\frac{\partial p_1}{\partial q_1} - ic_0(1-c_1\hbar\gamma)\frac{\partial p_0}{\partial q_0} + c_1c_0\left(\frac{\partial p_1}{\partial q_1}\frac{\partial p_0}{\partial q_0} - \frac{\partial p_0}{\partial q_1}\frac{\partial p_1}{\partial q_0}\right) \tag{2.97b}$$

$$\Phi = \frac{i}{\hbar}S_t - \frac{\gamma}{2}(1-c_1\hbar\gamma)(q_1-q_f)^2 - \frac{\gamma}{2}(1-c_0\hbar\gamma)(q_0-q_i)^2 - \frac{c_1}{2\hbar}(p_1-p_f)^2 - \frac{c_0}{2\hbar}(p_i-p_0)^2 + ic_0\gamma(p_i-p_0)(q_i-q_0) - ic_1(p_1-p_f)(q_1-q_f). \tag{2.97c}$$

One now invokes the initial value representation that changes an integral over q_1 into one over p_0,

$$\sum\int dq_1 = \int dp_0|M_{qp}| \tag{2.98}$$

and introduce the four blocks of the monodromy matrix:

$$M_{xy} = \frac{\partial x_t}{\partial y} \tag{2.99}$$

where $x = \{q,p\}$ and $y = \{q,p\}$ enables write the partial derivatives in Eq.(2.97) as

$$\begin{aligned}\frac{\partial p_1(q_1,q_0)}{\partial q_1} &= \frac{M_{pp}}{M_{qp}}, & \frac{\partial p_1(q_1,q_0)}{\partial q_0} &= \frac{-1}{M_{qp}}\\ \frac{\partial p_0(q_1,q_0)}{\partial q_1} &= \frac{1}{M_{qp}} & \frac{\partial p_0(q_1,q_0)}{\partial q_0} &= \frac{-M_{qq}}{M_{qp}}.\end{aligned} \tag{2.100}$$

By the symplectic property of the phase-space we have that $M_{qq}M_{pp} - M_{qp}M_{pq} = 1$. Using this properties of the monodromy matrices in Eq. (2.97) it can be rewritten as follows

$$K_{f,i} = (2\pi\hbar)^{-1} \int dp_0 \int dq_0 \mathcal{A}^{\frac{1}{2}} \exp(\Phi) \tag{2.101a}$$

$$\begin{aligned} \mathcal{A} = {} & 2\hbar c_0(1 - c_1\hbar\gamma)M_{qq} + 2\hbar c_1(1 - c_0\hbar\gamma)M_{pp} \\ & - 2i\hbar\gamma(1 - c_0\hbar\gamma)(1 - c_1\hbar\gamma)M_{qp} + 2i\hbar\gamma c_0 c_1 M_{pq} \end{aligned} \tag{2.101b}$$

$$\begin{aligned} \Phi = {} & \frac{i}{\hbar}S_t - \frac{\gamma}{2}(1 - c_1\hbar\gamma)(q_t - q_f)^2 - \frac{\gamma}{2}(1 - c_0\hbar\gamma)(q_0 - q_i)^2 - \frac{c_1}{2\hbar}(p_t - p_f)^2 \\ & - \frac{c_0}{2\hbar}(p_i - p_0)^2 + ic_0\gamma(p_i - p_0)(q_t - q_0) - ic_1(p_t - p_f)(q_t - q_f). \end{aligned} \tag{2.101c}$$

Finally choosing

$$c_0 = c_1 = \frac{1}{2\hbar\gamma}, \tag{2.102}$$

the Herman-Kluk expression for the probability amplitude takes its typical form for one dimensional systems:

$$K_{f,i} = (2\pi\hbar)^{-1} \int dp_0 \int dq_0 \langle p_f q_f | p_t q_t \rangle \langle p_0 q_0 | p_i q_i \rangle C_t \exp\left(\frac{i}{\hbar}S_t\right) \tag{2.103}$$

where

$$C_t = \left| \frac{1}{2}\left(M_{qq} + M_{pp} + \frac{\hbar\gamma}{i}M_{qp} + \frac{i}{\hbar\gamma}M_{pq} \right) \right| \tag{2.104a}$$

$$\langle p_0 q_0 | p_i q_i \rangle = \exp\left(-\frac{\gamma}{4}(q_0 - q_i)^2 - \frac{1}{4\hbar^2\gamma}(p_0 - p_i) + \frac{i}{2\hbar}(p_0 - p_i)(q_0 - q_i) \right). \tag{2.104b}$$

To evaluate the former expression, the action and the four blocks of the monodromy matrix should be propagated using the following set of coupled equations of motion for them [64]:

$$\dot{S}(t) = T(\mathbf{p}) - V(\mathbf{q}) \tag{2.105}$$

$$\dot{\mathbf{M}}_{\mathbf{pp}} = -\frac{\partial^2 V}{\partial \mathbf{q}^2}\mathbf{M}_{\mathbf{qp}} \tag{2.106}$$

$$\dot{\mathbf{M}}_{\mathbf{pq}} = -\frac{\partial^2 V}{\partial \mathbf{q}^2}\mathbf{M}_{\mathbf{qq}} \tag{2.107}$$

$$\dot{\mathbf{M}}_{\mathbf{qp}} = +\frac{\partial^2 T}{\partial \mathbf{p}^2}\mathbf{M}_{\mathbf{pp}} \tag{2.108}$$

$$\dot{\mathbf{M}}_{\mathbf{qq}} = +\frac{\partial^2 T}{\partial \mathbf{p}^2}\mathbf{M}_{\mathbf{pq}} \tag{2.109}$$

$$\tag{2.110}$$

Reference [64] provides a symplectic recipe to integrate this set of equations. Semiclassical approximations to the quantum propagator has been proven to be reliable methods to compute the autocorrelation function eq. (2.40) for systems of high dimensionality as molecules are. [4] Nonetheless, a very large number of trajectories (of the order of tenth of thousands or higher) are needed to converge the results and for chaotic systems achieve convergence is even harder.

Some of the difficulties of the semiclassical propagator of van-Vleck are surpassed, for concreteness let us list the issues here again:

(a) The root search problem is solved by including the transformation to initial values representation eq. (2.98).

(b) The problem of divergences at caustics remains for semiclassical amplitude [65].

(c) Numerical problems remains for chaotic trajectories.

(d) The dependence of the convergence (if even possible) on a large number of trajectories remains.

Although the progress in semiclassical propagation, an issue remains that hampers the application of semiclassical propagators currently and is that when the dynamics becomes chaotic,[66] it is found that the regular component is accurately represented by the SC-IVR,[5] but the quantum

[4] Most of this claim is based on proof of principle computations based in model, There are in the literature a few examples of on-the-fly semiclassical propagations.

[5] when using the Filinov integral conditioning technique

manifestations of the chaotic behavior is easily over-damped by the filtering factors.

Regarding the on-the-fly implementation of the semiclassical propagator of Herman and Kluk, in addition to facing the convergence problems of the method, the main bottleneck remains in the ab-initio computation of the Hessian for each step for each trajectory, making the applicability of this methodology for quantum propagation very limited, and even worth unsuitable for the solution of QOC problems.

Switching from unidimensional to multidimensional systems, the initial state typically is a Gaussian:

$$\phi_i(\mathbf{q}) = \langle \mathbf{q}|G(\gamma, \mathbf{Q}, \mathbf{P})\rangle \tag{2.111}$$

$$\langle \mathbf{q}|G(\gamma, \mathbf{Q}, \mathbf{P})\rangle = \left(\frac{\det\gamma}{\pi^D}\right)^{1/4} \exp\left(i\mathbf{P}\cdot(\mathbf{q}-\mathbf{Q})/\hbar - (\mathbf{q}-\mathbf{Q})\cdot\gamma\cdot(\mathbf{q}-\mathbf{Q})/2\right),$$

where $\mathbf{Q}(\mathbf{P})$ is the coordinate(momentum) centroid of the Gaussian in phase space, and γ is a positive definite matrix that determines the width of the Gaussian in each direction of the phase space.

In terms of the Feynman propagator:

$$K_{(T-t)}(\mathbf{q}, \mathbf{q}') = \left\langle \mathbf{q} \right| e^{-\frac{i}{\hbar}H_b(T-t)} \left| \mathbf{q}' \right\rangle, \tag{2.112}$$

the propagation of the wavefunction from the initial state, ϕ_i, at time zero; to the target wave function, $\tilde{\phi}_b$, at target time T, can be computed as:

$$\tilde{\phi}_b(\mathbf{q}) = \int \mathbf{dq}' K_{(T-t)}(\mathbf{q}, \mathbf{q}')\phi_i(\mathbf{q}). \tag{2.113}$$

Therefore, the time-autocorrelation that gives the optimal pulse shape, eq. (2.40), can be computed as:

$$C(t) = \int \mathbf{dq}\tilde{\phi}_b(\mathbf{q}) \int \mathbf{dq}' K_{(T-t)}(\mathbf{q}, \mathbf{q}')\phi_i(\mathbf{q}'). \tag{2.114}$$

In order to obtain the semiclassical approximation to the correlation function, $C^{sc}(t)$, the Feynman propagator is replaced by its semiclassical approximation:

$$K^{sc}_{t'}(\mathbf{q}, \mathbf{q}') = \frac{1}{(2\pi\hbar)^d} \int \mathbf{dP}_0 \int \mathbf{dQ}_0 R_{\mathbf{PQ}_{t'}} e^{\frac{i}{\hbar}S_{\mathbf{PQ}_{t'}}} \langle \mathbf{q}|G\left(\gamma, \mathbf{Q}_{t'}, \mathbf{P}_{t'}\right)\rangle \times \langle G(\gamma, \mathbf{Q}_0, \mathbf{P}_0)|\mathbf{q}'\rangle \tag{2.115}$$

where for compactness, we did the substitution $t' = (T - t)$. In this expression

$$S_{\mathbf{PQ}t'} = \int_T^t d\tau \mathbf{P}_\tau \cdot \dot{\mathbf{Q}}_\tau - H_b(\mathbf{P}_\tau, \mathbf{Q}_\tau), \tag{2.116}$$

stands for the classical action and the prefactor $R_{\mathbf{PQ}t'}$ is written in terms of the blocks of the stability matrix:

$$M_{qq} = \frac{\partial \mathbf{Q}_{t'}}{\partial \mathbf{Q}_0} \tag{2.117}$$

$$M_{qp} = \frac{\partial \mathbf{Q}_{t'}}{\partial \mathbf{P}_0} \tag{2.118}$$

$$M_{pq} = \frac{\partial \mathbf{P}_{t'}}{\partial \mathbf{Q}_0} \tag{2.119}$$

$$M_{pp} = \frac{\partial \mathbf{P}_{t'}}{\partial \mathbf{P}_0} \tag{2.120}$$

$$R_{\mathbf{PQ}t'} = \pm\sqrt{\det\left[\frac{1}{2}\left(M_{pp} + M_{qq} i\gamma\hbar M_{qp} + \frac{i}{\hbar}\gamma^{-1} M_{pq}\right)\right]} \tag{2.121}$$

The sign of the squared root is determined by keeping track of the continuity of $R_{\mathbf{PQ}t'}$. Replacing eq. (2.111) and eq. (2.115) into eq. (2.112) we obtain the semiclassical formula for the autocorrelation function:

$$\begin{aligned} C_{HK}^{sc}(t') = \frac{1}{(2\pi\hbar)^d} \int\int \mathbf{dP}_0 \mathbf{dQ}_0 R_{\mathbf{PQ}t'} e^{\frac{i}{\hbar} S_{\mathbf{PQ}t'}} \\ \times \exp\left[-\frac{1}{4}(\mathbf{Q}_{t'} - \mathbf{Q}_0)\cdot\gamma\cdot(\mathbf{Q}_{t'} - \mathbf{Q}_0) - \frac{i}{2\hbar}(\mathbf{P}_{t'} - \mathbf{P}_0)\cdot(\mathbf{Q}_{t'} - \mathbf{Q}_0)\right. \\ \left.\frac{1}{4\hbar^2}(\mathbf{P}_{t'} - \mathbf{P}_0)\cdot\gamma^{-1}\cdot(\mathbf{P}_{t'} - \mathbf{P}_0)\right] \\ \times \exp\left[-\frac{1}{4}(\mathbf{Q}_{t'} - \mathbf{Q}_0)\cdot\gamma\cdot(\mathbf{Q}_{t'} - \mathbf{Q}_0) + \frac{i}{2\hbar}(\mathbf{P}_{t'} - \mathbf{P}_0)\cdot(\mathbf{Q}_{t'} - \mathbf{Q}_0)\right. \\ \left.\frac{1}{4\hbar^2}(\mathbf{P}_{t'} - \mathbf{P}_0)\cdot\gamma^{-1}\cdot(\mathbf{P}_{t'} - \mathbf{P}_0)\right] \end{aligned} \tag{2.122}$$

However, This formula is unable to produce accurate results for the autocorrelation function when the Hamiltonian H_b induce chaotic classical trajectories, because for those trajectories the prefactor, $R_{\mathbf{PQ}t'}$, diverges. A rather *ad-hoc* approach to deal with this problem is just ignore in the average, those trajectories whose prefactor surpass a time dependent threshold.[67]

A more formal approach consist in compute the integral in eq. (2.122) employing its damped approximation:

$$I = \int \mathbf{dz} A(\mathbf{z}) e^{if(\mathbf{z})} \approx \int \mathbf{dz} A(\mathbf{z}) e^{if(\mathbf{z}) - \epsilon |\nabla f(\mathbf{z})|^2} \tag{2.123}$$

where ϵ is a tunable parameter. the damping factor, ϵ, washes out undesirable features in the dynamics due to regions of phase space not so well described within stationary phase approximation. The result is the so called cellularized frozen Gaussian approximation (CFGA) [68]:

$$C^{sc}_{CFGA}(t') = \frac{1}{(2\pi\hbar)^d} \int\int \mathbf{dP}_0 \mathbf{dQ}_0 R_{\mathbf{PQ}t'} e^{\frac{i}{\hbar} S_{\mathbf{PQ}t'}} \sqrt{\frac{(4\epsilon)^{-2d}}{\det[A_{pqt}]}} \times \exp\left[\frac{1}{4} \mathbf{b}_{pqt} \cdot A_{pqt} \cdot \mathbf{b}_{pqt} - c_{pqt}\right] \tag{2.124}$$

REGULAR ELECTRONIC STRUCTURE METHODS TO DETERMINE GROUND AND EXCITED STATES

The aim of this section is provide theoretical support to the electronic structure methods implemented for the thesis, and expose their connection with the determination of the ground [6] and excited PESs at the configuration interaction singles (CIS), configuration interaction singles and doubles (CISD), random phase approximation (RPA), and multi-configuration self consistent field (MCSCF) levels of theory.

Hartree-Fock method (HF)

The HF method has been derived to find the best solution to the electronic Schrödinger equation corresponding to the clamped-nuclei Hamiltonian:

$$[\hat{T}_e(\mathbf{r}) + \hat{V}_{eN}(\mathbf{r};\mathbf{R}) + \hat{V}_{NN}(\mathbf{R}) + \hat{V}_{ee}(\mathbf{r})]\Psi(\mathbf{r};\mathbf{R}) = E_0(\mathbf{R})\Psi(\mathbf{r};\mathbf{R}) \tag{2.125}$$

$$\left[-\frac{1}{2}\sum_{i=0}^{n}\nabla_i^2 + \sum_{Ai}\frac{Z_A}{r_{Ai}} + \sum_{A>B}\frac{Z_A Z_B}{R_{AB}} + \sum_{i>j}\frac{1}{r_{ij}}\right]\Psi(\mathbf{r};\mathbf{R}) = E_0(\mathbf{R})\Psi(\mathbf{r};\mathbf{R}),$$

[6] At the Hartree-Fock level of theory.

accomplished by one Slater determinant[7], Ψ. The solution that we are seeking for, $E_0(\mathbf{R})$, is the ground state PES for eq. (3.2a). The excited PESs can be computed using the state Ψ as a reference state from which start computing the excitations. Details regarding this issue will be provided in section 2.2.2.

We can solve either analytically or numerically the Schödinger equation for one electron in the field of one nuclei, therefore the simplest starting guess for a solution for a solution of eq. (2.125), is to assuming that the wave function is accomplished by a product of single electron spin orbitals $\Psi_{HP}(1,2,\cdots,n) = \phi_1(1)\phi_2(2)\cdots\phi_n(n)$. This is often called the Hartree product ansatz. However, this guess does not satisfies the antisymmetry principle, we have to antisymmetrize the ansatz via the operator $\mathcal{A}$ to account for it:

$$\Psi(1,2,\cdots,n;\mathbf{R}) = \mathcal{A}\Psi_{HP}(1,2,\cdots,n) = \begin{vmatrix} \phi_1(1) & \phi_2(1) & \cdots & \phi_n(1) \\ \phi_1(2) & \phi_2(2) & \cdots & \phi_n(2) \\ \vdots & \vdots & \ddots & \vdots \\ \phi_1(n) & \phi_2(n) & \cdots & \phi_n(n) \end{vmatrix} \tag{2.126}$$

$$\mathcal{A} = \frac{1}{\sqrt{n!}}\left[\mathbb{1} - \sum_{ij}\mathbf{P}_{ij} + \sum_{ijk}\mathbf{P}_{ijk} + \cdots\right] = \frac{1}{\sqrt{n!}}\sum_{p=0}^{n-1}(-1)^p\mathbf{P}, \tag{2.127}$$

where the $\mathbf{R}$ is to make explicit the parametric dependence of the Slater determinant on the molecular structure, dependence that is inherited to all the observables computed using it. The antisymmetrization operator has been written in terms of permutations($\mathbf{P}$). An important property of this operator that follows straightforward from its definition, is that $\mathcal{A}\mathcal{A} = \sqrt{n!}\mathcal{A}$. It is convenient here, to introduce shorthand notation for the one-

[7] Also called configuration state function (CSF).

and two-electrons terms in the electronic Hamiltonian:

$$\hat{h}_i(\vec{R}) = -\frac{1}{2}\sum_{i=0}^{n}\nabla_i^2 + \sum_{Ai}\frac{Z_A}{r_{Ai}} \tag{2.128}$$

$$\hat{g}_{ij} = \frac{1}{|\vec{r}_i - \vec{r}_j|} \tag{2.129}$$

$$V_{nn}(\vec{R}) = \sum_{A>B}\frac{Z_A Z_B}{R_{AB}} \tag{2.130}$$

$$\hat{H}_e(\vec{R}) = \sum_{i=1}^{n}\hat{h}_i + \sum_{i>j}^{n}\hat{g}_{ij} + V_{nn}(\vec{R}) \tag{2.131}$$

Where $\hat{h}_i(\vec{R})$ is the core Hamiltonian and $\hat{g}_{ij}$ is the electronic repulsion. Now it is possible to compute the energy of the Slater determinant, eq. (2.126):

$$\left\langle \Psi \middle| \hat{H}_e \middle| \Psi \right\rangle = \sum_p (-1)^p \left\langle \Psi \middle| \hat{H}_e \middle| \mathbf{P}\Psi \right\rangle. \tag{2.132}$$

For the core Hamiltonian, the unique nonzero contribution comes from the first term in the expansion of $\mathcal{A}$ in terms of permutations, and those contributions to the energy are of the form:

$$\sum_i \left\langle \Psi \middle| \hat{h}_i(\vec{R}) \middle| \Psi \right\rangle = \sum_i h_{ii}(\vec{R}). \tag{2.133}$$

As for the electronic repulsion, only two terms of the expansion of $\mathcal{A}$ in terms of permutations, have nonzero contributions, the $\mathbb{1}$ that originates the Coulomb term:

$$\langle \Psi | \hat{g}_{ij} | \Psi \rangle = \left\langle ii(1) \middle| \frac{1}{r_{12}} \middle| jj(2) \right\rangle = J_{ij} \tag{2.134}$$

and the $\mathbf{P}_{ij}$ that originates the exchange term:

$$\langle \Psi | \hat{g}_{ij} | \mathbf{P}_{ij}\Psi \rangle = \left\langle ij(1) \middle| \frac{1}{r_{12}} \middle| ij(2) \right\rangle = K_{ij}. \tag{2.135}$$

In summary, the electronic energy of the Slater determinant, eq. (2.126), should be:

$$E_0(\vec{R}) = \sum_i^n \left\langle \phi_i \right| \hat{h}_i(\vec{R}) \left| \phi_i \right\rangle + \frac{1}{2} \sum_{ij} \left(\left\langle \phi_j \right| \hat{J}_i \left| \phi_j \right\rangle - \left\langle \phi_j \right| \hat{K}_i \left| \phi_j \right\rangle \right) + V_{nn}(\vec{R}) \tag{2.136}$$

$$\hat{J}_i \left| \phi_j(2) \right\rangle = \left\langle \phi_i(1) \right| \hat{g}_{12} \left| \phi_i(1) \right\rangle \left| \phi_j(2) \right\rangle \tag{2.137}$$

$$\hat{K}_i \left| \phi_j(2) \right\rangle = \left\langle \phi_i(1) \right| \hat{g}_{12} \left| \phi_j(1) \right\rangle \left| \phi_i(2) \right\rangle \tag{2.138}$$

Now we are in position to show how is the set of molecular orbitals(MO) that makes the electronic energy stationary. To do so, we must constraint the variation of the MOs, to variations in which the MOs remains orthogonal and normalized. This is achieved by include a set of Lagrange multipliers λ_{ij}, the Lagrangian is:

$$\mathscr{L}(\vec{R}) = E_0(\vec{R}) - \sum_{ij} \lambda_{ij} \left(\langle \phi_i | \phi_j \rangle - \delta_{ij} \right) \tag{2.139}$$

The variation respect to the MOs is:

$$\delta\mathscr{L} = \delta E_0(\vec{R}) - \sum_{ij} \lambda_{ij} \left(\langle \delta\phi_i | \phi_j \rangle + \langle \phi_i | \delta\phi_j \rangle \right), \tag{2.140}$$

The variation in the energy is:

$$\begin{aligned} \delta E_0(\vec{R}) =& \sum_i^n \left(\left\langle \delta\phi_i \right| \hat{h}_i(\vec{R}) \left| \phi_i \right\rangle + \left\langle \phi_i \right| \hat{h}_i(\vec{R}) \left| \delta\phi_i \right\rangle \right) \\ &+ \frac{1}{2} \sum_{ij} \left(\left\langle \delta\phi_i \right| \hat{J}_j - \hat{K}_j \left| \phi_i \right\rangle + \left\langle \phi_i \right| \hat{J}_j - \hat{K}_j \left| \delta\phi_i \right\rangle \right. \\ &\left. + \left\langle \delta\phi_j \right| \hat{J}_i - \hat{K}_i \left| \phi_j \right\rangle + \left\langle \phi_j \right| \hat{J}_i - \hat{K}_i \left| \delta\phi_j \right\rangle \right) \\ =& \sum_i^n \left(\left\langle \delta\phi_i \right| \hat{h}_i(\vec{R}) \left| \phi_i \right\rangle + \left\langle \phi_i \right| \hat{h}_i(\vec{R}) \left| \delta\phi_i \right\rangle \right) \\ &\sum_{ij} \left(\left\langle \delta\phi_i \right| \hat{J}_j - \hat{K}_j \left| \phi_i \right\rangle + \left\langle \phi_i \right| \hat{J}_j - \hat{K}_j \left| \delta\phi_i \right\rangle \right). \end{aligned} \tag{2.141}$$

Defining the Fock operator (explicit dependence on the molecular geometry was omitted during the derivation but is recovered here):

$$\hat{F}_i(\vec{R}) = \hat{h}_i(\vec{R}) + \sum_j^n \left(\hat{J}_j(\vec{R}) - \hat{K}_j(\vec{R})\right) \tag{2.142}$$

$$\delta E_0(\vec{R}) = \sum_i^n \left(\left\langle \delta\phi_i \right| \hat{F}_i(\vec{R}) \left| \phi_i \right\rangle + \left\langle \phi_i \right| \hat{F}_i(\vec{R}) \left| \delta\phi_i \right\rangle\right). \tag{2.143}$$

We are looking for the set of MOs that makes energy stationary, the energy must be real and the MOs orthogonal. This imply:

$$\langle \delta\phi | \phi \rangle = \langle \phi | \delta\phi \rangle^\star \tag{2.144}$$

$$\left\langle \delta\phi \right| \hat{F} \left| \phi \right\rangle = \left\langle \phi \right| \hat{F} \left| \delta\phi \right\rangle^\star, \tag{2.145}$$

this eqs. (2.144) and (2.145) are manifestations of the hermiticity of the operators. The stationarity condition respect to the variations of the Lagrangian, eq. (2.139), imply that:

$$\begin{aligned} \delta\mathscr{L} = &\sum_i^n \left\langle \delta\phi_i \right| \hat{F}_i(\vec{R}) \left| \phi_i \right\rangle - \sum_{ij} \lambda_{ij} \langle \delta\phi_i | \phi_j \rangle \\ &+ \sum_i^n \left\langle \delta\phi_i \right| \hat{F}_i(\vec{R}) \left| \phi_i \right\rangle^\star - \sum_{ij} \lambda_{ij} \langle \delta\phi_i | \phi_j \rangle^\star = 0 \end{aligned} \tag{2.146}$$

The variation of either $\langle \delta\phi |$ or $\langle \delta\phi |^\star$, must make stationary the Lagrangian. Taking the complex conjugate of the last two terms and subtracting them from the first two terms we get:

$$\sum_{ij} \left(\lambda_{ij} - \lambda_{ij}^\star\right) \langle \delta\phi_i | \phi_j \rangle = 0 \tag{2.147}$$

therefore, $\lambda_{ij} = \lambda_{ij}^\star$, that imply the hermiticity of the Lagrange multipliers. Knowing one of the relations between the Lagrange multipliers that make the Lagrangian stationary with respect to any of the two variations is equivalent to know the relation involving the other vatiation. The variation respect to $\langle \delta\phi |$ gives the set of Hartree-Fock(HF) equations:

$$\hat{F}_i(\vec{R})\phi_i = \sum_j^n \lambda_{ij}(\vec{R})\phi_j \tag{2.148}$$

Further simplification can be achieved by performing a unitary transformation that diagonalize λ_{ij} originating the set of canonical MOs:

$$\hat{F}_i(\vec{R})\phi_i' = \sum_i^n \epsilon_i(\vec{R})\phi_i' \tag{2.149}$$

This exposes the physical interpretation of the Lagrange multipliers as the energy of the MOs. But here we start to be in predicament, because the HF depends on all the occupied MOs, but the right occupied MOs are unknown. Therefore the standard approach is start by a initial guess for the occupied MOs and solve eq. (2.149) iteratively by a self-consistent field (SCF) cycle.

Finally the total energy of the molecule can be written in terms of the energies of the MOs as:

$$E_0(\vec{R}) = \sum_i \epsilon_i(\vec{R}) - \frac{1}{2}\sum_{ij}^n (J_{ij}(\vec{R}) - K_{ij}(\vec{R})) + V_{nn}(\vec{R}). \tag{2.150}$$

Linear combination of atomic orbitals (LCAO) approach to the HF equations

The aim here is show how the expansion of the MO as a LCAO, transform the integro-differential electronic Schödinger equation into a set of algebraic equations that can be solved using standard techniques of linear algebra.

Writing the MOs as a linear combination of atomic orbitals χ_i, see appendix A.1, the MO can written as:

$$\phi_i = \sum_\alpha^{N_b} c_{\alpha i}\chi_\alpha \tag{2.151}$$

where each MO, ϕ_i, is expanded as a linear combination of atomic orbitals LCAO, χ_α, and N_b is the number of basis functions. It is important to remark that as in section 2.1.1, regular electronic structure is based in pseudospectral methods where the localized basis are centered at the nuclei. The functional form of the basis functions χ_α is chosen to fulfill two criteria: the first is physically motivated and is the requirement that the functions must go to zero asymptotically with the distance between the nucleus and

the electrons, the second is pragmatic and is the expedite computation of the matrix elements of the electronic Hamiltonian. Besides be solutions of the Schrödinger equation for one electron in a Coulomb potential,[69] the usage of Slater orbitals in molecular electronic structure is not popular due to the lack of efficient methods to compute the electronic repulsion integrals. In contrast, gaussian basis sets.[70] the evaluation of the integrals for all the matrix elements of the electronic Hamiltonian is feasible, therefore cartesian gaussians [59] will be used in this work.

Replacing the LCAO, eq. (2.151), in the HF equation for the canonical MO, eq. (2.149), The Hartree-Fock equations takes the form:

$$\hat{F}_i(\vec{R}) \sum_{\alpha}^{N_b} c_{\alpha i}\chi_\alpha = \sum_{i}^{n} \epsilon_i(\vec{R}) \sum_{\alpha}^{N_b} c_{\alpha i}\chi_\alpha \tag{2.152}$$

Projecting on the left on a specific MO and integrating yields the following system of equations:

$$\begin{aligned} \mathbf{F}(\vec{R})\mathbf{c} =& \mathbf{S}(\vec{R})\mathbf{c}\boldsymbol{\epsilon}(\vec{R}) \\ F_{\alpha\beta}(\vec{R}) =& \left\langle \chi_\alpha \right| \hat{F}(\vec{R}) \left| \chi_\beta \right\rangle \\ S_{\alpha\beta} =& \langle \chi_\alpha | \chi_\beta \rangle \end{aligned} \tag{2.153}$$

This system of coupled equations is known as the Roothaan–Hall Hartree-Fock equation (RHHF). Here $F_{\alpha\beta}(\vec{R})$ is the matrix representation of the Fock operator, eq. (2.142), $\mathbf{S}(\vec{R})$ is the matrix of overlaps.[8] Introducing the electronic charge-density matrix:[9]

$$D_{\gamma\delta} = \sum_{j}^{occ} c_{\gamma j} c_{\delta j}, \tag{2.154}$$

where tha index j takes values on the occupied MOs, the matrix element of

[8] In general, this two matrices are hermitian and can be diagonalized by unitary transformations.

[9] Also called bond-order matrix.

the Fock operator is:

$$\begin{aligned}\left\langle \chi_\alpha \right| \hat{F}(\vec{R}) \left| \chi_\beta \right\rangle &= \left\langle \chi_\alpha \right| \hat{h}(\vec{R}) \left| \chi_\beta \right\rangle + \sum_j^{occ} \left\langle \chi_\alpha \right| \hat{J}_j(\vec{R}) + \hat{K}_j(\vec{R}) \left| \chi_\beta \right\rangle \\ &= \left\langle \chi_\alpha \right| \hat{h} \left| \chi_\beta \right\rangle + \sum_j^{occ} (\langle \chi_\alpha \phi_j | \, \hat{g} \, | \chi_\beta \phi_j \rangle - \langle \chi_\alpha \phi_j | \, \hat{g} \, | \phi_j \chi_\beta \rangle) \\ &= \left\langle \chi_\alpha \right| \hat{h} \left| \chi_\beta \right\rangle + \sum_{\gamma\delta} D_{\gamma\delta} (\langle \chi_\alpha \chi_\gamma | \, \hat{g} \, | \chi_\beta \chi_\delta \rangle - \langle \chi_\alpha \chi_\gamma | \, \hat{g} \, | \chi_\delta \chi_\beta \rangle)\end{aligned} \tag{2.155}$$

For its implementation in a computer code, result of convenience to write the former equation in more compact notation by the introduction of the tensor of repulsion integrals $\mathbf{G}$:

$$F_{\alpha\beta} = h_{\alpha\beta} + \sum_{\gamma\delta} G_{\alpha\beta\gamma\delta} D_{\gamma\delta}. \tag{2.156}$$

The matrix element $\langle \chi_\alpha \chi_\gamma | \, \hat{g} \, | \chi_\beta \chi_\delta \rangle$ have following permutational invariance respect to the indexing of the basis functions:

$$\begin{aligned}\langle \chi_\alpha \chi_\gamma | \, \hat{g} \, | \chi_\beta \chi_\delta \rangle &= (\mu\nu|\lambda\sigma) \\ (\mu\nu|\lambda\sigma) &= (\nu\mu|\lambda\sigma) = (\mu\nu|\sigma\lambda) = (\nu\mu|\sigma\lambda) \\ &= (\sigma\lambda|\nu\mu) = (\lambda\sigma|\nu\mu) = (\lambda\sigma|\mu\nu)\,,\end{aligned} \tag{2.157}$$

Therefore the restriction to the computation of the unique electronic repulsion integrals (ERIs) is guaranteed if the following restrictions in the indexing are fulfilled:

$$\begin{aligned}\mu \geq & \nu \\ \lambda \geq & \sigma \\ \mu(\mu+1)/2 + \nu \geq & \lambda(\lambda+1)/2 + \sigma.\end{aligned}$$

The tensor of repulsion integrals can be mapped to a vector, $ERIs$, introducing the compound index of ERIs:

$$\mu\nu = \mu(\mu+1)/2 + \nu, \tag{2.158}$$

$$\lambda\sigma = \lambda(\lambda+1)/2 + \sigma,$$

$$\mu\nu\lambda\sigma = \mu\nu(\mu\nu+1)/2 + \lambda\sigma, \tag{2.159}$$

$$G_{\alpha\beta\gamma\delta} = ERIs(\alpha\gamma\beta\delta) - ERIs(\alpha\gamma\delta\beta).$$

Starting from eq. (2.150) and following analogous steps to the derivation of eq. (2.155), it is possible to derive the following expression for the total energy of the molecule:

$$E_0(\mathbf{R}) = \sum_{\alpha\beta}^{M} D_{\alpha\beta} h_{\alpha\beta} + \frac{1}{2} \sum_{\alpha\beta\gamma\delta}^{M} \left(D_{\alpha\beta} D_{\gamma\delta} - D_{\alpha\delta} D_{\gamma\beta} \right) (\alpha\gamma|\beta\delta) + V_{nn}(\vec{R}) \tag{2.160}$$

The techniques and notation used to compute the matrix elements can be traced back to the reference [71], and has been reviewed and modernized in reference [16]. The appendix A.1 summarizes the derivation of all the electronic integrals involved in a HF computation that where implemented for the thesis.

Single-reference methods for the computation of excited states.

Following reference [72], the methods for the computation of excited states starting from a single reference wavefunction, begins by choosing a Hartree-Fock determinant, ψ_{HF}, as a reference for the ground state of the molecule:

$$\psi_{HF} = (n!)^{-1/2} \det\{\chi_1 \chi_2 \cdots \chi_i \chi_j \cdots \chi_N\}. \tag{2.161}$$

where then molecular spin orbitals are given in terms of an optimized combination of atomic basis functions as follows:

$$\chi_p = \sum_{\mu}^{M} c_{\mu p} \phi_\mu. \tag{2.162}$$

The following notation will be used: μ, ν, λ, σ, $\cdots$, stands for atomic orbitals; i, j, k, l, $\cdots$, stands for molecular orbitals which are occupied in the ground state; a, b, c, d, $\cdots$, stands for virtual or molecular orbitals that are empty in the ground state; p, q, r, s, $\cdots$, stands for generic molecular spin orbitals. The optimized coefficients of combination, $c_{\mu p}$, can be computed by a self-consistent field (SCF) computation, details for the implementation of the SCF procedure are given in the Theoretical Developments and computational implementations section of the thesis.

Here is enough to consider that the $c_{\mu p}$ are the optimal solution to the Hartree-Fock equations:

$$\sum_{\mu} (F_{\mu\nu} - \epsilon_p S_{\mu\nu}) c_{\mu p} = 0. \tag{2.163}$$

Here $F_{\mu\nu}$ are matrix elements of the Fock-operator given by eq. (2.156), $S_{\mu\nu}$ are matrix elements of the matrix of overlaps, and ϵ_p are canonical eigenvalues of the Fock operator. If $n = N/2$ is the number of occupied orbitals, [10] $n(M-n)$ possible singly excited determinants obtained by the action of all the allowed single excitation operators in eq. (A.82) on the reference determinant eq. (2.161), such a excited determinants and associated energies are:

$$\psi_{ia} = (n!)^{-1/2} det\{\chi_1\chi_2\cdots\chi_a\chi_j\cdots\chi_N\}, \tag{2.164}$$

$$E_{ia} = E_{HF} + \epsilon_a - \epsilon_i - \tilde{G}_{iaia} \tag{2.165}$$

where $\tilde{G}$ stands for the spin-adapted ERIs after the transformation from atomic to molecular orbitals representation:

$$\tilde{G}_{pqrs} = \sum_{\mu\nu\lambda\sigma} c_{\mu p} c_{\nu q} c_{\lambda r} c_{\sigma s} G_{\mu\nu\lambda\sigma} \tag{2.166}$$

Thus we can build a pseudospectral basis to determine the excited state using linear combinations of ψ_{ia}:

$$\psi_{CIS} = \sum_{ia} x_{ia}\psi_{ia}, \tag{2.167}$$

the combination coefficients are given by the normalized eigenvectors of the CIS Hamiltonian matrix:

$$\langle\psi_{ia}|\,|\psi_{jb}\rangle = [E_{HF} + \epsilon_a - \epsilon_i]\delta_{ij}\delta_{ab} - \tilde{G}_{jaib}. \tag{2.168}$$

This procedure is known in literature as the full configuration interaction in the subspace of single substitutions of CI Singles. We can get further improvements if the second order Møller–Plesset perturbative correction:

$$\begin{aligned}\Delta_{iajb} = &-\frac{1}{4}\sum_{ijab}\frac{\left\langle\psi_{CIS}\right|\hat{H}\left|\psi_{ijab}\right\rangle}{\epsilon_a + \epsilon_b - \epsilon_i - \epsilon_j - \Delta_{CIS}} \\ &-\frac{1}{36}\sum_{ijkabc}\frac{\left\langle\psi_{CIS}\right|\hat{H}\left|\psi_{ijkabc}\right\rangle}{\epsilon_a + \epsilon_b + \epsilon_c - \epsilon_i - \epsilon_j - \epsilon_k - \Delta_{CIS}}\end{aligned} \tag{2.169}$$

[10] In consistency with the notation followed in appendix A.2, In the case of a closed-shell molecule, the number of occupied orbitals is one half of the total number of electrons.

standing for the correlations due to the electro-electron repulsion is added. Such corected method is referred to as CI-Singles-MP2. The additional matrix elements are given by:

$$\left\langle \psi_{CIS} \right| \hat{H} \left| \psi_{ijab} \right\rangle = \sum_{c} [x_{ic}\tilde{G}_{abcj} - x_{jc}\tilde{G}_{abci}] + \sum_{k} [x_{kb}\tilde{G}_{kaij} - x_{ka}\tilde{G}_{kbij}] \tag{2.170}$$

$$\begin{aligned}\left\langle \psi_{CIS} \right| \hat{H} \left| \psi_{ijkabc} \right\rangle =& x_{ia}\tilde{G}_{jkbc} + x_{ib}\tilde{G}_{jkca} + x_{ic}\tilde{G}_{jkab} + x_{ja}\tilde{G}_{kibc} \\ &+ x_{jb}\tilde{G}_{kica} + x_{jc}\tilde{G}_{kiab} + x_{ka}\tilde{G}_{ijbc} + x_{kb}\tilde{G}_{ijca} + x_{kc}\tilde{G}_{ijab}.\end{aligned} \tag{2.171}$$

The new matrix elements stands out for correction due to triples, eq. (2.170), and quadruples, eq. (2.171), substitutions, and the Δ_{CIS} and x are given by the eigensystem of eq. (2.168). Using state of the art paralization tools the computation of this corrections can be paralellized automaticly.

Chapter 3

Theoretical Developments and Computational Implementations

The application of pseudospectral methods to wavepacket dynamics, section 2.1.1, and regular electronic structure theory, sections 2.2.1 and 2.2.2; have shown a long tradition of success. Our aim in this chapter is attempt to borrow ideas from those pseudospectral methodologies in order to achieve three goals: in the first place, formulate a pseudospectral solution to the QOC optimization problem with experimental realm; in the second place, formulate a modular [1] methodology to obtain an on-the-fly approximated solution of the TDSE that takes into account the full dimensionality of the molecules and non-adiabatic transitions between the PESs; and in third place, we implemented extensions of the Hartree-Fock and single reference methods of regular electronic structure theory in order to describe properly the interaction of the molecule with a time-dependent Electric field for broader regions of the frequency*versus* intensity diagram fig. 1.1.

We believe that the combination of this three achievements will provide worth contributions in order to fulfill *the need for accurate ground and excited potential energy surfaces to design optimal pulses a priory, as well as to interpret the mechanism of pulses that are found by experimental optimization.*[29] In this section we also collect the theoretical derivations giving place to numerical implementations performed in order to test in a systematic manner the proposed methodologies.

[1] Modularity in the sense of keep under control the computational expenses of the on-the-fly computations.

In order to expose the essential features that are necessary to take into account to achieve the QOC of molecular events, let us recall here the theoretical formulation of the excited state dynamics theory. The wavefunction, Ψ, of a molecular system composed of N nuclei with coordinates $\mathbf{R} = (\mathbf{R_1}, \mathbf{R_2}, \ldots, \mathbf{R_I}, \ldots, \mathbf{R_N})$, and n electrons with coordinates $\mathbf{r} = (\mathbf{r_1}, \mathbf{r_2}, \ldots, \mathbf{r_i}, \ldots, \mathbf{r_n})$ can be calculated by solving the time-dependent Schrödinger equation (atomic units will be used hereafter)

$$\frac{\partial \psi}{\partial t} = -i\hat{H}(t)\psi, \tag{3.1}$$

here $\hat{H}(t) = \hat{\mathcal{H}}_0 + \hat{\mathcal{H}}^{\text{int}}(t)$, where $\hat{\mathcal{H}}_0$ is the molecular Hamiltonian, and $\hat{\mathcal{H}}^{\text{int}}(t)$ is the interaction of the system with a pulse of light.

Under the Born-Oppenheimer ansatz[73] for the wavefunction of eq. (3.1), the evolution of the nuclear wavepacket, χ_k, can be obtained by tracing out the electronic degrees of freedom:

$$\left[\mathcal{T}(\mathbf{R}) + E_k(\mathbf{R})\right] \chi_k(\mathbf{R};t) + \sum_l \mathcal{C}_{kl}\chi_k(\mathbf{R};t) = i\frac{\partial}{\partial t}\chi_k(\mathbf{R};t), \tag{3.2a}$$

$$\mathcal{C}_{kl}(\mathbf{R}) = \langle \Phi_k | \mathcal{T}(\mathbf{R}) | \Phi_k \rangle - \sum_J \frac{1}{M_J} \langle \Phi_k | \nabla_J | \Phi_l \rangle \nabla_J, \tag{3.2b}$$

here, $E_k(\mathbf{R})$ is the $k-$th potential energy surface (PES) corresponding to electronic state $|\Phi_k\rangle$, that can be the ground or any excited state of the molecule, and $\mathcal{C}_{kl}(\mathbf{R})$ are diabatic couplings between electronic states $|\Phi_k\rangle$ and $|\Phi_l\rangle$. This expression is in the adiabatic picture, but it can be transformed by a unitary similarity transformation to a picture in which the kinetic and not the potential operator is diagonal, the so called diabatic picture.

The electronic state, $|\Psi_k\rangle$, can be computed employing electronic structure methods as the exposed in sections 2.2.1 and 2.2.2 (in such a case, it is often called *on-the-fly* quantum dynamics, see reference [49]), or as a model potential, typically harmonic, whose parameters has been fitted to a grid of results from electronic structure computations, The most prominent example of the second kind of approach is the vibronic coupling Hamiltonian model [22, 23, 74, 75].

In order to enable the possibility of control, in some extent, the state of the molecule, it must be coupled to a source of energy that must be coherent and highly tunable. It is typically, a train of laser pulses, that in terms of the physical field can be written as:

$$\boldsymbol{\varepsilon}_{phys}(t) = \frac{1}{2\pi}\int_{-\infty}^{+\infty} \tilde{\boldsymbol{\varepsilon}}(\omega)e^{i\omega t}d\omega \tag{3.3}$$

$$\boldsymbol{\varepsilon}(t) = \boldsymbol{\varepsilon}^{(+)}_{phys}(t). \tag{3.4}$$

Standing for the pulse shape decomposed into a range of monochromatic waves, the superscript $(+)$ refers to the positive part of the spectrum of the physical field. The light-molecule interaction, $\hat{\mathcal{H}}^{\text{int}}$, is considered semiclassically. Within the dipole and non-relativistic region of fig. 1.1, the light-molecule interaction is described properly by the dipolar approximation,

$$\mathcal{H}^{\text{int}}_{kl}(\mathbf{R}, t) \approx -4\pi\mu_{kl}(R)\varepsilon(t), \tag{3.5}$$

where μ_{kl} is an element of the electronic transition dipole matrix. Within the non-dipole and non-relativistic region of fig. 1.1, higher multipole moments must be summed up to represent properly the light-molecule interaction:

$$\mathbf{p} = \mathbf{p}_0 + \boldsymbol{\alpha}\cdot\vec{\varepsilon} + \frac{1}{2!}\vec{\varepsilon}\cdot\beta\vec{\varepsilon} + \cdots \tag{3.6}$$

built by concatenating the vectors of genes of the N LCPs, $\mathbf{E}_i = \{y_1, y_2, \cdots, y_N\}$. Where $\mathbf{p}_0$ stands for the dipole coupling whose matrix elements are those in eq. (3.5), $\boldsymbol{\alpha}$ is the polarizability matrix and is related to how easy is move electron from occupied to empty orbitals as response to the field, and β is the second order hyperpolarizability and has to do with nonlinear responses to the field.

The eqs. (3.1), (3.2a), (3.2b) and (3.4) to (3.6) summarizes the different aspects of the QOC problem on which we are attempting to contribute. The developments are grouped as follows: In the first section a novel pseudospectral methodology to solve and analyze QOC problems is proposed and tested using models as proof-of-principle demonstrations, we also provide in this section details for a generalized and efficient implementation of the method of Alvarellos and Metiu [76] for the propagation of wavepackets on coupled PESs as in eqs. (3.2a) and (3.2b) focused to offer good performance for models whose Hamiltonian involves an arbitrary number of PES

in one and two dimensions. In the second section we propose a modular methodology to compute approximate solutions to the TDSE for molecules, eqs. (3.1), (3.2a) and (3.2b), taking into account the full dimensionality of the molecules, the non-adiabatic effects and the light-molecule interaction. In the third section, we extend the previous method to solve on-the-fly the TDSE for molecules in which the Franck-Condon and conical intersection zones are populated with trimmed portions of a von-Neumann lattice, that has been constructed in the phase space of normal coordinates and transformed back to Cartesian coordinates; details for an efficient implementation of this methodology tailored to run in any high performance computing facility are exposed and applied to the QOC of the $\pi \rightarrow \pi^{\star}$ decay in the ethylene molecule. In the fourth section, we expose the details regarding the from-the-scratch implementation of a single-reference method for the determination of the ground and excited PESs, their mechanical and electric responses, taking into account the light-molecule interaction and attempting to describe properly interactions until the non-dipole, non-relativistic zone of fig. 1.1.

In order to support and produce the results in this document and the content of the published papers, a computational package that we call *HELIOS* has been written from the scratch. The capabilities of *HELIOS* covers from quantum dynamics based on models in one and two dimensions using the split-operator method, to computation of approximated solutions to the TDSE for systems higher dimensionality employing the pseudospectral approach exposed in section 3.2, also is supported on-the-fly solutions to the TDSE supported by the GAMESS for the computation of molecular responses via the coupled-perturbed Hartree-Fock equations. Regarding electronic structure methods, *HELIOS* is capable of perform all the molecular integrals in appendix A.1 and determine the ground state PES of polyatomic molecules at the state of the art, also are implemented in *HELIOS* the MP2 method to recover the electronic correlation, the CIS [77], random-phase approximation and CISD [78] for the computation of excited PES. Mechanical molecular responses are available within *HELIOS* using finite differences and with them is possible to run direct dynamics. Finally, regarding QOC, *HELIOS* have available an implementation of the Krotov procedure and the pseudospectral formulation that will be proposed in section 3.1 including the acquisition of data for principal component analysis of the optimal path. No other software has being used unless that it is explicitly mentioned and cited.

Algorithm 2 Krotov self-consistent procedure.

Propagate the initial state $\psi(\mathbf{R},T)=\hat{U}(0,T;\varepsilon_f=cte.)\psi(\mathbf{R},0)$
while $\int_0^T \|\varepsilon_f(t)-\varepsilon_b(t)\|>\kappa$ **do**
  Initialize the Lagrange multiplier: $\chi(\mathbf{R},T)=|\phi_f(\mathbf{R})\rangle\langle\phi_f(\mathbf{R})|\psi(\mathbf{R},T)\rangle$.
  for each backward time step: **do**
    $\varepsilon_b(t)=-\Im\langle\chi(t)|\,\mu_k\,|\psi(t)\rangle$
    $\chi(\mathbf{R},t-\Delta t)=\hat{U}(t-\Delta t,t;\varepsilon_b(t))\chi(\mathbf{R},t)$
    $\psi(\mathbf{R},t-\Delta t)=\hat{U}(t-\Delta t,t;\varepsilon_f(t))\psi(\mathbf{R},t)$
  end for
  Initialize the wavepacket: $\psi_i(\mathbf{R})=\varphi(\mathbf{R})$.
  for each forward time step: **do**
    $\varepsilon_f(t)=-\Im\langle\chi(t)|\,\mu_k\,|\psi(t)\rangle$
    $\chi(\mathbf{R},t+\Delta t)=\hat{U}(t+\Delta t,t;\varepsilon_b(t))\chi(\mathbf{R},t)$
    $\psi(\mathbf{R},t+\Delta t)=\hat{U}(t+\Delta t,t;\varepsilon_f(t))\psi(\mathbf{R},t)$
  end for
end while

TOWARDS A PSEUDOSPECTRAL FORMULATION OF QOC

Type (i) and type (ii) methods of section 1.1 have as common goal to attain a large transition probability from the initial wave-packet to a final, target, wave-packet by shaping an external laser field while minimizing the energy that the field transfers to the molecule. For this purpose the Lagrangian for the standard QOC problem eq. (2.43) should be optimized.

The optimality condition is given in the form of the set of coupled Euler-Lagrange equations, eqs. (2.46) to (2.48), Here the evolution of both, the state $\psi(\mathbf{R},0)$ and the Lagrange multiplier $\chi(\mathbf{R},T)$ depends on the field intensity. Similarly, the field intensity $\varepsilon(t)$ depends on both $\psi(\mathbf{R},t)$ and $\chi(\mathbf{R},t)$. As a consequence, the calculation of the optimal pulse shape must be performed in a self-consistent fashion.

Adopting a time discretization (i.e., $t_j=j\times\Delta t$, where $j=0,1,2,3,...,N$ and $N\Delta t=T$, and k is an index to count the number of iterations) the self-consistent procedure in algorithm 2 was implemented. Use of a strong

field as the initial guess at the line 1 of algorithm 2 is a necessary condition to achieve convergence. In fact, the initial field should be strong enough to take the iterative optimization procedure to a neighborhood in the Lagrangian manifold that put within reach a local optimal solution to the QOC problem at hand. In more intuitive terms, this means that the guess field used in the initial propagation must be enough to achieve some amount of overlap between initial and target states.

Within low dimensionality systems one can tailoring the strength and orientation of the field to achieve the non-negligible amount of overlap that needs the procedure in algorithm 2 to converge [79], but it is cumbersome in systems of high-dimensionality as polyatomic molecules.

In order to expose the meaning of the claim *"Strong enough"* we will apply the procedure algorithm 2 to a wavepacket propagating in a double well potential and expose in closer details the features of the method.

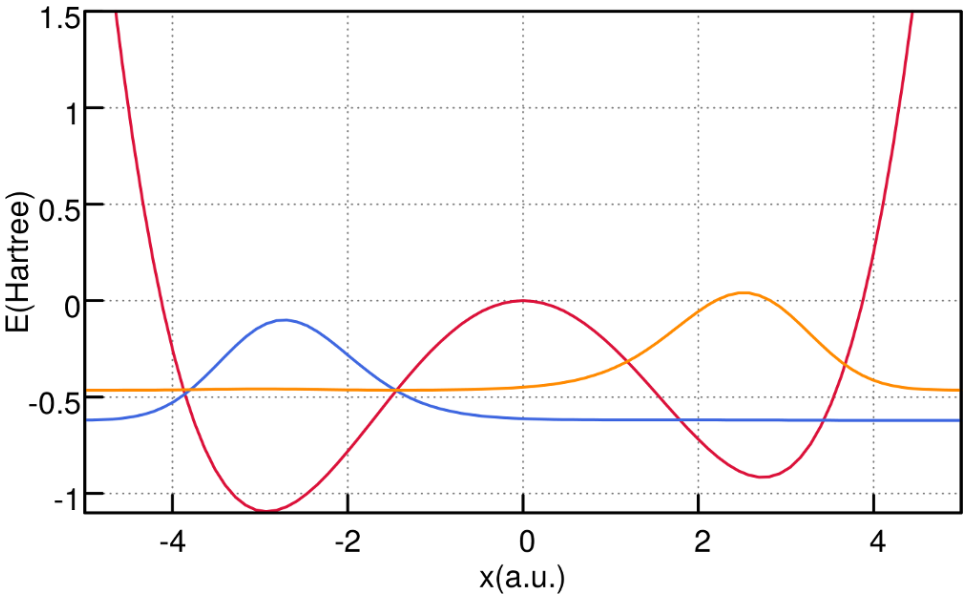

Figure 3.1: *Initial(blue), $\psi(\mathbf{R}, 0)$, and target(yellow), $\chi(\mathbf{R}, T)$, states of the double well potential(red). The QOC consist in optimize a pulse convert the initial state into the target one in a prescribed propagation time with minimum expenditure of energy.*

The initial and target states of the problem are shown in fig. 3.1. Having

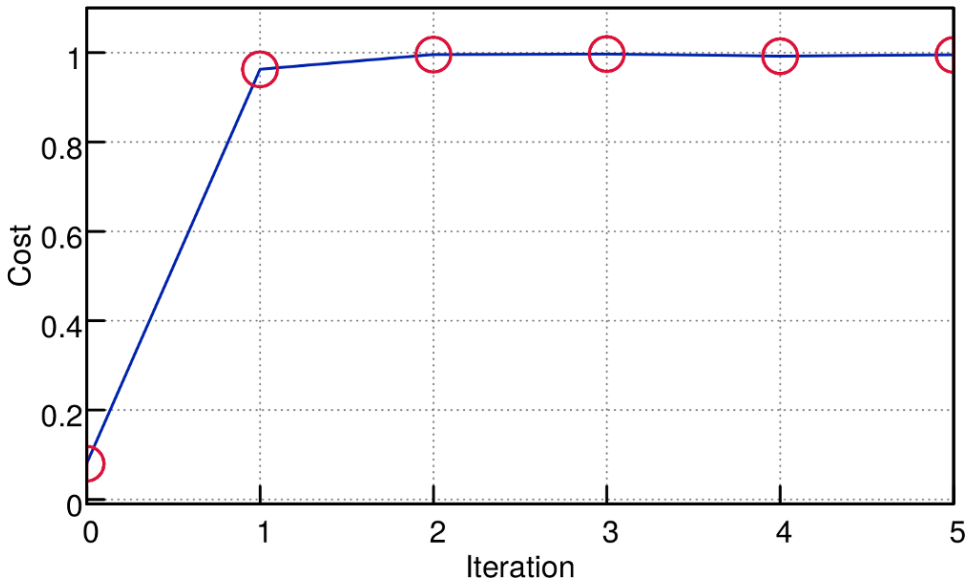

Figure 3.2: *Values achieved by the Lagrangian for each iteration of the procedure algorithm 2.*

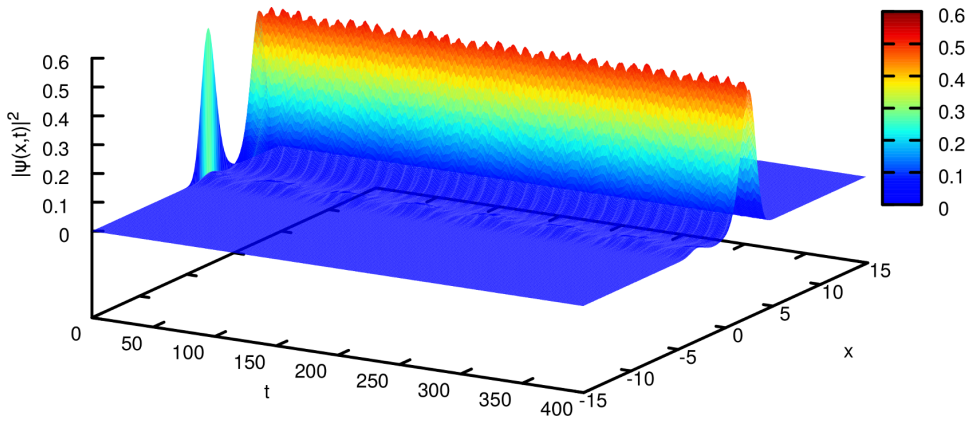

Figure 3.3: *Propagation of the initial condition steered by the optimal pulse.*

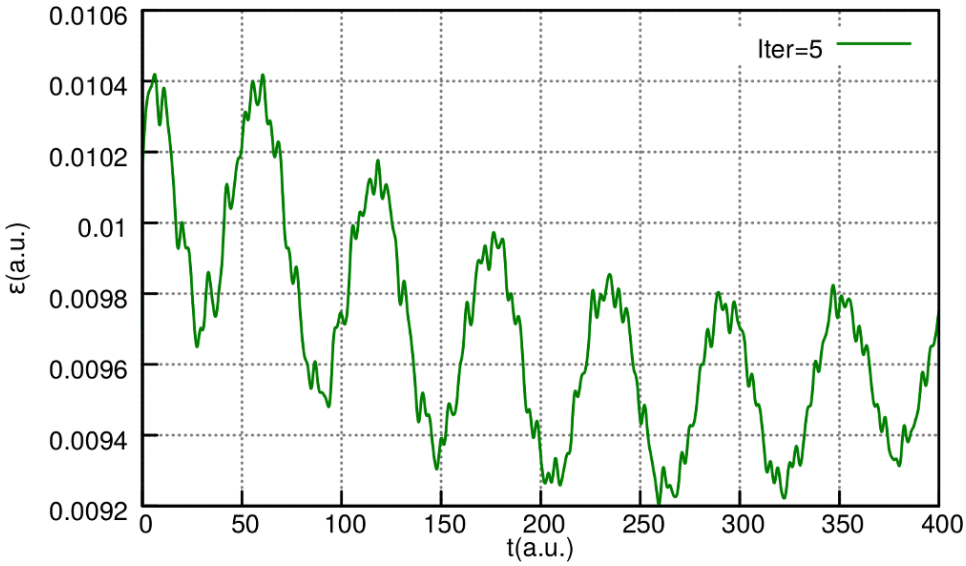

Figure 3.4: *Optimal pulse shape obtained usign the procedure algorithm 2 at the fifth iteration.*

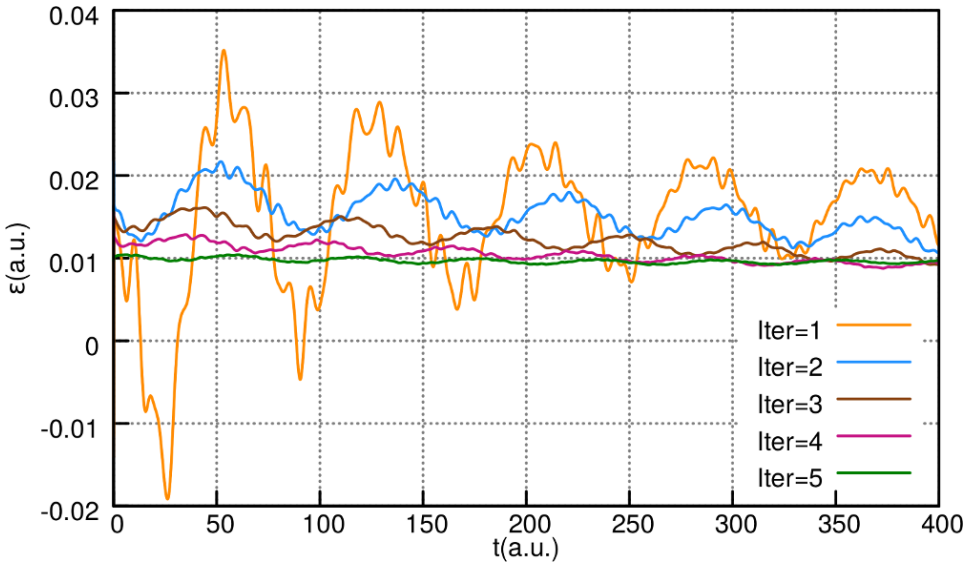

Figure 3.5: *History of the optimal pulse shape as function of the iteration number for the procedure algorithm 2. The intensity of the pulse shape for the first iteration is about 1 order of magnitude bigger than the intensity for the optimal pulse.*

the local optimal solution within reach, the procedure in algorithm 2 converges quickly to the optimal pulse shape as shown in fig. 3.2. As shown fig. 3.3, the final optimal pulse, fig. 3.4, is very efficient preparing the target state.

One of the main issues regarding the applicability of the procedure in algorithm 2 to molecular systems stands out in fig. 3.5. When the electric field of the pulse achieve high values, it may cause changes in the chemical identity of the system that we are attempting to control. Inducing undesirables photochemical processes or making impossible to attempt for on-the-fly computation of the PESs.

Aiming to manage this difficulty we attempt to achieve a pseudospectral formulation of the QOC optimization procedure as follows: expressing the pulse shape as a unknown linear combination of band-width limited pulse functions; we used a genetic algorithms (GA) in order to optimize the Lagrangian eq. (2.43), doing an meta-heuristic search within a region of the space of parameters that have experimental realm; finally keeping a record of time averaged observations and performing a principal component analysis on the recorded data (Markov chain) we can shed lights on *how to interpret the mechanism of pulses that are found by our experimental optimization.*[29]

Linearly chirped pulses (LCP) are very good candidates to be used as a pseudospectral basis for band-width limited pulse functions, because LCPs have been used successfully to control photochemical reactions [80, 35, 81, 82, 83, 84, 85, 86]. The time profile of a LCP can be written as:

$$\mathcal{V}(t) = E_0 \exp\left(-\frac{(t-\tau_0)^2}{2\tau^2}\right) \cos\left(\frac{1}{2}c(t-\tau_0)^2 + \omega_0(t-\tau_0)\right), \tag{3.7}$$

here τ_0 is the time shift, E_0 is the pulse amplitude, c is the chirp rate, ω_0 is the central frequency, and τ is the pulse width. As observed, the instantaneous frequency of a LCP changes linearly with time.

In order to perform the optimization of the pulse shape, we use a genetic algorithm (GA) to score the resulting pulse shapes using as fitness function the Lagrangian $J_{\hat{O}}$. For an observable $\hat{O}$ the fitness function we used the

following:

$$J_{\hat{O}} = J_{\hat{O}}^{(1)}[\Psi] + J^{(2)}[\varepsilon(t)], \tag{3.8}$$

$$J_{\hat{O}}^{(1)}[\Psi] = \left\langle \Psi(T) \middle| \hat{O} \middle| \Psi(T) \right\rangle, \tag{3.9}$$

$$J^{(2)}[\varepsilon(t)] = -\int_0^T \|\varepsilon(t)\|^2 dt \tag{3.10}$$

here $J^{(2)}[\varepsilon(t)]$ again penalizes the fluence of the laser. In order to allow more selective optimizations, we propose the multi-target fitness function:

$$J = J_{\hat{O}_1} + \sum_{i=2}^{k} \frac{1}{J_{\hat{O}_i}} \tag{3.11}$$

to maximize observable $\hat{O}_1$, while minimizing observables $\hat{O}_{i\neq 1}$.

In order to implement the pseudospectral optimization of the pulse shape for a given QOC problem, we express the pulse, $\varepsilon(t)$, as a linear combination of LCPs. In our GA implementation, the chromosome of the i-th individual, the linear combination of LCPs

$$\varepsilon(t) = \sum_i \mathcal{V}_i(t), \tag{3.12}$$

built by concatenating the vectors of genes of the N LCPs, $\mathbf{E}_i = \{y_1, y_2, \cdots, y_N\}$. Each LCP is represented by a 5-vector $y_j = (E_0, \tau_0, c, \tau, \omega_0)$. We propose two genetic operations to evolve the N LCPs: (1) a mutation to change one or more genes with probability $\boldsymbol{\pi}_M$, and (2) a crossover operation acting on two individuals to generate a new individual with probability $\boldsymbol{\pi}_X$. The chromosome of the new individual are generated as a fitness-weighted linear combination of the chromosome of the parents. Optimizations were carried out following the next steps:

0. Initialize the population with a list of individuals whose chromosomes were generated randomly. [2]

1. Propagate individuals using the same initial condition and calculate their scores with the fitness function of eq. (3.11). also compute along the propagation the averaged quantity to be employed in the PCA analysis.

[2] It is crucial to limit the generation of the initial list of individuals to the region of the parameters space with experimental relevance.

2. Sort individuals in descending order according to their fitness.
3. Compute the cumulative fitness of the entire population.
4. Keep those individuals with fitness greater or equal than the cumulative fitness. Discard the remainder.
5. Replace those individuals discarded in step 4 with new ones generated by crossing over the survivors with probability π_X.
6. Go through the new population list sampling the probability of mutation of each gene with a Monte Carlo scheme. Mutate those genes with probabilities lower than π_M.
7. Go back to step 1 if the maximum number of generations has not been reached.

Machine learning concepts are useful tools when we need to gain intuition on a set of observations. One in common usage is unsupervised learning. The technique of unsupervised learning consists of a learner trying to find a hidden structure in a set of observations, to use it in decision making, aiming to predict future outcomes.[87]

One simple way to obtain a probabilistic model from a set of observations is to assume that the data follow a Gaussian distribution and that the structure of the data distribution is encoded in its covariance matrix. The structure can be retrieved in two steps: 1) perform a singular value decomposition (SVD) of the covariance matrix to obtain singular values, W, and singular vectors P. 2) Identify the directions with highest variance in the set of observations. The steps of this procedure are presented in algorithm 3. The higher the W the higher the variance of the set of observations along the corresponding P. This procedure is known as principal components analysis (PCA) of the set of observations.

We can enrich our understanding of the intricate sequence of events resulting from the effects of the optimization of the pulse shape for a given QOC problem by using unsupervised learning techniques. To this aim, we built a set of observations by recording the time-averaged expected values of the dynamics for each surviving individual along the total GA evolution, it may be the transition moment integrals (TA-TMI) as we did in reference [88] or any other process of interest. The resulting set of observations narrows around the most frequent values along the optimal path in a statistical

Algorithm 3 Principal components analysis.

1: Compute the average $\vec{\mu}$ of the total (N) set of observations$\{P^1\}, \cdots, \{P^N\}$.
2: Compute the covariance matrix with matrix elements $\Sigma_{i,j} = \langle (P_i - \mu_i)(P_j - \mu_j) \rangle$.
3: Compute the SVD of Σ.

sense.

Perform a PCA of this data set enhance our understanding on *how to interpret the mechanism of pulses that are found by experimental optimization.*[29]

Controlling a biomolecule

[3]

Biological realm

Rhodopsin, the protein of vision in vertebrates' retina, is a light-sensitive receptor of rod cells and a well known GPCR (G protein-coupled receptor) [89]. The chromophore of rhodopsin, 11-*cis*-retinal, is covalently bound to the protein via a protonated Schiff base. Although today is not completely understood how the chromophore motion interacts with its surroundings in the protein [89, 90, 91, 92, 93], it is known that the absorption of one photon causes the photoisomerization of the chromophore to all-*trans*-retinal, which induces the activation of the protein and triggers a cascade of events in the tertiary structure of the protein ending up in an electric impulse to the brain[93].

The photoisomerization process occurs within 200 fs,[91] an ultrafast process compared to the time-scale of the protein activation and comparable to, or shorter than, the period of torsional vibrations of the chromophore. This short time indicates that in the first steps of vision the coherence of light is transferred to the chromophore. An even more interesting fact, is to explore the possibility that the coherent motion of the chromophore continues after the molecule decays onto the ground electronic surface [94, 95, 96].

[3] To be submitted to J. Chem. Phys.

In bacteriorhodopsin, a protein found in halobacteria, Prokhorenko *et al.* [97] have found experimentally that the efficiency of the isomerization from all-*trans*-retinal to 13-*cis*-retinal (K intermediary) can be manipulated by excitation with tailored light pulses: In their experiments they controlled the absolute yield of 13-*cis*-retinal over a 40% range and 20 ps after the excitation by the actinic pulse. They obtained excitation pulses capable of enhance or suppress the isomerization yield by $\pm 20\%$, when amplitude and phase are both optimized (anti-optimized) from the transform-limited pulse. In the same work, the authors also observed a 4% yield difference due to effect of changing the phase constrained to the same frequency spectrum, *i.e.*, phase control [97, 98].

One-photon phase control have been studied from a theoretical and computational perspective [99, 100, 101, 102, 103]. These studies show that phase control is possible for open quantum systems where the photo-processes are treated beyond the Markovian approximation. In their work, Arango and Brumer [101] modeled the retinal by a 27 degrees of freedom system[**?**] semiclassically driven by a linear chirped laser pulse. These authors used multi-configurational time dependent Hartree (MCTDH)[104] method to propagate the entire photo-process from the 11-*cis*-retinal ground state. Although some degree of phase control was observed, this work was restricted to single linear chirped pulses. However as a first approach, in this work we neglect the coupling to the protein in such a way that the photoisomerization process remains unitary but subject to relaxation due to internal conversion.

Gradient base optimal control,[105, 106] feedback loop based optimal control,[107] and coherent control,[108, 109, 97, 98] require high intensity fields that necessarily implies multi-photon adsorption, and consequently, the coupling to higher electronic states that are not involved in the natural biological response. Therefore, a method to perform quantum optimal control (QOC) constrained to linear combinations of low-intensity analytical pulse shapes is desirable. Recently we proposed a method to achieve analytical optimal pulse shaping whit the aid of genetic algorithms (AOPS+GA),[88] the method was designed to meet this needs and our aim in this paper is to apply the method on the control of the photoisomerization of retinal.

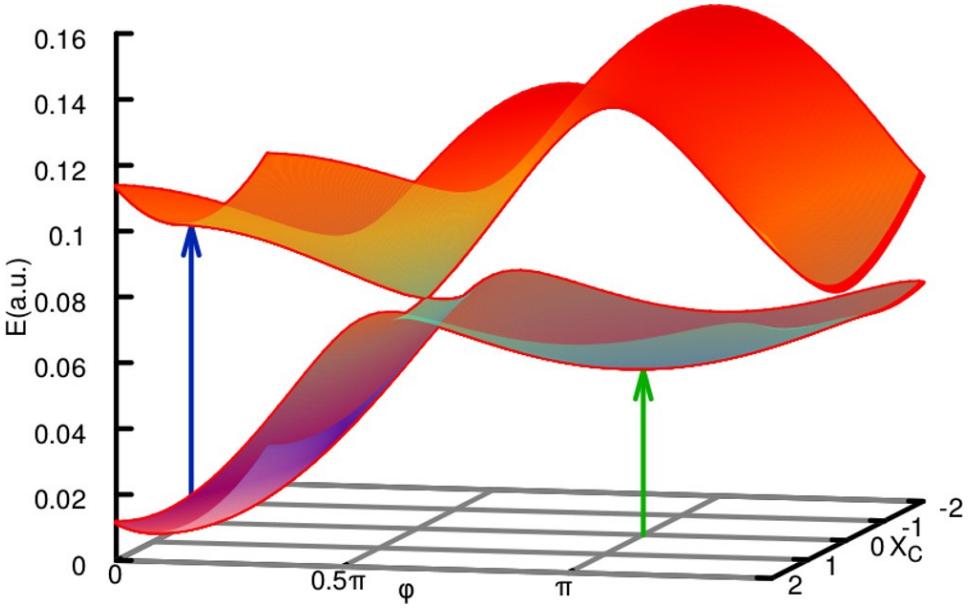

Figure 3.6: *PES of the rovibronic Hamiltonian for the retinal molecule introduced in reference [75]. showing the ground and excited adiabatic PES as a function of the isomerization angle φ and of the coupling mode X_C. The blue arrow shows the initial state of the wavepacket, The green arrow shows the target region for the QOC.*

The Hamiltonian

The 2-dimensional model of Hahn and Stock[75] for the *cis-trans* photoisomerization of retinal includes two electronic curves, FIG.3.6, with a torsional, φ, and a coupling, q, degrees of freedom. The coupling coordinate $q = \sqrt{\frac{m\omega}{\hbar}} X_C$ mainly stands for the stretching of the active C=C bond. Within the rotating wave and Condom approximations,[4] the Hamiltonian including the coupling to the radiation is: (atomic units will be used hereafter)

$$\begin{aligned}\hat{\mathcal{H}}(t) &= \hat{\mathcal{T}} + \hat{\mathcal{V}} + \hat{\mathcal{H}}^{\text{int}} \qquad (3.13)\\ &= -\frac{1}{2m}\frac{\partial^2}{\partial\varphi^2} + \frac{\omega}{2}\frac{\partial^2}{\partial q^2}\\ &\quad + \begin{pmatrix} V_{11} & V_{12} \\ V_{21} & V_{22} \end{pmatrix} - \varepsilon(t) \begin{pmatrix} 0 & \mu \\ \mu & 0 \end{pmatrix}\end{aligned}$$

$$V_{11} = \frac{1}{2}W_1(1-\cos(\varphi)) + \frac{\omega}{2}q^2 \qquad (3.14)$$

$$V_{22} = E_1 - \frac{1}{2}W_2(1-\cos(\varphi)) + \frac{\omega}{2}q^2 + \kappa q \qquad (3.15)$$

$$V_{12} = V_{21} = \lambda q \qquad (3.16)$$

$$\varepsilon(t) = \sum_i \mathcal{V}_i(t), \qquad (3.17)$$

the constant μ is taken to be 1 au.[110] As in a previous work,[88] we will express $\varepsilon(t)$, as a linear combination of linearly chirped pulse (LCP) functions. The time profile of a LCP can be written as:

$$\mathcal{V}(t) = E_0 \exp\left(-\frac{(t-\tau_0)^2}{2\tau^2}\right)\cos\left(\frac{1}{2}c(t-\tau_0)^2 + \omega_0(t-\tau_0)\right), \qquad (3.18)$$

here τ_0 is the time shift, E_0 is the pulse amplitude, c is the chirp rate, ω_0 is the central frequency, and τ is the pulse width.

The state of the molecule as a function of time, $|X(\varphi,q;t)\rangle$, can be expressed in the diabatic basis as a vector of nuclear configurations:

$$|X(\varphi,q;t)\rangle = \begin{pmatrix} \chi_1(\varphi,q;t) \\ \chi_2(\varphi,q;t) \end{pmatrix}. \qquad (3.19)$$

[4] Neglecting any dependence of the transition dipole moment, μ, on the molecular coordinates.

Because of the coupling with the field, the formal solution of the time-dependent Schödinger equation(TDSE):

$$\frac{\partial}{\partial t}\left|X(\varphi,q;t)\right\rangle = -i\hat{\mathcal{H}}(t)\left|X(\varphi,q;t)\right\rangle, \tag{3.20}$$

or propagator, is $\hat{U}(t) = e^{-i\int_0^{2\delta t}[\hat{\mathcal{H}}(t)]dt} \approx e^{-i\mathcal{H}(t+\delta t/2)\delta t}$. As we used in a previous work,[88] we get this result by approximating $\hat{U}$ by employing the midpoint rule to compute the time integration for short times, in combination with the Symmetric Strang splitting. The accuracy of such an approximation have been shown that is of the order δt^2.

We have chosen as initial condition a Gaussian with its centroid in the *cis*-configuration of the retinal PES, $\varphi = 0$ and $q = 0$, of width 16.0 in both variables. Since our interest is to control the wave packet on the excited PES, we assume that the initial condition has been suddenly excited from the ground to the excited PES.

For the optimization of the pulse, we will employ the following multi-target fitness function:

$$J = J_{T1} + J_{CI} + \frac{10^{-2}}{J_{C1}} + \frac{10^{-2}}{J_{C2}} + \frac{10^{-2}}{J_{T2}} \tag{3.21}$$

$$J_{Ti} = \frac{1}{T}\int_0^T dt' Y_{Ti}(t') \tag{3.22}$$

$$J_{CI} = \frac{1}{M}\int_0^T \Im\left\langle\chi_1\right|\hat{p}_\varphi\left|\chi_1\right\rangle \delta(\varphi - 0.52\pi)dt, \tag{3.23}$$

$$J_{Ci} = \frac{1}{T}\int_0^T dt' Y_{Ci}(t') \tag{3.24}$$

$$\begin{aligned} Y_{Ti}(t) = &\int_{-2}^{2} dq \int_{-\frac{\pi}{2}}^{\frac{3\pi}{2}} d\varphi \left\langle\chi_i(t)|\chi_i(t)\right\rangle \\ &\times \theta(\varphi - 0.52\pi)\theta(1.48\pi - \varphi) \end{aligned} \tag{3.25}$$

$$\begin{aligned} Y_{Ci}(t) = &\int_{-2}^{2} dq \int_{-\frac{\pi}{2}}^{\frac{3\pi}{2}} d\varphi \left\langle\chi_i(t)|\chi_i(t)\right\rangle \\ &\times \theta(\varphi + 0.52\pi)\theta(0.52\pi - \varphi) \end{aligned} \tag{3.26}$$

where $\theta(\varphi)$, is the Heaviside step function. This choice of the fitness function allows us to maximize the *trans*-population of the ground state, J_{T1},

and the current through the conical intersection, J_{CI}; while minimizing all the *cis*-population J_{C1-2} and the excited *trans*-population, J_{T2}. The coefficient 10^{-2} weight the importance of minimize J_{C1}, J_{C2} and J_{T2} respect to maximize J_{T1}; suitable values for this numerical constant was chosen looking at the maximum yields for the free evolution.

Table 3.1: *Boundaries of the LCP parameters space used in our GA approach.*

Parameter	Minimum	Maximum
E_0(a.u.)	9.0×10^{-3}	3.5×10^{-2}
τ_0(a.u.)	2.5×10^2	9.8×10^3
τ(a.u.)	5.0×10^2	1.5×10^3
ω(a.u.)	0.02	0.17
c(a.u.)	-1.0×10^{-4}	1.0×10^{-4}

The optimal pulse shape is obtained employing a genetic algorithm using as fitness function the equation eq. (3.21).

Results and discussion

In this section we discuss the results obtained for the the propagation of the nuclear wavepackets computed using midpoint rule combined with symmetric Strang splitting. We computed the free evolution of the wavepacket, fig. 3.7, as a reference for comparison with the dynamics of the wavepacket when it is driven by the optimal pulse, fig. 3.11.

The free evolution of the wavepacket, fig. 3.7, shows the projection on the isomerization coordinate, φ, of the wavepacket in the panels A and C, and the projection on the coupling coordinate, q, in the panels B an D. The evolution starts with a *cis*-wavepacket centered at $q = 0$ with zero momentum in the excited state, fig. 3.7C-D. For times between 25 fs and 80 fs approximately, 50% of the initial *cis*-wavepacket is distributed as follows: 24% the *trans*-excited, 16% at the *cis*-ground, and a 10% at the *trans*-ground configurations of the PES; been the latter the maximum *trans*-yield that can be achieved from the free evolution of the wavepacket.

While the the torsional component of the wavepacket, fig. 3.7C, reach the conical intersection between 50 fs and 100 fs, the maximum amplitude of

the coupling mode for the excited state, fig. 3.7D, is reached at approximately 120 fs and for this time the yield of the *cis*-configuration of the ground state is minimum. This means that the torsional and coupling components of the wavepacket are out of synchrony.

It is important to remark, that at 120 fs the relaxation via internal conversion is maximum showing that the strength of the relaxation via internal conversion is correlated to the amplitude of oscillation of the coupling mode on the ground and excited PESs.

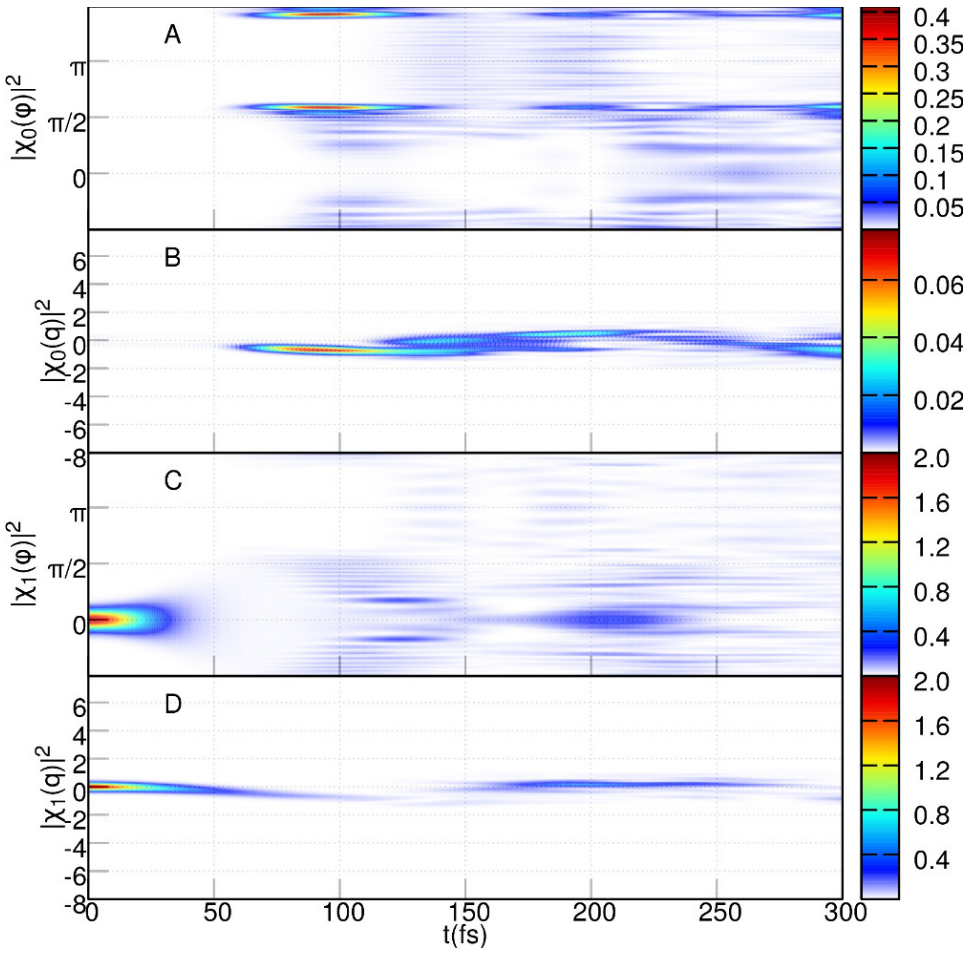

Figure 3.7: *Free evolution of the wavepacket on the ground (A and B), and excited (C and D) PESs. Panels A and C show the projection on the reaction coordinate, φ. Panels B and D show the projection on the coupling coordinate, q.*

The AOPS+GA was performed using 6 LCPs as basis set, evolving the genetic algorithm during 30 generations, with 16 individuals each. The optimal pulse shape is presented in fig. 3.8. It is accomplished by six LCPs: the first centered at $\tau_0 = 99.3$ fs and $\omega_0 = 0.1$ au ($\lambda = 455.6$ nm), the second at $\tau_0 = 131.3$ fs and $\omega_0 = 0.14$ au ($\lambda = 325.5$ nm), the third at $\tau_0 = 159.9$ fs and $\omega_0 = 0.01$ au ($\lambda = 4.556 \times 10^3$ nm), the fourth at $\tau_0 = 170.3$ fs and $\omega_0 = 0.022$ au ($\lambda = 2.071 \times 10^3$ nm), the fifth at $\tau_0 = 188.4$ fs and $\omega_0 = 0.053$ au ($\lambda = 859.7$ nm) and finally the sixth at $\tau_0 = 235.8$ fs and $\omega_0 = 0.042$ au ($\lambda = 1.085 \times 10^3$ nm). The corresponding power spectrum and Wigner transform of this pulse are presented in figures fig. 3.9 and fig. 3.13 respectively.

Figure 3.11B in combination with fig. 3.13 shows that the first LCP of fig. 3.8 transfers population from the *cis*-component of the initial wavepacket to the coupling mode on the ground state with nonzero amplitude triggering the population transfer from *cis*-excited to *trans*-ground via internal conversion.

Figure 3.11A in combination with fig. 3.13 shows that the second LCP of fig. 3.8 localizes the *cis*- and *trans*-portions of the wavepacket at the bottom of the respective wells of the ground PES.

Figure 3.11B in combination with fig. 3.13 shows that the third LCP of fig. 3.8 attempts to localize the projection on the direction of the coupling mode of the wavepacket to switch off the internal conversion mechanism to stop the lack out of the *trans*-ground population.

Figure 3.11A in combination with fig. 3.13 shows that the fourth and fifth LCPs of fig. 3.8 again attempts to localize the *cis*- and *trans*-portions of the wavepacket at the bottom of the respective wells of the ground PES.

Finally 3.11A in combination with fig. 3.13 shows that the sixth LCP of fig. 3.8 selectively localize the *trans*-component of the wavepacket in the ground state PES.

The synchrony between the maximum amplitude in the coupling mode (approximately at 100 fs in 3.11D) and the biggest amount of population going from *cis*- to *trans*-configuration in both, the ground(fig. 3.11A) and the excited(fig. 3.11C) states, constitutes the main mechanism of control that enables to maximize the yield of the *trans*-photoproduct.

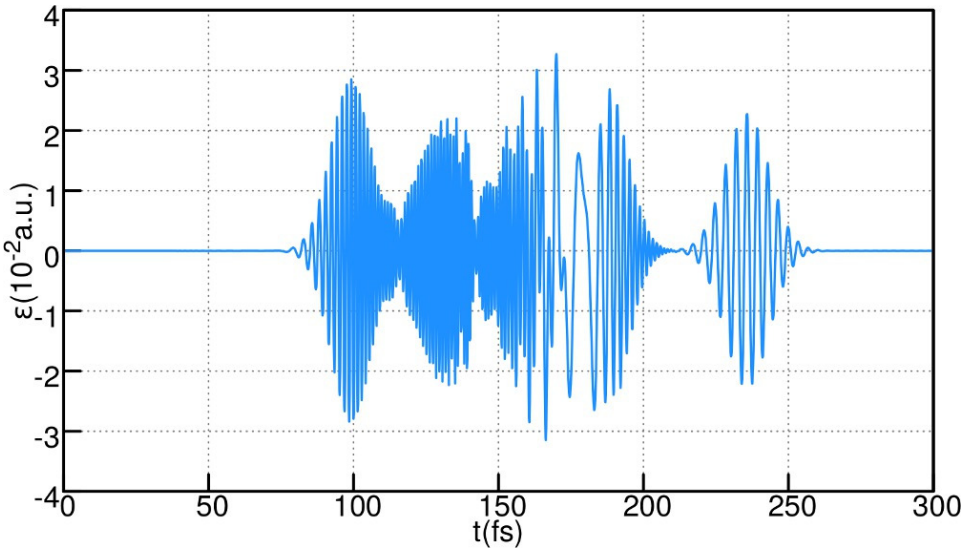

Figure 3.8: *Optimal pulse calculated to maximize J (eq.* (3.21)*).*

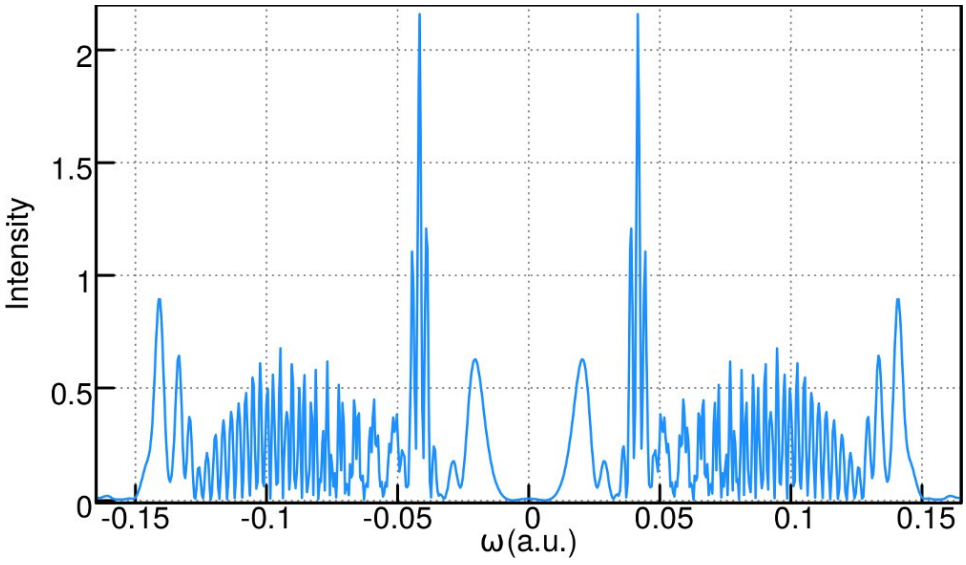

Figure 3.9: *Spectral power of the optimal pulse in fig. 3.8 .*

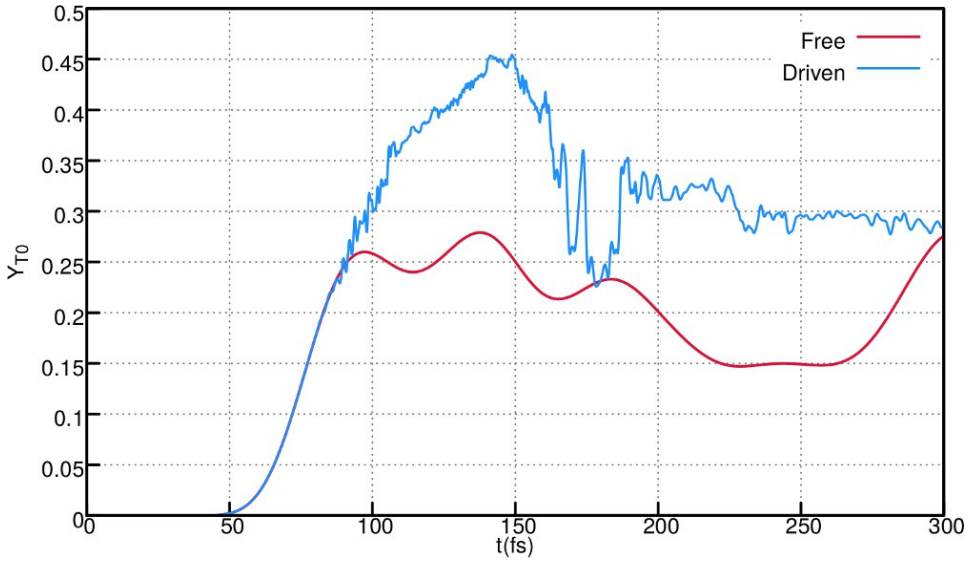

Figure 3.10: *Yields for the* trans*-photoproduct for the free and driven evolutions.*

With the aim of asses the amount of control on the yield of the *trans*-photoproduct on the ground state, we present the ratio $Y_{T1}/(Y_{T2}+Y_{C1}+Y_{C2})$ in fig. 3.10. The increment in the *trans*-yield of the ground PES between 90 and 150 fs approximately, is due to the combined action of the first five LCPs in fig. 3.8. Between 150 and 180 fs, part of the portion of the wavepacket that is on the *trans*-ground well of the PES reaches again the conical intersection and is distributed between the *cis*-excited and *cis*-ground populations via internal conversion. Finally the sixth LCP in fig. 3.8 attempts to deplete the lack of population of the *trans*-ground well localizing the remaining portion of the wavepacket to the bottom of the well producing a peak around 180 fs; this population remains nearly trapped at the *trans*-ground well.

The principal component analysis (PCA) was performed using the decomposition of the decomposition into *cis*- and *trans*-components of the average of the term in the Hamiltonian that couples the molecule to the light. We found that the process $(-0.997, -0.078)$ with weight 0.13 dominates along the optimal path that maximizes eq. (3.21) in comparison with the process $(-0.078, +0.997)$ that have weight 2.01×10^{-3}. The principal effect induced by dominant process is deplete the energy of the *cis*-component

Figure 3.11: *Controlled evolution of the wavepacket on the ground (A and B), and excited (A and B) PESs. Panels A and C show the projection on the reaction coordinate. Panels B and D show the projection on the coupling coordinate.*

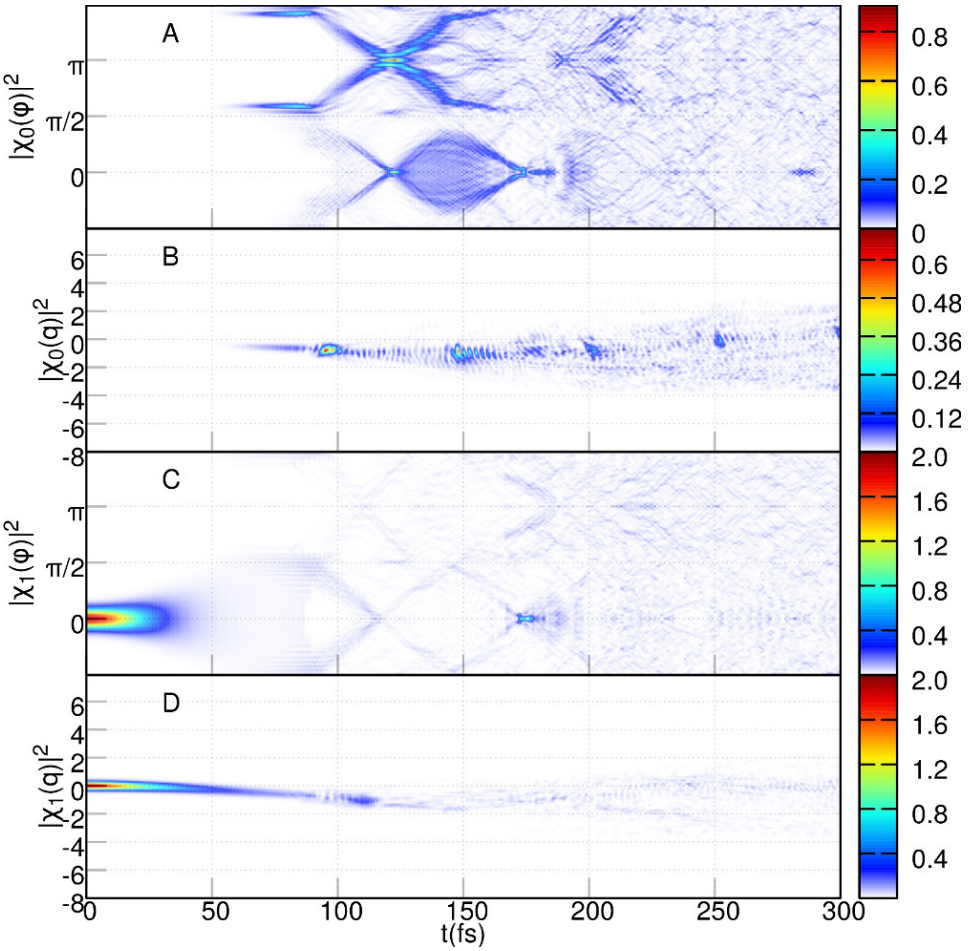

of the wavepacket. To support this result, we computed the decomposition of the light-molecule interaction term for the free(fig. 3.12A) and driven(fig. 3.12B) evolutions of the wavepacket, and effectively the main effect of the interaction with of the optimal pulse ,fig. 3.8, is to reduce the energy content of the *cis*-component of the wavepacket.

The maximum QOC on the *trans*-yield that we get is around 15% that is not so huge, taking into account that our optimal pulse covers wavelengths ranging from infrared to near ultraviolet in about 200 fs. Perhaps, in view

Figure 3.12: *decomposition of the coupling term of the Hamiltonian, eq.* (3.13) *In its* Cis- *and* Trans-*components for the free(A) and driven(B) wavepackets.*

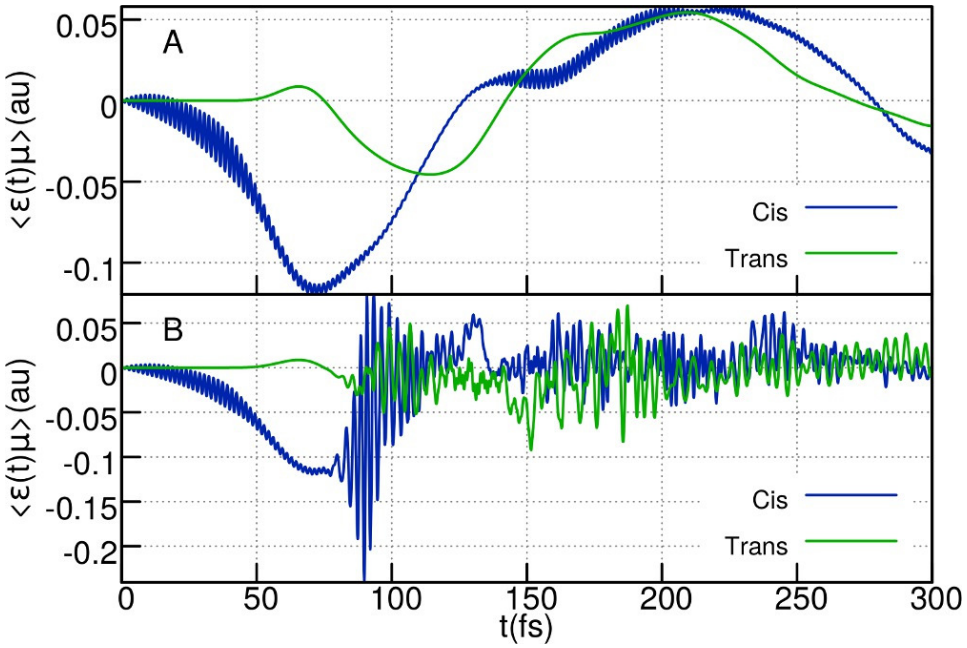

Figure 3.13: *Wigner transform of the optimal pulse-shape assembled with 6 LCPs of figure* 3.8.

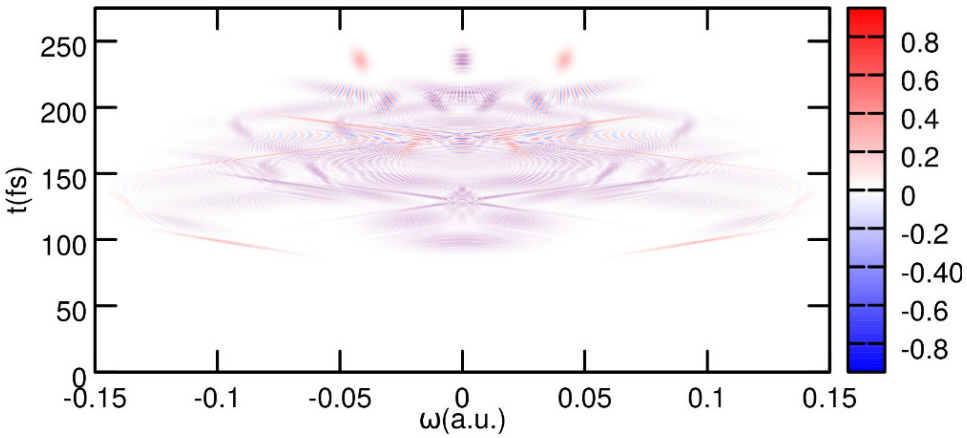

that light of this wavelengths is too abundant in our environment the low-yield mechanisms of isomerization have been favored during the evolution of the mechanism of vision in mammals.

Summary

Controlling the retinal photoisomerization during initial stage of the vision is of current research interest in the field of coherent control. We have used the ratio $Y_{T1}/(Y_{T2} + Y_{C1} + Y_{C2})$ for quantifying the yield of trans-photoproduct in the retinal photoisomerization. We have shown that this ratio can be actively enhanced (increased) with respect to the free dynamics by employing laser pulses obtained by quantum optimal control. Although our method allows the use of an arbitrary amount of LCPs, we employed a minimal basis of 6 LCPs with the aim to obtain realistic pulses that can be tested in the laboratory. The optimal pulse achieved the goal of controlling the amount of trans photo-isomer on the ground electronic surface. Besides the optimal pulse shape and the parameters necessary to build it in the laboratory, we presented a detailed analysis of the pulses and the projections of the wave packet on the relevant coordinates, this allowed us to pinpoint clue aspects of the mechanism of control.

Now that we have developed a methodology to optimize pulse shapes for a given QOC problem, we need additional methodological features enabling us to compute approximated solutions to the TDSE, taking into account the full dimensionality of the molecule, such methodological features should be tailored to compute the solutions using modest computational resources. Next section is devoted to introduce pseudo-spectral methodologies to compute the solution of the TDSE for molecules.

PSEUDOSPECTRAL METHOD TO COMPUTE APPROXIMATED SOLUTIONS TO THE TDSE USING TRIMMED VON-NEUMANN LATTICES

In order to formulate our methodology, we will proceed here in the spirit of reference [111] with the difference that our starting point to build up our pseudospectral basis is a von-Neumann lattice (vNL) of coherent states,

eq. (2.111), whose spacing in position and momentum are given as follows:

$$\Delta q_\alpha = \sqrt{\frac{2\pi}{\gamma_{\alpha\alpha} N}} \tag{3.27}$$

$$\Delta p_\alpha = \sqrt{\frac{2\pi\gamma_{\alpha\alpha}}{N}} \tag{3.28}$$

In order to achieve modularity in the procedure, we proceed to construct an skeleton of displacements for a trimmed versions of the vNL (TvNL). The listing for the *C++* subroutine that we implemented to achieve this point is presented in listing 3.1, All the implementation of the thesis are based on the *Amadillo* library [112] and the Standard Templates Library of *C++*. In the subroutine, s controls the neighborhood order to perform the trim, each displacement should be scaled according to eqs. (3.27) and (3.28).

```
void GBMK::Skeleton(int s, int dim , vec &basis_pnt, vector<vec> &
    bas)
{

  int n=s;
  int d=dim;
  int i,i_max;
  bool cond=false;

  if(d>0){
    const int i_max = sqrt((double)n);
    for(i=-i_max; i<=i_max; i++)
      {
  /*basis_pnt.size() must be equal to de dimensionality of the
    phase space*/
  basis_pnt[basis_pnt.size() - d] = i;
  Skeleton(n - i*i, d - 1, basis_pnt, bas);
      }
  }else{
    bas.push_back(basis_pnt);
  }

}
```

Listing 3.1: *Procedure to build the skeleton for a trimmed vNL*

The number of basis functions in the trimmed vNL per degree of freedom scales as follows:

$$N_s = 2^s \binom{2f}{s} \tag{3.29}$$

Therefore, the total number of basis function in TvNL that takes into account up to s_0 neighbors is given by:

$$N_b = \sum_{s=0}^{s_0} N_s. \tag{3.30}$$

In order to provide an intuitive perspective of the procedure, we will use the case of the spectroscopic Morse potential for the CO molecule [113] to illustrate the rest of the procedure.

Figure 3.14: *TvNL at 8-th order of neighborhood superimposed to the isocontours of the Hamiltonian for the CO molecule for $t = 0$. Based on the harmonic approximation we used $\gamma_{\alpha\alpha} = \sqrt{k_\alpha \mu_\alpha}$ been k_α the constant of elasticity of the PES and μ_α the reduced mass of the corresponding degree of freedom. A density of $N = 1$ coherent states per Planck cell where used to obtain this TvNL.*

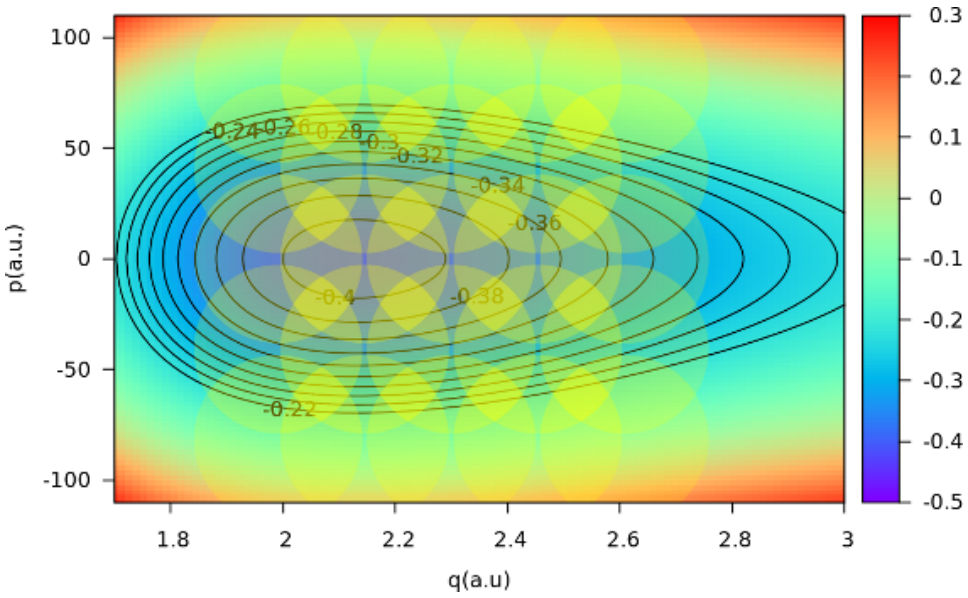

An example of a TvNL is shown in fig. 3.14. The TvNL has been generated around the central basis function. The isocontours of the Hamiltonian corresponds to the allowed solutions of the Hamilton equations of motion, in such a way that the classical evolution of each basis function follows the isocontour on which it started on, in a clockwise sense. The position in phase space of the basis function after half oscillation period(fig. 3.15) and one oscillation(fig. 3.16) period are also shown.

Figure 3.15: *TvNL of fig. 3.14 after half oscillation period, $t = T/2$.*

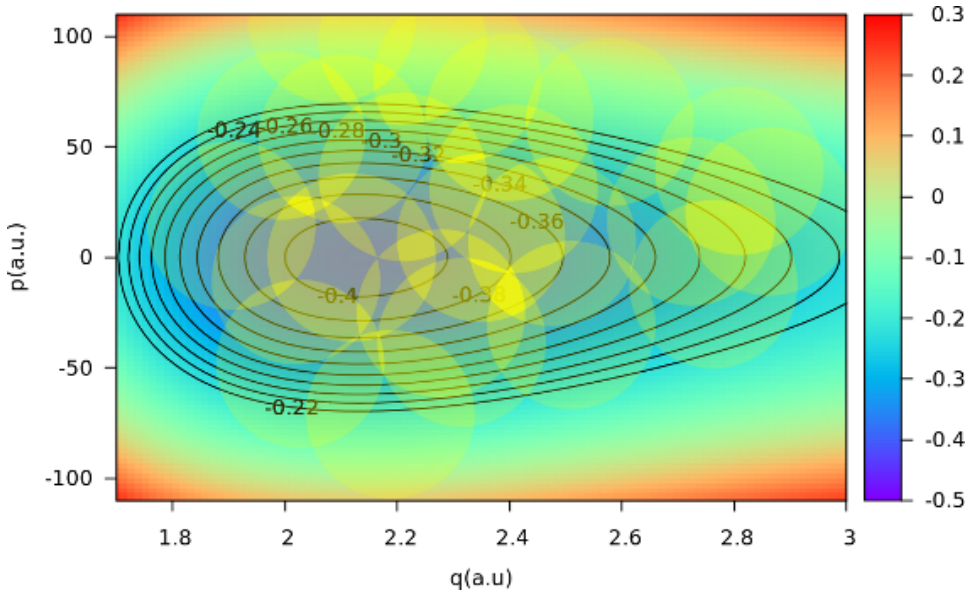

Figure 3.16: *TvNL of fig. 3.14 after one oscillation period, $t = T$.*

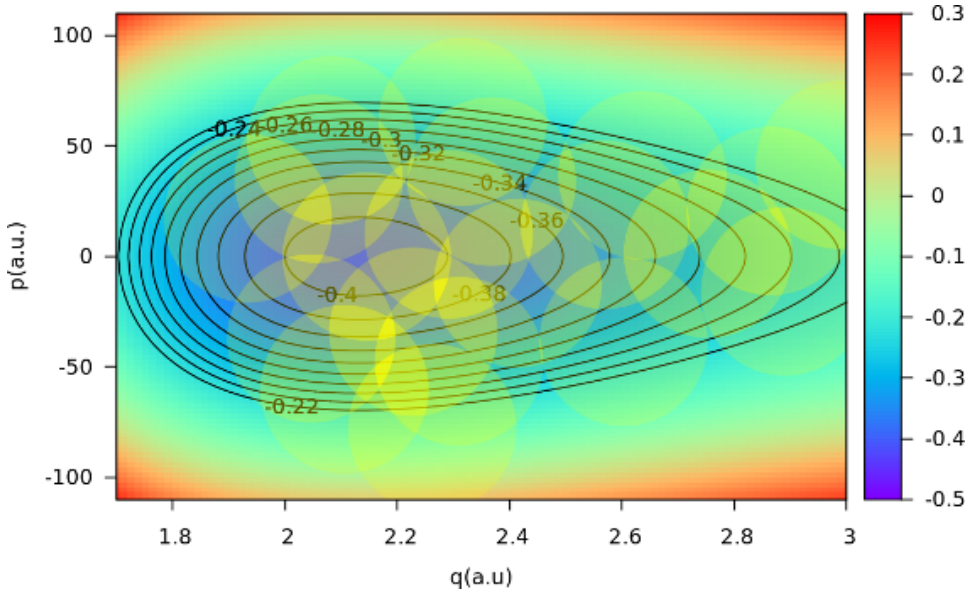

In analogy with the FMS method [49], in order to obtain an approximated solution to the TDSE we use as guess a linear combination of basis function of unknown complex coefficients:

$$|\psi^I(t)\rangle = \sum_{\alpha}^{N_b^I} c_\alpha^I(t)\,|G_\alpha(\mathbf{R}(t))\rangle = c_\alpha^I(t)\,|\alpha^I(t)\rangle\,, \tag{3.31}$$

where uppercase letters, $I, J, K, L, \cdots$, standing for the electronic PESs; and greek letters, $\alpha, \beta, \cdots$, stands for basis functions within a given electronic states . Replacing this ansatz in eqs. (3.2a) and (3.2b), we get the following:

$$\sum_{i}^{N_b^I}\left[\dot{c}_i^I(t)\,|G_i(\mathbf{R}(t))\rangle + c_i^I(t)\frac{\partial}{\partial t}\,|G_i(\mathbf{R}(t))\rangle\right] = \left[-\frac{i}{\hbar}\hat{H} + \sum_L \mathcal{C}_{IL}(\mathbf{R})\right] \times \sum_i^{N_b^I} c_i^I(t)\,|G_i(\mathbf{R}(t))\rangle\,, \tag{3.32}$$

representing the basis set as a vector, $\mathbf{c}$, and projecting the former equation on another arbitrary basis function, we get a closed set of working equations to solve eqs. (3.2a) and (3.2b) on the TvNL:

$$\mathbf{S}^I(t)\dot{\mathbf{c}}^I(t) = \left[-\frac{i}{\hbar}\mathbf{H}(t) + \mathbf{D}^I(t) + \sum_L \mathbf{H}_{IL}\right]\mathbf{c}^I(t) \tag{3.33}$$

$$\dot{\mathbf{S}}^I(t) = \mathbf{D}^{I\dagger}(t) + \mathbf{D}^I(t) \tag{3.34}$$

$$\mathbf{S}^I(t) = \langle\alpha^I|\beta^I\rangle \tag{3.35}$$

$$\mathbf{D}^I(t) = \langle\alpha^I|\dot{\beta}^I\rangle \tag{3.36}$$

$$|\dot{\beta}^I(t)\rangle = \left[\dot{\mathbf{Q}}_\beta^I(t)\cdot\gamma\cdot(\mathbf{q}-\mathbf{Q}_\beta^I(t)) + \frac{i}{\hbar}\left(\dot{\mathbf{P}}_\beta^I\cdot(\mathbf{q}-\mathbf{Q}_\beta^I(t)) - \mathbf{P}_\beta^I(t)\cdot\dot{\mathbf{Q}}_\beta^I(t)\right)\right. \tag{3.37}$$

$$\left. + i\dot{\mathbf{P}}_\beta^I(t)\cdot\mathbf{Q}_\beta^I(t) + i\dot{\mathbf{Q}}_\beta^I(t)\cdot\mathbf{P}_\beta^I(t)\right]|\beta^I\rangle\,. \tag{3.38}$$

$$\dot{\mathbf{Q}}_\beta^I(t) = \frac{\mathbf{P}_\beta^I(t)}{\mu_\beta} \tag{3.39}$$

$$\dot{\mathbf{P}}_\beta^I(t) = -\frac{\partial E_I}{\partial \mathbf{Q}_\beta^I} \tag{3.40}$$

Here the $\mathbf{D^I}$ as well as $\mathbf{H}_{IL}$ are often called nonadiabatic couplings(NAC), therefore for clarity we will reserve the name nonadiabatic coupling for the

$\mathbf{H}_{IL}$ and call dynamical couplings (DC) the $\mathbf{D}^{\mathbf{I}}$.

As it is common to all pseudospectral methods, in order to solve the TDSE eq. (3.33), we have to compute all the matrix elements. In our experience the easy way to compute the required integrals consist on use the following identity derived from the functional dependence of the basis function on $\mathbf{Q}$ and $\mathbf{q}$:

$$\begin{aligned}\langle q|\gamma,Q,P\rangle &= \left(\frac{det\gamma}{\pi^D}\right)\exp\left(i\mathbf{P}\cdot\ (\mathbf{q}-\mathbf{Q})/\hbar\ -(\mathbf{q}-\mathbf{Q})\cdot\gamma\cdot(\mathbf{q}-\mathbf{Q})/2\right)\\ \frac{\partial\langle q|\gamma,Q,P\rangle}{\partial\mathbf{q}} &= -\frac{\partial\langle q|\gamma,Q,P\rangle}{\partial\mathbf{Q}}.\end{aligned} \tag{3.41}$$

The property eq. (3.41) enables us to derive the matrix element of the kinetic energy from the overlap matrix element. Within the harmonic approximation, the property eq. (3.41) enables us to derive the formulas for all the needed matrix elements. The results can be summarized as follows:

Introducing the short hand notation:

$$g = \mathbb{1}\mu^{-1} \tag{3.42}$$
$$M_p = (\gamma_\alpha+\gamma_\beta)^{-1} \tag{3.43}$$
$$M_q = \gamma_\alpha M_p \gamma_\beta \tag{3.44}$$
$$\mathbf{Q}_{\alpha\beta} = M_p(\gamma_\alpha\mathbf{q}_\alpha+\gamma_\beta\mathbf{q}_\beta) \tag{3.45}$$
$$\mathbf{P}_{\alpha\beta} = M_p(\gamma_\beta\mathbf{p}_\alpha+\gamma_\alpha\mathbf{p}_\beta) \tag{3.46}$$
$$\mathbf{\Delta}q = \mathbf{q}_\alpha-\mathbf{q}_\beta \tag{3.47}$$
$$\mathbf{\Delta}p = \mathbf{p}_\alpha-\mathbf{p}_\beta \tag{3.48}$$
$$\mathbf{p}_{eff} = \mathbf{P}_{\alpha\beta}+i\hbar M_q\mathbf{\Delta}q \tag{3.49}$$

The set of closed expression for the matrix elements are:

$$\begin{aligned}S_{\alpha\beta} = \left[\frac{4\det(\gamma_\alpha\gamma_\beta)}{\det(\gamma_\alpha+\gamma_\beta)^2}\right]^{1/4}\exp\left(-\frac{1}{2}\left(\mathbf{\Delta}q\cdot M_q\cdot\mathbf{\Delta}q+\frac{1}{\hbar^2}\mathbf{\Delta}p\cdot M_p\cdot\mathbf{\Delta}p\right)\right.\\ \left.+\frac{i}{\hbar}\mathbf{\Delta}q\cdot M_p\cdot\mathbf{P}_{\alpha\beta}-\frac{i}{2\hbar}(\mathbf{q}_\alpha\cdot\mathbf{p}_\alpha-\mathbf{q}_\beta\cdot\mathbf{p}_\beta)\right)\end{aligned} \tag{3.50}$$

Here the chain rule, $\frac{\partial}{\partial t} f(q(t)) = \frac{\partial f}{\partial q}\dot{q}$, where used.

$$D_{\alpha\beta} = \Bigg(\dot{\mathbf{p}}_\beta(t) \cdot (\frac{1}{\hbar^2} M_p \cdot (\mathbf{\Delta} p + \frac{i}{\hbar}\gamma_\alpha \mathbf{\Delta} q) + \frac{i}{2\hbar}\mathbf{p}_\beta) \\ \dot{\mathbf{q}}_\beta(t) \cdot (M_q \cdot \mathbf{\Delta} q - \frac{i}{\hbar}\mathbf{P}_{\alpha\beta} + \frac{i}{2\hbar}\mathbf{q}_\beta) \Bigg) S_{\alpha\beta} \tag{3.51}$$

$$T_{\alpha\beta} = \frac{1}{2} \left(\mathbf{p}_{eff} \cdot g \cdot \mathbf{p}_{eff} + \hbar^2 Tr(M_q \cdot g) \right) S_{\alpha\beta} \tag{3.52}$$

$$V_{\alpha\beta} = \left(V(\mathbf{Q}_{\alpha\beta}) + \frac{i}{\hbar}\dot{\mathbf{p}}_\beta(t) \cdot M_p \cdot \mathbf{\Delta} p - \frac{1}{2}\mathbf{\Delta} p \cdot M_p \cdot \frac{\partial^2 V}{\partial \mathbf{R}} \, |_{\mathbf{Q}_{\alpha\beta}} \cdot M_p \cdot \mathbf{\Delta} p \right) \tag{3.53}$$

As can be seen from equation 3.53, the potential matrix element is evaluated using Taylor expansion of the potential up to second order. This is compatible with *ab-initio* computation of gradient and Hessian.

Before starting the propagation of the wavepacket according to eqs. (3.2a) and (3.2b), we need to fit the initial condition, the central Gaussian of the tvNL, as a linear combination of the portion of the basis on the electronic state I. To do so, we write the initial wavepacket as an unknown linear combination of basis functions:

$$|\Psi_0\rangle = \sum_\beta c_\beta |\beta\rangle \tag{3.54}$$

and project it on each state of the lattice, this generalizes to a system of equations in unknown coefficients:

$$\langle \alpha | \Psi_0 \rangle = \sum_\beta c_\beta \langle \alpha | \beta \rangle , \tag{3.55}$$

$$\boldsymbol{b} = \boldsymbol{S}\boldsymbol{c}. \tag{3.56}$$

The numerical solution of the former system of equation gives the fitting

coefficients. The error in the fitting is given by:

$$\begin{aligned}\left\|\sum_j c_j\left|\beta_j\right\rangle-\left|\Psi_0\right\rangle\right\|^2 &= \left[\sum_k c_k\left|\beta_k\right\rangle-\left|\Psi_0\right\rangle\right]^\dagger\left[\sum_k c_j\left|\beta_j\right\rangle-\left|\Psi_0\right\rangle\right] \\ &= \sum_{jk} c_k^\star c_j\left\langle\beta_k|\beta_j\right\rangle-\sum_k c_k^\star\left\langle\beta_k|\Psi_0\right\rangle-\sum_j c_j\left\langle\Psi_0|\beta_j\right\rangle+1 \\ &= \boldsymbol{c}^\dagger\boldsymbol{S}\boldsymbol{c}-\boldsymbol{c}^\dagger\boldsymbol{b}-\boldsymbol{b}^\dagger\boldsymbol{c}+1\end{aligned} \tag{3.57}$$

to illustrate the fitting we will show it in one dimension. The spacing of the grid in phase space was chosen as:

$$\Delta_q=\sqrt{\frac{2\pi}{N\gamma}} \tag{3.58}$$

$$\Delta_p=\hbar\sqrt{\frac{2\pi\gamma}{N}} \tag{3.59}$$

$$\Delta_q\Delta_p=\frac{h}{N} \tag{3.60}$$

where N is the number of coherent states per Planck's cell. To attain an extra degree of freedom in the choice of the shells, we will allow the functions in the shell to squeeze equally with respect the initial Gaussian.

In order to do an analysis of the performance of the fitting respect to the amount of squeezing in the basis, we parametrized both, the exponent of the initial Gaussian and those of the basis in units of γ_0 that can be taken from the local harmonic approximation to the potential at hand: $\gamma_0=m\omega$.

Fixing the exponent of the initial Gaussian at $1.5\gamma_0$, fig. 3.17 presents the error in the fitting, eq. (3.58), as a function of the density of coherent states per Planck's cell $N_\hbar$ and the squeezing of the basis, employing exponents between $0.01\gamma_0$ and $7.0\gamma_0$.

Figure 3.17: *Error in the fitting for $\gamma = 1.5\gamma_0$, in log_{10} scale as a function of the squeezing and the density of states for aggregation of shells of 1-th(A), 2-nd(B),3-rd(C), 4-th(D), 5-th(E), 6-th(F) neighboring orders. When the initial state is one of the basis functions, the fitting can be performed within machine accuracy.*

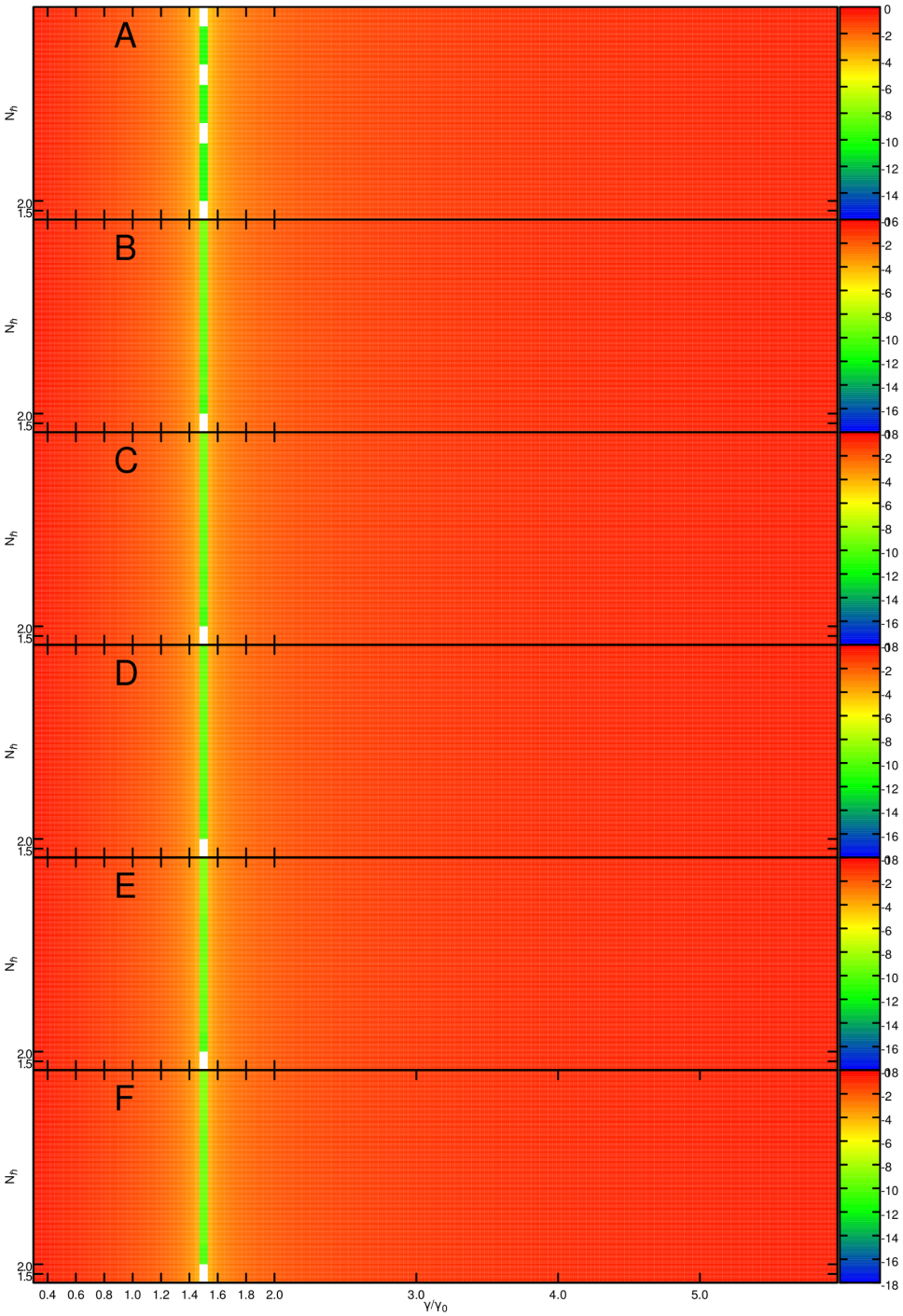

Is very important to have a good initial fitting of the initial, fig. 3.17, state because the error in the fitting accumulates for each propagation step depleting the accuracy of the solution to the TDSE. From a mathematical point of view, the errors in fig. 3.17 when the initial Gaussian is not one of the basis function are due to loss of accuracy in resolve the identity due to use a TvNL.

With the fitting available we get ready to start propagating the eq. (3.33) for the basis functions on each electronic state. Modularity is achieved using these methodology, because to build up the basis, we can employ TvNL of different order of truncation centered on the initial wavepacket, eq. (3.54), and TvNL centered at regions of the PESs that present Franck-Condon or diabatic activity for the problem at hand. To keep under control the computational expenses in the case of on-the-fly computations, use initially the lower neighboring aggregation orders in the construction of TvNL and increase the order as needed.

In order to solve the TDSE, eq. (3.33), we integrated directly this equation using the quantum-classical embedding procedure that is inspired in the one given in reference [50]. The procedure that we implemented is show in algorithm 4.

The problems to compute the inverse of the overlap matrix are well known [114], therefore we workaround that by assuming a least squares approximant [114]. The $\tilde{\mathbf{H}}$ matrix in the step 2 of algorithm 5 corresponds to the solution of the system eq. (3.33) in the least squares sense. We have implemented three methods in order to solve the differential equation in the step 3 of algorithm 5: implicit Euler, fourth order Runge-Kutta and Gear's predictor-corrector method of order 1th to 5th with the aim of switch the electronic integration method at will. A benchmark computation of the methodology is show in fig. 3.18. It shows that the methodology offers a good compromise between performance and accuracy, it is clear that the method is exact only if the exact matrix elements are available for all the terms of the Hamiltonian and the basis set is complete. But the possibility of control the neighboring order of the TvNL combined with the modular distribution of additional TvNLs centered at regions of the PESs that present Franck-Condon or diabatic activity, put the approximate solutions of the nonadiabatic TDSE with the full dimensionality of the molecule within reach.

Algorithm 4 Quantum-Classical embedding procedure to solve eq. (3.33).

Add to the basis set a TvNL of chosen order to fit on it the initial condition
Add to the basis another TvNL in oder to cover zones of the PESs that present Franck-Condon or diabatic activity.
for each nuclear time step: **do**
    $\mathbf{P}^I_\beta = \mathbf{P}^I_\beta + g \cdot \mathbf{F}^I_\beta \frac{\Delta t}{2}$
    Build a copy of $\mathbf{c}$: $\mathbf{c}_0 = \mathbf{c}(t)$
    Initialize the counter of bisections: $p = 1$
    while $\|\mathbf{c}_0 - \mathbf{c}_1\| \geqslant$ threshold: **do**
        $\mathbf{c}_1 = \hat{U}_e(t + \frac{\Delta t}{2^p}, t)\mathbf{c}(t)$
        $p = p + 1$
        $\mathbf{c}(t) = \mathbf{c}_0$
    end while
    for $i_e = 0$ to $i_e = 2^p/2 = \frac{\Delta t}{2}$: **do**
        $\mathbf{c}(t + \frac{\Delta t}{2^p}) = \hat{U}_e(t + \frac{\Delta t}{2^p}, t)\mathbf{c}(t)$
        $t = t + \frac{\Delta t}{2^p}$
    end for
    $\mathbf{Q}^I_\beta = \mathbf{Q}^I_\beta + g \cdot \mathbf{P}^I_\beta \Delta t$
    for $i_e = 0$ to $i_e = 2^p/2 = \frac{\Delta t}{2}$: **do**
        $\mathbf{c}(t + \frac{\Delta t}{2^p}) = \hat{U}_e(t + \frac{\Delta t}{2^p}, t)\mathbf{c}(t)$
        $t = t + \frac{\Delta t}{2^p}$
    end for
    $\mathbf{P}^I_\beta = \mathbf{P}^I_\beta + g \cdot \mathbf{F}^I_\beta \frac{\Delta t}{2}$
end for

Algorithm 5 Quantum propagator $\hat{U}_e(t + \frac{\Delta t}{2^p}, t)$ of algorithm 4.

Build $\mathbf{S}^I$,$\mathbf{H}$,$\mathbf{D}^I$, $\mathbf{H}_{IL}$ for all the electronic states.
Find $\tilde{\mathbf{H}}$: $min \left\| \mathbf{S}^I \tilde{\mathbf{H}} - \left[-\frac{i}{\hbar}\mathbf{H}(t) + \mathbf{D}^I(t) + \sum_L \mathbf{H}_{IL} \right] \right\|$
Integrate $\dot{\mathbf{c}}(t) = \tilde{\mathbf{H}}\mathbf{c}(t)$ from t to $t + \frac{\Delta t}{2^p}$.

Figure 3.18: *Benchmark of the quantum-classical embedding procedure algorithm 4, we used for the propagation the 8th order TvNL in fig. 3.14 that corresponds to 25 classical trajectories. To test the performance of the method, we propagate the same initial condition using the Split-operator algorithm, algorithm 1, on a grid with 256 points, and compute the overlap between the split-operator($\pi_{sp}(r)$) and pseudospectral($\pi_{gbm}(r)$) wavepackets in panel A. we employed the same time step, $\Delta t = \frac{T}{100}$, in both propagations.*

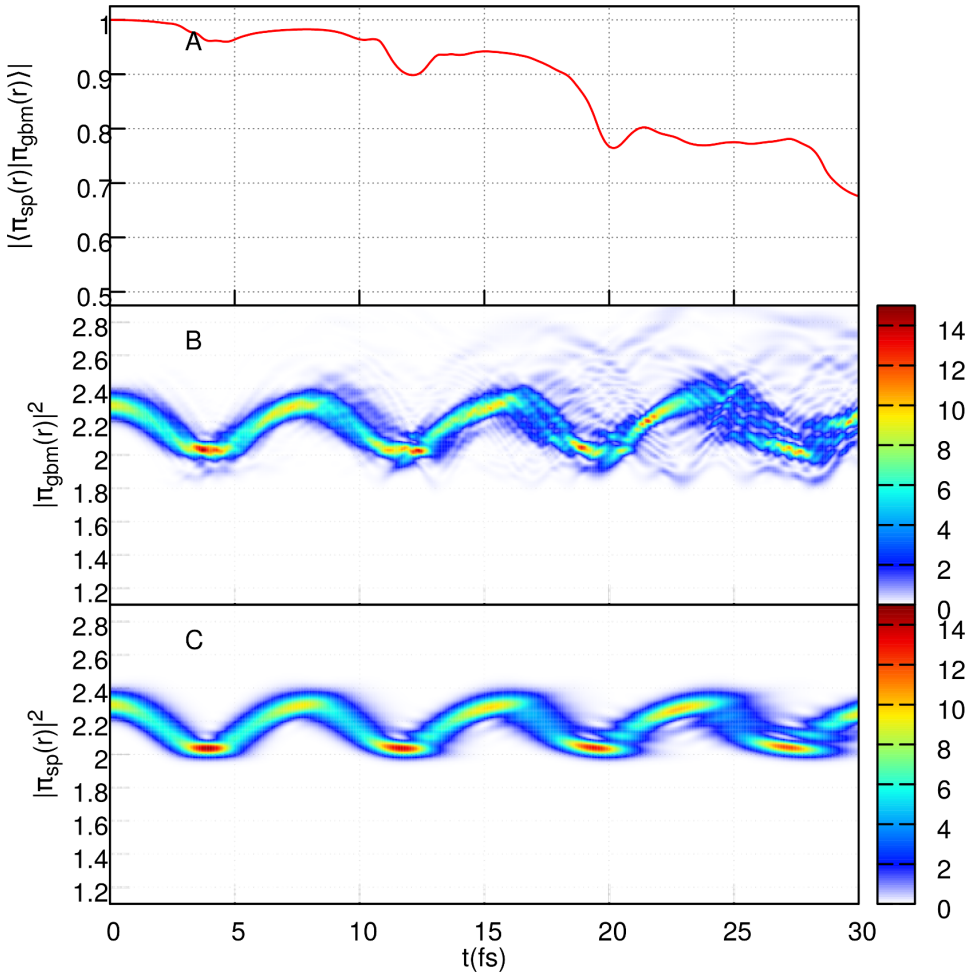

Application to linear and nonlinear spectroscopies

A vibronic coupling Hamiltonian model where developed for the Pyrazine molecule in reference [74]. The model describes the ground state, S_0, the first excited state, $S_1(n\pi^\star)$, and the second excited state, $S_2(\pi\pi^\star)$, of Pyrazine at the CASSCF level of theory. This model describes the vibrational motion of the molecule in normal mode coordinates, withing the subspace of the five totally symmetric normal modes $\nu_1, \nu_2, \nu_{6a}, \nu_{8a}, \nu_{9a}$ and the $S1-S2$ coupling mode ν_{10a} that is of B_{1g} Symmetry, and therefore, it is decoupled of the other modes. The description of the vibrational motion of the molecule is given by the Hamiltonian

$$h_k = h_0 + E_k + \sum_i \kappa_i^{(k)} Q_i + \sum_{i,j} \gamma_{i,j}^{(k)} Q_i Q_j \tag{3.61}$$

$$h_0 = \sum_i \left(-\frac{1}{2m_i} \frac{\partial}{\partial Q_i^2} + \frac{1}{2} k_i Q_i^2 \right) \tag{3.62}$$

where the parameters in the Hamiltonian are defined as:

$$\kappa_i^{(k)} = \left(\frac{\partial E}{\partial Q_i} \right)_0 \tag{3.63}$$

corresponding to the numerical gradient of the $k-$th excitation energy centered in the equilibrium geometry. This terms are nonzero only for the five totally symmetric modes.

$$\gamma_{i,j}^{(k)} = \frac{1}{2} \left(\frac{\partial^2 E_k}{\partial Q_i \partial Q_j} \right)_0 \tag{3.64}$$

Corresponding to the numerical Hessian of the $k-$th excitation energy centered in the equilibrium geometry. Its off-diagonal terms originate the so called Dushinsky rotation of normal mode coordinates [115], and are nonzero only for modes of the same symmetry in the D_{2h} point group of the molecule. Finally E_k correspond to vertical excitation energies.

A four dimensional model of the molecule Pyrazine is considered here. The degrees of freedom that we will consider are: $Q_1 = \nu_1$, $Q_2 = \nu_{6a}$, $Q_3 = \nu_{9a}$ and $Q_4 = \nu_{10a}$. The parameters of the Hamiltonian where computed at the state averaged CASSCF level of theory, employing a DZP basis set using

MOLPRO. Atomic units will be used to list the parameters:

$$k = \begin{pmatrix} 4.884\,39 \times 10^{-3} \\ 3.061\,86 \times 10^{-3} \\ 6.137\,38 \times 10^{-3} \\ 4.419\,65 \times 10^{-3} \end{pmatrix} \tag{3.65}$$

$$m = \begin{pmatrix} 204.734 \\ 326.599 \\ 162.936 \\ 226.263 \end{pmatrix} \tag{3.66}$$

$$E = \begin{pmatrix} 0.00000 \\ 0.144792 \\ 0.179704 \end{pmatrix} \tag{3.67}$$

$$\gamma^{(0)} = 0 \tag{3.68}$$

$$\gamma^{(1)} = \begin{pmatrix} -1.690\,47 \times 10^{-5} & -5.843\,14 \times 10^{-5} & 4.40991894e^{-6} & 0. \\ -5.843\,14 \times 10^{-5} & 7.055\,87 \times 10^{-5} & 4.299\,67 \times 10^{-5} & 0. \\ 4.40991894e^{-6} & 4.299\,67 \times 10^{-5} & -1.370\,75 \times 10^{-4} & 0. \\ 0. & 0. & 0. & -6.614\,88 \times 10^{-4} \end{pmatrix} \tag{3.69}$$

$$\gamma^{(2)} = \begin{pmatrix} 1.014\,28 \times 10^{-4} & -1.605\,95 \times 10^{-4} & 3.674\,93 \times 10^{-5} & 0. \\ -1.605\,95 \times 10^{-4} & -2.473\,23 \times 10^{-4} & 7.607\,11 \times 10^{-5} & 0. \\ 3.674\,93 \times 10^{-5} & 7.607\,11 \times 10^{-5} & 9.812\,07 \times 10^{-5} & 0. \\ 0. & 0. & 0. & -6.614\,88 \times 10^{-4} \end{pmatrix} \tag{3.70}$$

$$\kappa^{(0,1,2)} = \begin{pmatrix} 0. & -2.969\,35 \times 10^{-3} & -8.2098 \times 10^{-3} \\ 0. & -3.447\,09 \times 10^{-3} & 3.781\,51 \times 10^{-3} \\ 0. & 5.552\,82 \times 10^{-3} & 1.870\,54 \times 10^{-3} \\ 0. & 0. & 0. \end{pmatrix} \tag{3.71}$$

Introducing the transition-dipole-moment:

$$\hat{\mu}_{fi} = |\Psi_f\rangle\, \hat{e} \cdot \boldsymbol{\mu}_{fi}(\mathbf{R})\, \langle\Psi_i| \tag{3.72}$$

where $\hat{e}$ is a unitary vector in the direction of the external field, the transition-dipole-moment accounts for transitions from one initial, Ψ_i, to a final, Ψ_f, PESs induced by the external field. If the dependence of the transition-dipole-moment function on the molecular coordinates is weak, as in the present case, Condon approximation can be used, $\boldsymbol{\mu}_{fi}(\mathbf{R}) \approx \boldsymbol{\mu}_{fi}$. Defining the time-correlation function:

$$\Phi_v^{kk'}(t) = \left\langle v \right| \hat{\mu}_{0k} e^{-iHt} \hat{\mu}_{k'0} \left| 0 \right\rangle . \tag{3.73}$$

The absorption cross section can be computed as follows:

$$\sigma_A(\omega) = \frac{2\pi}{3}\alpha\omega 2\Re\mathcal{F}\left[\sum_k \Phi_v^{kk'}(t)\right] \tag{3.74}$$

where α is the fine structure constant, in atomic units $\alpha = \frac{1}{137}$. The computation of the time-correlation function using the pseudospectral methodology corresponds to propagate the wavepacket on the k' electronic PES and compute its overlap with a copy of the initial state that remains frozen at the PES k:

$$\Phi_v^{kk'}(t) = \mathbf{c}(0)\cdot\mathbf{S}_{0t}\cdot\mathbf{c}(t) \tag{3.75}$$

where the overlap matrix $(0)\cdot\mathbf{S}_{0t}$ plays the role of the metric matrix nonorthogonal basis, whose matrix elements can be computed using eq. (3.50) and involves the basis functions of the wavepacket and the basis function of the copy of the wavepacket remaining frozen at $t = 0$.

Is remarkable the resemblance between eq. (3.73) and eq. (2.40), what means that the optimal pulse shape to maximize the electronic transition $k \to k'$ within TDPT result from an intermediate step in the computation of the absorption spectrum. This idea remains valid in the case of nonlinear spectra computations.

Due to the finite time propagation, the computation of the absorption spectrum using eq. (3.73) is equivalent to convolute the correlation function with an step function producing undesired negative values in the spectrum. to workaround this difficulty we convolute the correlation function with a

To test the pseudospectral approach to the dynamics of the Pyrazine molecule, we used the quantum/classical embedding algorithm , algorithm 5, to compute the correlation function, eq. (3.73), and the resulting spectrum, using a basis set accomplished by TvNL of first order of neighborhood around the minimum of the S_0 PES and a copy of it placed at the $S_2(\pi\pi^\star)$ PES. that corresponds to the minimal level of description.

A continuation in fig. 3.19 we will present results for the adsorption spectrum of the Pyrazine molecule. The diffusion of the peaks when we

move from $\lambda = 0$ to $\lambda = 0.1676(eV)$ is a signature of the $S_1(n\pi^\star) \rightarrow S_2(\pi\pi^\star)$ coupling that induces relaxation via internal conversion. It is expected that the description of the relaxation improves as the neighboring order of the TvNL increases but we are interested to remain within a minimal basis size in order to show the performance of the method.

Figure 3.19: *Computation of $S_2(\pi\pi^\star)$ the absorption spectrum of the Pyrazine molecule employing the first shell corresponding to 34 classical trajectories. Although the small number of trajectories, adiabatic effects can be observed in the diffusion of the peaks without appeal to phenomenological broadening.*

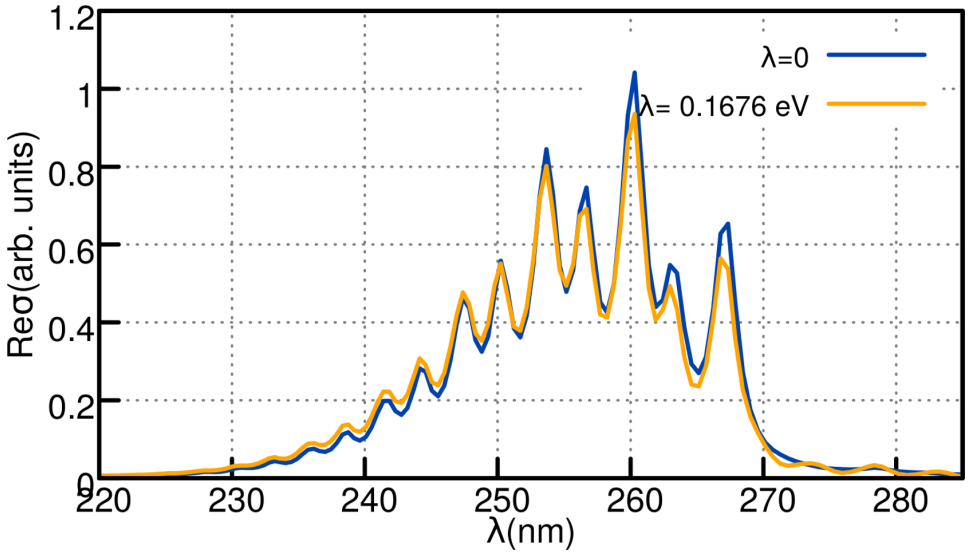

Figure 3.20: *Computation of the cross correlation function of Pyrazine molecule employing the first shell corresponding to 34 classical trajectories for four degrees of freedom. The pulse shape in the figure correspond to the solution of the QOC problem of maximize the the $S_0 \rightarrow S_2(\pi\pi^\star)$ transition in the molecule Pyrazine.*

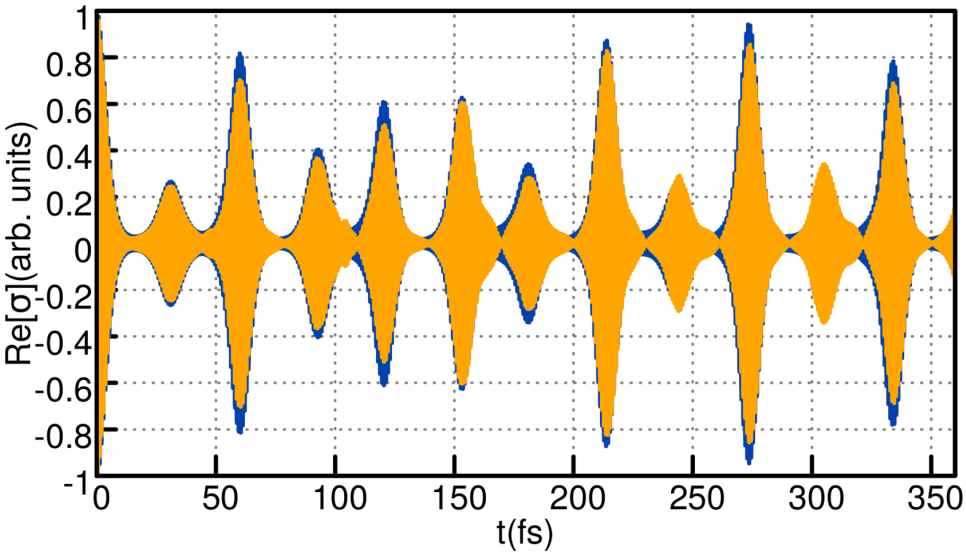

ON-THE-FLY MOLECULAR DYNAMICS USING THE PSEUDOSPECTRAL METHOD.

In order to apply the pseudospectral method in section 3.2 to the study of on-the-fly nonadiabatic molecular dynamics we need a suitable system of coordinates in which to build up the TvNL. Normal-mode coordinate have a long tradition helping to chemists and chemical-physicist in the analysis of molecular motions and therefore is the system of coordinates of choice in order to construct the TvNL. On the other side, cartesian coordinate help us to represent molecular geometries in a human readable way, therefore, our approach tho the initial setup of the pseudospectral basis is build the TvNL in normal coordinates and transform it to cartesian coordinates that is the systems in which the time-evolution will be computed.

In order to do the formal derivation of the matrix, $\mathbf{U}$, that transform the molecular structure from normal to cartesian coordinates we proceed as follows. Following [116], we consider the quantities involved in a conju-

gate gradient procedure of optimization of a given molecular structure. In this procedure the ground state energy is a function of the molecular geometry, been $\mathbf{R}_i = (R_{i_x}, R_{i_y}, R_{i_z})$ the cartesian coordinates the i-th atom in the structure, *e.g.* $i = \{C_1, C_2, H_3, H_4, H_5, H_6\}$ in the case of the ethylene molecule. The aim of the algorithm is construct a series of steps leading to a stationary point of the energy, if we consider the gradient $\mathbf{g}_i = \frac{\partial E_0}{\partial \mathbf{R}_i}$, the stationarity condition is reached if $\mathbf{g} = \sum_i \mathbf{g}_i = 0$.

The information for the energies, E^a, and gradients, $\mathbf{g}^a$, the structures, $\mathbf{R}^a$, as well as an approximated Hessian matrix, $\mathbf{F}_{ij} = \frac{\partial^2 E^a}{\partial \mathbf{R}_i \partial \mathbf{R}_j}$, is collected along the iterations of the conjugate gradient algorithm. writing the new, eq. (3.77), and old, eq. (3.78), estimates of the Hessian as:

$$\tilde{\mathbf{r}}_i^a = (\mathbf{R}_i^a - \mathbf{R}_i^0) - \sum_{b=1}^{a-1} \mathbf{r}_i^b \sum_j (\mathbf{R}_j^a - \mathbf{R}_j^0) \cdot \mathbf{r}_j^b \tag{3.76}$$

$$\mathbf{k}_n^{ab} = \frac{\sum_i (g_i^a - g_i^0) \cdot \mathbf{r}_i^b - \sum_{c=1}^{a-1} \mathbf{k}_n^{cb} \sum_i (\mathbf{R}_i^a - \mathbf{R}_i^0) \cdot \mathbf{r}_i^c}{\sum_l (\mathbf{R}_l^a - \mathbf{R}_l^0) \cdot \mathbf{r}_l^a} \tag{3.77}$$

$$\mathbf{k}_0^{ab} = \mathbf{k}_0^{ab} = \sum_{ij} \mathbf{r}_i^a \cdot F_{ij} \cdot \mathbf{r}_j^b. \tag{3.78}$$

The approximations to the matrix of constants of force is given by:

$$\mathbf{F}_{ij}^{new} = \mathbf{F}_{ij}^{old} + \sum_{b \geqslant a}^{m} (\mathbf{k}_n^{ab} - \mathbf{k}_0^{ab}) \left[\mathbf{r}_i^a \cdot \mathbf{r}_j^b + (1 - \delta_{ab}) \mathbf{r}_i^a \cdot \mathbf{r}_j^b \right] \tag{3.79}$$

As long as the number of iterations of the conjugated gradient algorithm increases, increases the projection of the Schmidt orthogonalization, eq. (3.76) along the normal coordinates. From an intuitive point of view, it is expected the the largest configurational changes along the conjugate gradient optimization, should be along the so called essential modes [117], in terms of which the main spectral features can be described.

Is of common use that the the matrix of constants of force is computed in terms of mass weighted coordinates in the electronic structure packages, dividing all f the elements in each row and in each column by the square root of the appropriate mass in atomic mass units. The normal mode coordinates and its associated frequencies are obtained as eigenvectors and eigenvalues of the matrix of constants of force. In virtue of Noether's theorem, [61], because of the conservation of the linear momentum there are

3 constants of motion, and because of the conservation of the angular momentum, there are another 3 constants of motion or 2 in case of a linear molecule. Since rotations and translations have not been separated yet, six eigenvalues must be pretty close to zero. projecting out this part of the spectral decomposition of the matrix of constants of force can be achieved as follows: if the orthogonal set of vector that represent translations and rotation is $\mathbf{Z}$ then the projection matrix is given by:

$$P_{ij} = -\sum_k Z_{ik}Z_{jk}, \text{ if } i \neq j \; P_{ii} = 1 - \sum_k Z_{ik}Z_{ik}. \tag{3.80}$$

and the projected matrix of constants of force is given by:

$$\mathbf{F}_{TR} = \mathbf{PFP}^t \tag{3.81}$$

The matrix that transform from normal to cartesian coordinates, $\mathbf{U}$, is given by the eigendecomposition of $\mathbf{F}_{TR}$ as follows:

$$\mathbf{UF}_{TR} = \Omega\mathbf{U}. \tag{3.82}$$

In the case of the ethylene molecule there are $3 \times 6 - 6 = 12$ degrees of freedom after that the constants of motion has been removed, the phase space for the molecule is therefore of 24 dimensions. We used the listing in 3.1 in oder to generate the corresponding TvNL, the result is presented in fig. 3.21.

In order to compute the dynamics on-the-fly we need the excited state energies, the gradients of the excited states, and the nonadiabatic coupling matrix element. All this quantities are efficiently computed by using the multi-configurational self-consistent-field response theory [55]. In order to improve the computational efficiency, this methodology was implemented in the computational package GAMESS using iterative method in the Krylov subspace [118].

The algorithmic approach to the propagation of the wavepacket should be modified in order to minimize the number on-the-fly computations as in algorithm 6.

the results shown in fig. 3.23 were computed at the sate averaged complete active space level of theory using 3 states with four active orbital for fur electrons. The flowchart that we followed to perform the computation is shown in section 3.3, it is has been automatized within *HELIOS*.

Figure 3.21: *TvNL fo the ethylene, The figure is accomplished by the 73 possible unitary displacements of the structure of the molecule in phase space, This is the TvNL is analogous to the TvNL presented in fig. 3.14 for the CO molecule, with the difference that in the present case we used first order in neighborhood. We used this module twice in the initial setup of the pseudospectral method for the the $\pi \rightarrow \pi^{\star}$ internal conversion, one unpopulated, at the π electronic state and the other at the $\pi^{\star}$ electronic state.*

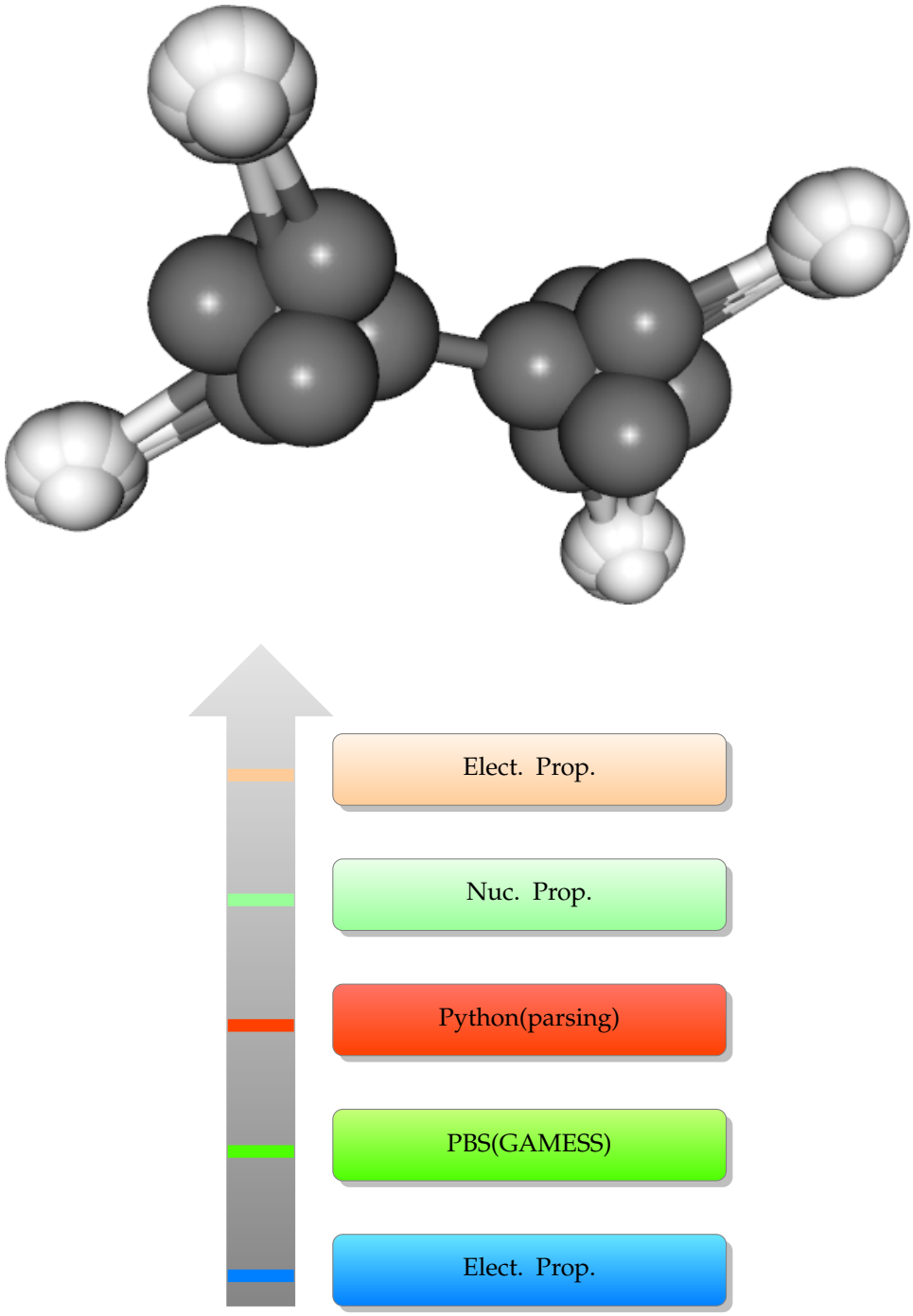

Algorithm 6 Quantum-Classical embedding procedure to solve eq. (3.33) using on-the-fly computations.

Add to the basis set a TvNL of first order in the $\pi^\star$ electronic state
Add to the basis another TvNL of first order in the π electronic state.
for each nuclear time step: **do**
    Build a copy of $\mathbf{c}$: $\mathbf{c}_0 = \mathbf{c}(t)$
    Initialize the counter of bisections: $p = 1$
    while $\|\mathbf{c}_0 - \mathbf{c}_1\| \geqslant$ threshold: **do**
        $\mathbf{c}_1 = \hat{U}_e(t + \frac{\Delta t}{2^p}, t)\mathbf{c}(t)$
        $p = p + 1$
        $\mathbf{c}(t) = \mathbf{c}_0$
    end while
    for $i_e = 0$ to $i_e = 2^p/2 = \frac{\Delta t}{2}$: **do**
        $\mathbf{c}(t + \frac{\Delta t}{2^p}) = \hat{U}_e(t + \frac{\Delta t}{2^p}, t)\mathbf{c}(t)$
        $t = t + \frac{\Delta t}{2^p}$
    end for
    $\mathbf{P}^I_\beta = \mathbf{P}^I_\beta + g \cdot \mathbf{F}^I_\beta \frac{\Delta t}{2}$
    $\mathbf{Q}^I_\beta = \mathbf{Q}^I_\beta + g \cdot \mathbf{P}^I_\beta \Delta t + \frac{\Delta t^2}{2} g \cdot \mathbf{F}$
    for $i_e = 0$ to $i_e = 2^p/2 = \frac{\Delta t}{2}$: **do**
        $\mathbf{c}(t + \frac{\Delta t}{2^p}) = \hat{U}_e(t + \frac{\Delta t}{2^p}, t)\mathbf{c}(t)$
        $t = t + \frac{\Delta t}{2^p}$
    end for
end for

Algorithm 7 Quantum propagator $\hat{U}_e(t + \frac{\Delta t}{2^p}, t)$ of algorithm 6.

Build $\mathbf{S}^I$,$\mathbf{H}$,$\mathbf{D}^I$, $\mathbf{H}_{IL}$ for all the electronic states.
Find $\tilde{\mathbf{H}}$: $min \left\| \mathbf{S}^I \tilde{\mathbf{H}} - \left[-\frac{i}{\hbar}\mathbf{H}(t) + \mathbf{D}^I(t) + \sum_L \mathbf{H}_{IL} \right] \right\|$
Integrate $\dot{\mathbf{c}}(t) = \tilde{\mathbf{H}}\mathbf{c}(t)$ from t to $t + \frac{\Delta t}{2^p}$.

Figure 3.22: *Populations of the $\pi^{\star}$(green) and π(blue) electronic states as a function of the time.*

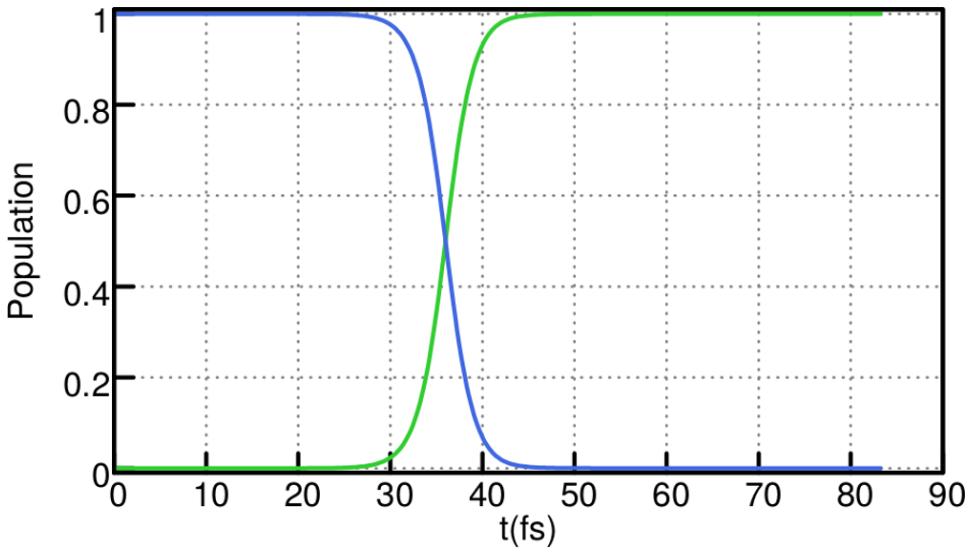

EXCITED STATES COMPUTATIONS BASED ON SINGLE REFERENCES

In order to incorporate the light-molecule interaction in the *ab-initio* determination of the ground and excited PESs, we added an interaction term to the electronic Hamiltonian in the electronic Schrödinger equation to take into account the interaction between the electrons in the molecule and the external field $\mathbf{E}$, reference [15] can be consulted. Taking the molecule-field interaction into account, the electronic Schrödinger equation takes the form:

$$[\hat{T}_e(\mathbf{r}) + \hat{V}_{eN}(\mathbf{r};\mathbf{R}) + \hat{V}_{NN}(\mathbf{R}) + \hat{V}_{ee}(\mathbf{r}) + \hat{V}_{Ee}]\Psi(\mathbf{r};\mathbf{R}) = E_0(\mathbf{R})\Psi(\mathbf{r};\mathbf{R}) \tag{3.83}$$

$$\left[H_e(\mathbf{r};\mathbf{R}) + \mathbf{E}\cdot\sum_i \mathbf{r}_i\right]\Psi(\mathbf{r};\mathbf{R}) = E_0(\mathbf{R})\Psi(\mathbf{r};\mathbf{R}).$$

The additional term involves single particle interactions, therefore it modifies the core Hamiltonian only and in the case of a time-dependent field, the explicit time-dependence is inherited to the core Hamiltonian. The first

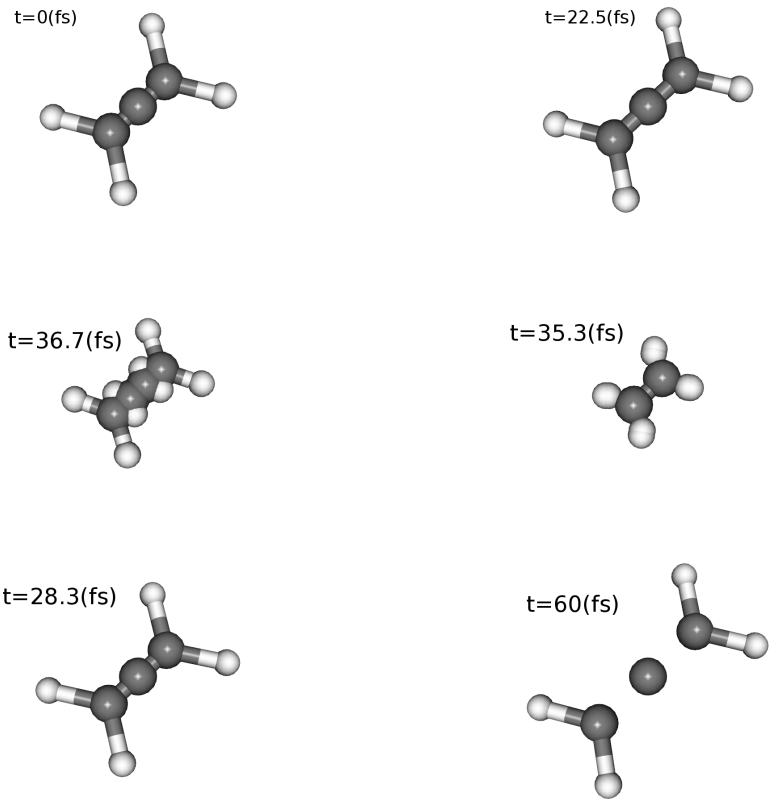

Figure 3.23: *Snapshots of the evolution of the average position of the wavepacket. This results were computed at the SA-3-CAS(4/4) level of theory using a double zeta basis set. Using 32 cores in a cluster this computation takes 6 hours. The black ball at the middle of the double bond represents portion of the wavepacket with zero population at the respective PES.*

step to determine excited states using a single reference methodology is to determine a reference state against which to perform our excitations. As it was mentioned in section 2.2.2 a determinant computed at the Hartree-Fock level of theory is a good starting reference because it is the best single determinantal solution to the Hartree-Fock equations. details regarding the self-Consistent field solution to the Hartree-Fock equations will be given in the next section.

Self-Consistent field(SCF) cycle

In a very intuitive way, the SCF cycle works as follows: The set of eigenvectors that diagonalizes the core Hamiltonian, $\mathbf{h}$, can be used as initial guess to build the initial charge-density matrix $\mathbf{D}_0$, [5] using eq. (2.154). Having available $\mathbf{D}_0$ enables us to compute the initial guess for the Fock matrix $\mathbf{F}_0$, using eq. (2.156), the set of eigenvectors of $\mathbf{F}_0$ provides an improved guess for the charge-density matrix $\mathbf{D}_1$ for the next iteration. [6] The stopping condition for the SCF cycle is achieved when the changes between the charge-density matrices of two consecutive iterations decreases below a threshold. [7] In such a case we can say that the self-consistency in the electronic mean field has been achieved.

In order to perform a SCF cycle, the basis set should be orthogonalized. Exist various methods to achieve this goal, but two methods are in common use, the symmetric and the canonical orthogonalization methods [15].

The overlap matrix $\mathbf{S}$ is a manifestation of the non-orthogonality of the basis set. The orthogonalization procedure consist in find a transformation $\mathbf{X}$, that no need to be unitary, such that:

$$\mathbf{X}^{\dagger}\mathbf{S}\mathbf{X} = \mathbb{1} \tag{3.84}$$

In the symmetric orthogonalization procedure:

$$\mathbf{X}_S = \mathbf{S}^{-1/2} = \mathbf{U}\mathbf{s}^{-1/2}\mathbf{U}^{\dagger}, \tag{3.85}$$

[5] This is the so called H-core guess described below. Further performance can be achieved using more chemically inspired guess as the Hückel one.

[6] From the mathematical point of view an SCF cycle is analogous to a fixed-point iteration where the molecular energy stands for the function and the electronic density stands for the variable.

[7] Typical Threshold values are 10^{-9} for the L_2-distance between charge-density matrices.

where $\mathbf{s}$ is the diagonal matrix of eigenvalues and $\mathbf{U}$ is the matrix of eigenvectors of the overlap matrix. The caveat of this procedure is that if exist eigenvectors that are nearly linearly dependent, one or more eigenvalues in $\mathbf{s}$ will be close to zero making $\mathbf{X}_S$ ill-conditioned depleting the numerical accuracy of the SCF cycle.

Canonical orthogonalization procedure can manage the linear dependence problem mentioned above. In the canonical orthogonalization procedure

$$\mathbf{X}_C = \mathbf{U}\mathbf{s}^{-1/2}, \tag{3.86}$$

where each eigenvector is divided by the square root of its correspondent eigenvalue. The problem of linear dependences in the basis set can be managed by ordering the eigensystem of $\mathbf{S}$ in descending order in the eigenvalues and truncating the columns of $\mathbf{X}_C$ neglecting eigenpairs whose eigenvalue fall below a threshold. 1.0^{-5} is a threshold value of common use.

We also need a diagonalization procedure in order to perform a SCF. The diagonalization involves a orthogonalization intermediate step as follows:

$$\tilde{\mathbf{F}} = \mathbf{X}^{\dagger}\mathbf{F}\mathbf{X} \tag{3.87}$$

$$\tilde{\mathbf{F}}\tilde{\mathbf{c}} = \boldsymbol{\epsilon}\tilde{\mathbf{c}} \tag{3.88}$$

$$\mathbf{c} = \mathbf{X}\tilde{\mathbf{c}}. \tag{3.89}$$

Is not necessary to transform the energies because the eigenvalues are independent of the representation of the matrix that we are diagonalizing. The steps through an SCF cycle are given in algorithm 8. Is remarkable the resemblance between algorithm 8 and algorithm 2, the difference is that while algorithm 2 explores the set of allowed pulse shapes, algorithm 8 explores the allowed set of electronic configuration for the given molecule.

In fact, using the H-Core guess the electronic configuration of lowest energy correspond to distribute the electrons on the atomic orbitals of the heaviest atom of the molecule at hand. When the electronic repulsion is turned on, The electrons in the higher orbitals, start migrating towards neighboring atoms until only remains the core orbitals of the atom plus a few electrons in the valence atomic orbital. The same process occurs at the neighboring atoms of the molecular geometry during the remaining steps of the SCF until the convergence or equilibration of this charge migration is achieved.

Algorithm 8 H-Core guess SCF procedure

1: Initialize the density: $\mathbf{D}_0 = 0$
2: **while** $\left\|\mathbf{c}^k - \mathbf{c}^{k-1}\right\| \geqslant$ threshold and $k > 2$: **do**
3: Build the Fock matrix, $\mathbf{F}$, using eq. (2.156).
4: Store a copy to check for convergence:$\mathbf{c}^{k-1} = \mathbf{c}^k$.
5: Obtain a new set of orbitals, $\mathbf{c}^k$, using the diagonalization eq. (3.88).
6: Build a new electronic charge-density matrix using $\mathbf{c}^k$ and eq. (2.154).
7: Increase the iteration counter: $k = k + 1$.
8: **end while**

Within a SCF procedure is easy to move away electrons from one atom to the neighboring atom, but is hard bring the electrons back. Sometimes occurs that during the initial steps of the SCF one or more core electrons are moved away to the wrong set of neighboring atoms and in such situation the SCF procedure does not achieve convergence. [8] To workaround this situation one can use a shifting in the diagonalization as follows:

$$(\tilde{\mathbf{F}} - \sigma \mathbf{S}\frac{\mathbf{D}}{2}\mathbf{S})\tilde{\mathbf{c}} = \boldsymbol{\epsilon}'\tilde{\mathbf{c}} \tag{3.90}$$

where the $\boldsymbol{\epsilon}'$ is a vector of energies that takes into account the redistribution of electrons among the molecular orbital caused by the shift.

Aiming to test the implementation in algorithm 8 we selected a small set of molecules and perform a computation of the ground state at the Hartree-Fock level of theory with $\mathbf{E} = 0$. The discrepancy between our results and the corresponding energies for the same molecular geometry, and using the same basis set, published by the web page of the NIST is show in fig. 3.24, the difference in energies are around a few micro-Hartrees showing a good agreement between our results and the energies published by the NIST. In oder to study the effects on the energies and orbitals induced by the electric field, we focus on the ethylene molecule. The input for *HELIOS* consist in the molecular geometry in a XYZ format with the chemical symbols replaced by the nuclear charge as shown in the listing 3.2 .

[8] The use of a chemically appealing guess may alleviate this problem.

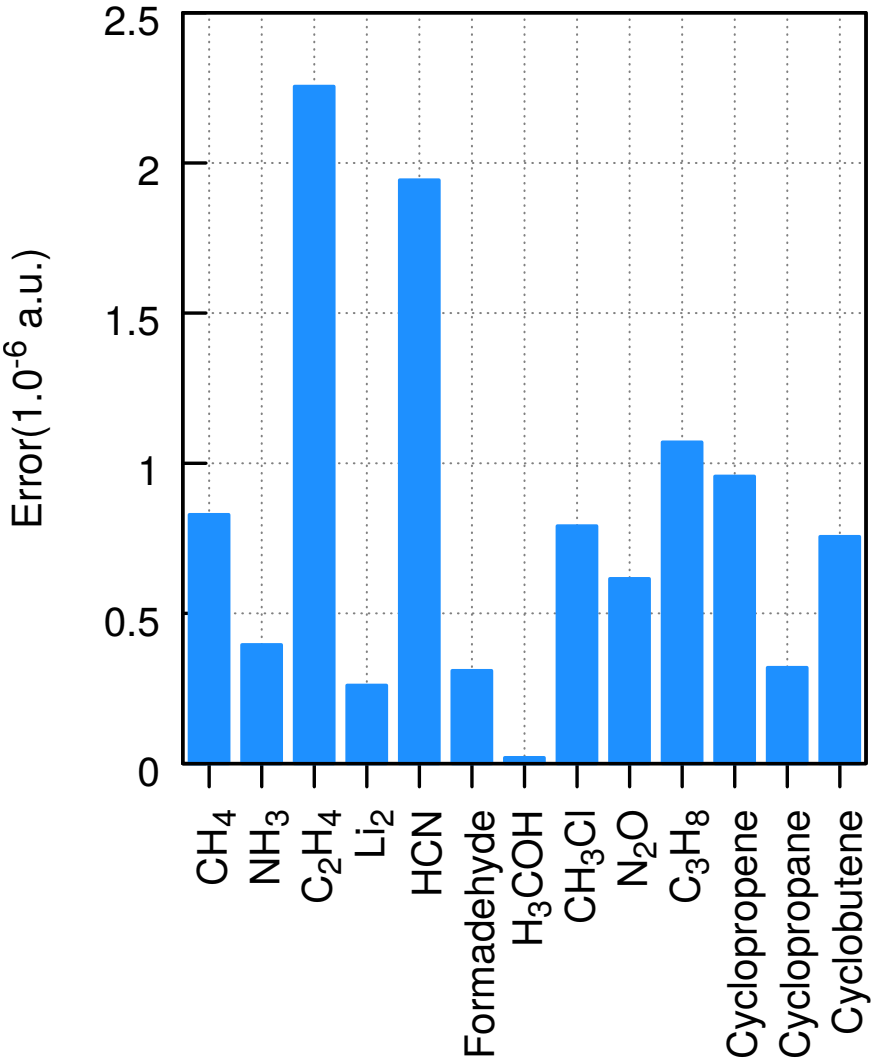

Figure 3.24: *Average Discrepancy against NIST database for computations performed using as basis set: STO-3G, 3-21G, 6-31G, 6-311G.*

```
6
6  0.000  0.000  0.658
6  0.000  0.000  −0.658
1  0.000  0.911  1.225
1  0.000  −0.911   1.225
1  0.000  −0.911   −1.225
1  0.000  0.911  −1.225
```

Listing 3.2: *Molecular geometry for the Ethylene molecule given in Angstroms.*

In order to check the eigenvectors that we are obtaining we computed the isosurfaces for the electronic wavefunction:

$$\Psi_j(\mathbf{R}) = \sum_k c_{kj}\chi_k(\mathbf{R}). \tag{3.91}$$

where $\chi_k(\mathbf{R})$ is the set of contracted cartesian Gaussian primitives of the corresponding basis set [59]. The orbitals showed in fig. 3.25 corresponds to the HOMO-2(A,F), HOMO-1(B,G), HOMO[9](C,H), LUMO[10](D,I) and LUMO+1(E,J) using a 3-21G basis set.

In order to obtain a closed form of the real-time electronic propagator, we will used a Padé approximant of the electronic propagator in its scalling-squaring form:

$$\exp(\tau\mathbf{H}) = \left(\exp\left(2^{-s}\tau\mathbf{H}\right)\right)^{2^s} \tag{3.92}$$

where $\tau = -i\frac{\Delta t}{\hbar}$, following [119], the squaring is chosen to satisfy that $\|2^{-s}\tau\mathbf{H}\|_\infty \leqslant \frac{1}{2}$. with the former conditions fulfilled we can write the propagator by scaling and squaring its Padé approximant for short times:

$$\left(P_{pp}(2^{-s}\tau\mathbf{H})\right)^{2^s} = \exp(\tau\mathbf{H} + \mathbf{E}), \tag{3.93}$$

$$P_{pp}(x) = \begin{cases} 1 + \frac{2x\sum_{k=0}^{p/2-1} c_{2k+1}x^{2k}}{\sum_{k=0}^{p/2} c_{2k}x^{2k} - x\sum_{k=0}^{p/2-1} c_{2k+1}x^{2k}} & \text{if } p \text{ is even,} \\ -1 - \frac{2\sum_{k=0}^{(p-1)/2} c_{2k}x^{2k}}{x\sum_{k=0}^{(p-1)/2} c_{2k+1}x^{2k} - \sum_{k=0}^{(p-1)/2} c_{2k}x^{2k}} & \text{if } p \text{ is odd,} \end{cases} \tag{3.94}$$

$$c_k = c_{k-1}\frac{p+1-k}{(2p+1-k)k}, \tag{3.95}$$

where $\mathbf{E}$ is an pretty small error[11] that deviates the propagation of being unitary. In order to manage the error to manage such error, we choose the

[9] Highest Occupied Molecular Orbital.

[10] Lowest Unoccupied Molecular Orbital.

[11] The error is of the order of 1.0^{-15} if $p = 6$ is used in the Padé approximant.

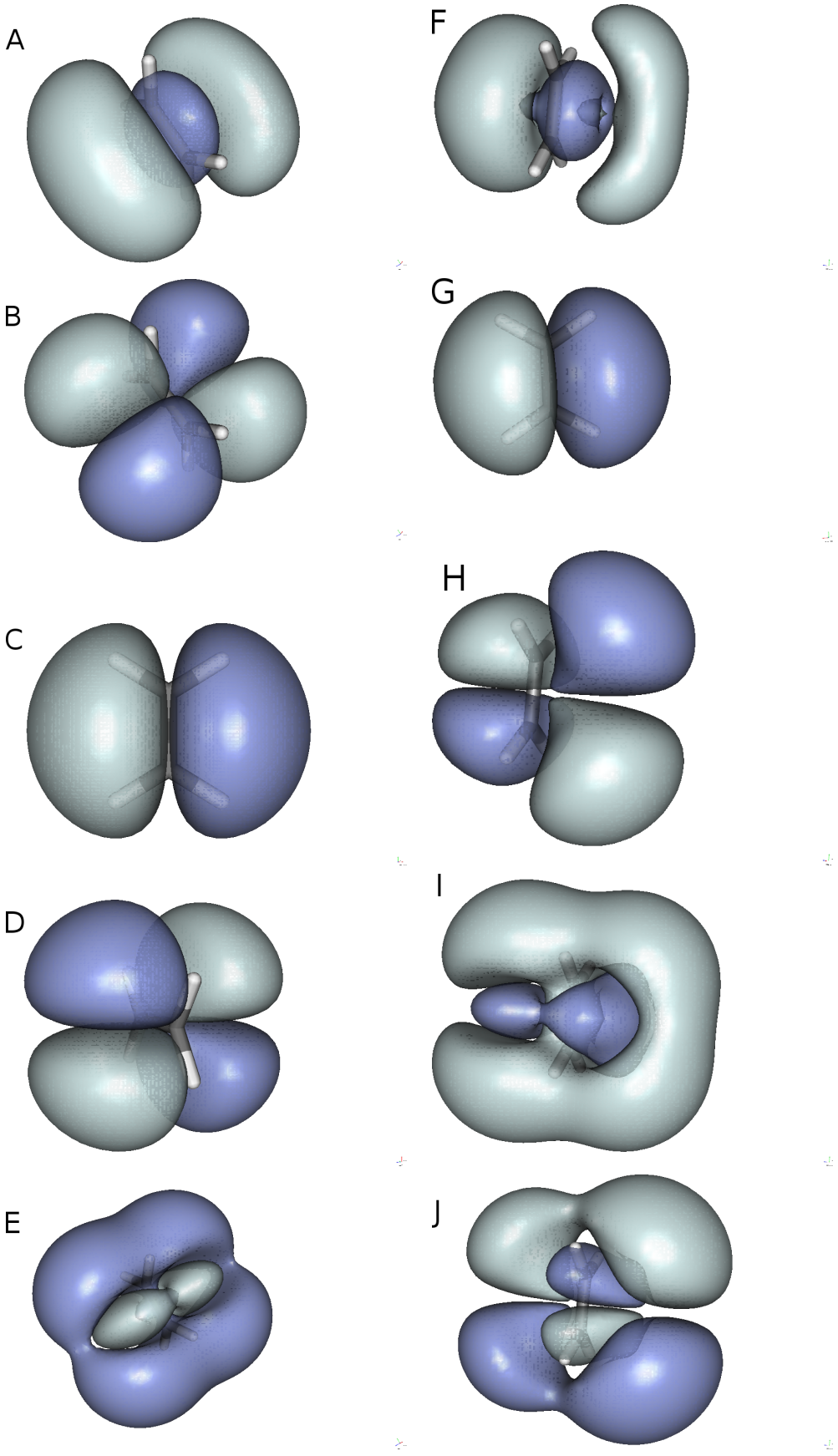
A
B
C
D
E
F
G
H
I
J

number of terms in the Padé approximant adaptively as follows: We increase the number of terms, $p \rightarrow p+3$, until $\|\mathbf{U}_p(t+\Delta t) - \mathbf{U}_{p+3}(t+\Delta t)\| \leqslant 1.0^{-14}$. We used the same trick in section 3.1.1.2 to speed up the step 5 of algorithm 1, and achieve an efficient implementation of the Alvarellos and Metiu procedure [76]. But the highest impact of this ideas is expected from its application to the real-time propagation of slater determinants.

In view that in the case of a closed shell molecule, the molecular energy is computed as:

$$E_0 = \mathrm{tr}\left(\mathbf{P}\frac{1}{2}(\mathbf{h}+\mathbf{F})\right) = \mathrm{tr}\left(\mathbf{P}\frac{1}{2}\left(2\mathbf{h}+\mathbf{J}-\frac{1}{2}\mathbf{K}\right)\right) \tag{3.96}$$

we used:

$$\mathbf{H} = \frac{1}{2}\left(2\mathbf{h}+\mathbf{J}-\frac{1}{2}\mathbf{K}\right) \tag{3.97}$$

as the molecular Hamiltonian to evaluate the propagator. In order to allow to computing the electronic propagator in the presence of a time-dependent field, we used the time-dependent electronic Hamiltonian:

$$\mathbf{H}(t) = \frac{1}{2}\left(2\mathbf{h}(t)+\mathbf{J}-\frac{1}{2}\mathbf{K}\right) \tag{3.98}$$

where the time-dependence of the field has been included in the core Hamiltonian and the density matrix, $\mathbf{P}$, the Coulomb interaction, $\mathbf{J}$, and the exchange interaction, $\mathbf{K}$, have being evaluated using the instantaneous orbitals that result from a SCF cycle, and as in reference [88] we employed the midpoint rule in the computation of the propagator, eq. (2.20), as follows:

$$\hat{U}(t+\Delta t, t) = \exp\left(-\frac{i}{\hbar}\int_t^{t+\Delta t} d\tau \mathbf{H}(\tau)\right) \approx \exp\left(-\frac{i}{\hbar}\mathbf{H}(t+\frac{\Delta t}{2})\Delta t\right). \tag{3.99}$$

We can evaluate the former expression using the Padé approximant in eq. (3.93). If the unitarity of the exact quantum propagator is preserved in its numerical approximant the molecular energy must be preserved along the propagation. In order to check the accuracy of our implementation of the electronic propagator, we computed the difference in energy between the Hartree-Fock energy at $t = 0$ and the molecular energy as a function of time

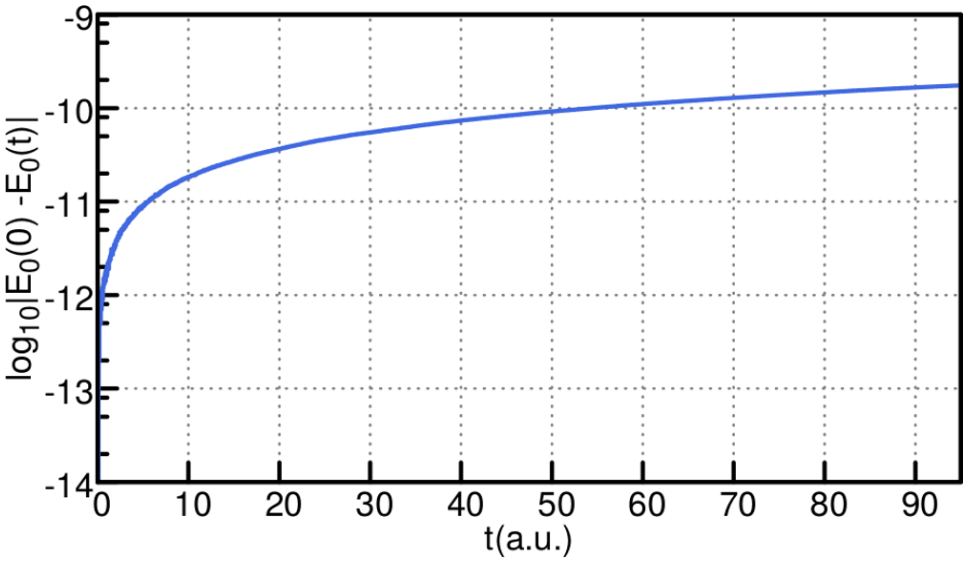

Figure 3.26: *Benchmark of the numerical propagator, eq.* (3.93)*, using the ethylene molecule with the 3-21G basis set, the initial molecular energy is* $E_0(0) = -77.600988$.

for a molecular orbital that has been propagated using eq. (3.93), the results for this test are shown in fig. 3.26.

In order to study the effects of a time-dependent field on the molecular orbitals, we will use as pulse shape a LCP, eq. (3.18), for the external field. The HOMO-LUMO gap gives a rough approximation to the excitation energy of a molecule, 15.447 eV in the case of the ethylene molecule. Therefore we will employ as carrier frequency, $\omega_0 = 5.6584 \times 10^{-1}$(a.u.), as electric field, $E_0 = 1.0 \times 10^{-1}$,[12] as pulse width, $\tau = 10$(a.u), as time shift, $\tau_0 = 50$(a.u.), and as chirp rate, $c = 1.0^{-5}$. The time profile of the pulse is shown in fig. 3.27.

Results for the study of the effects of a LCP on the dynamics of an Slater determinant are shown in fig. 3.28, although the pulse does not induce a complete HOMO-LUMO transition, as it can be seen in panel F, Is remarkable the level of selectivity of the LCP affecting only the HOMO, panel C and LUMO, panel D molecular orbitals, in the case of the LUMO orbital, the excitation due to the pulse induce induces an excitation in the wavefunction originating the appearance of an additional node in the wavefunction.

[12]The optical intensity in terms of the field is: $I = \frac{c\varepsilon_0 n}{2}|E|^2 = 5.45106|E|^2$(a.u.)

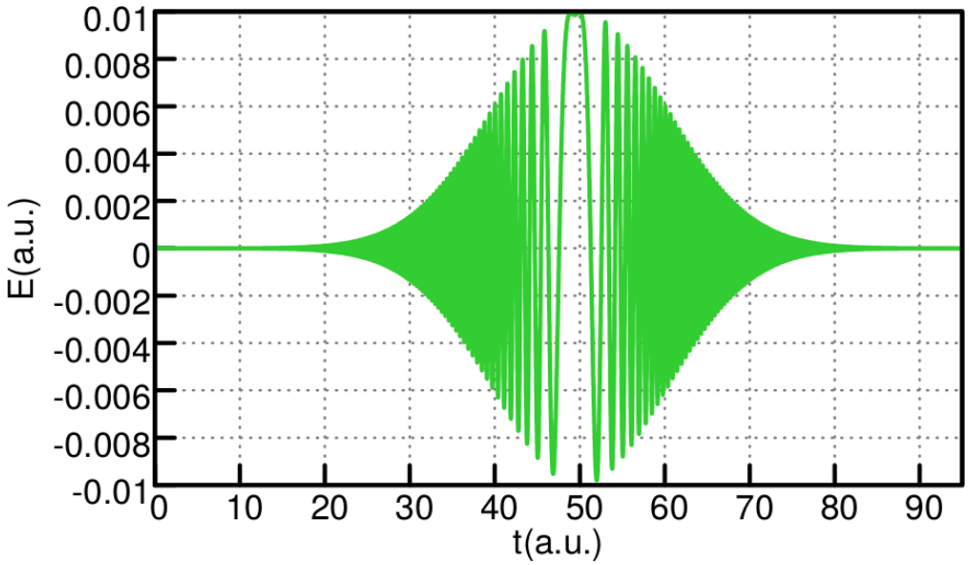

Figure 3.27: *Time-dependence of the electric field that is steering the state of the Ethylene molecule.*

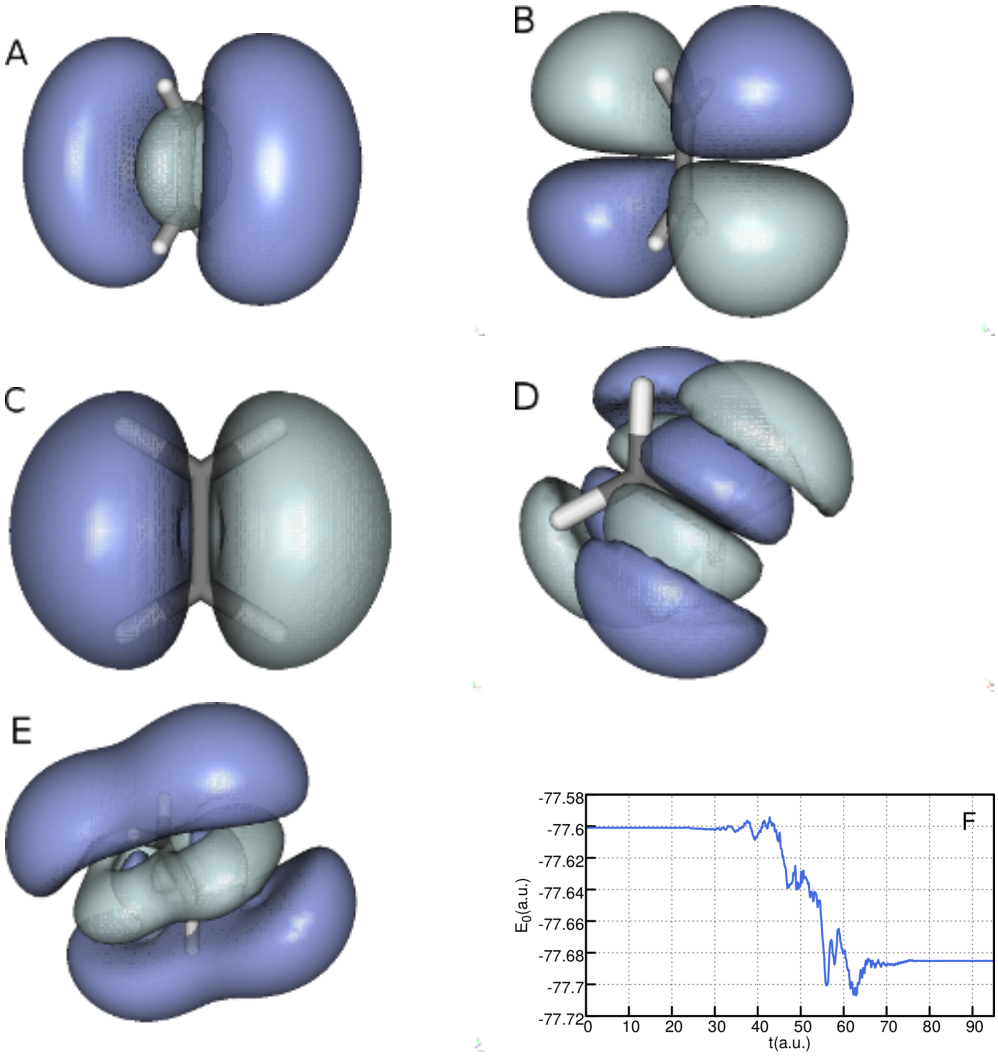

Figure 3.28: *Real part of the orbitals after* 100*(a.u.) of propagation using the Padé approximant of the electronic propagator. The initial conditions of the orbitals corresponds to the left column of fig. 3.25, and the carrier frequency of the chirped pulse is resonant with an HOMO-LUMO excitation causing the additional node in see panel D.*

Chapter 4

Conclusions and Perspectives

Concluding Remarks

The pseudospectral approach to the solution of QOC problems proposed here offer the following set of advantages: In the first place, the optimization can be constrained to pulse shapes of experimental realm and complex multi-target Lagrangian functions can be optimized in order to achieve higher selectivity. In the second place, the procedure of optimization is based on meta-heuristic experiments making the method capable of perform optimization in spaces of parameters of high dimensionality and at the same time provides information regarding the most probable sequence of events that takes place along the optimal path. In the third place, in virtue that the optimization procedure is global, the convergence of the method does not depend on large fields, making our method the first method available that is compatible with on-the-fly determination of the PESs and NACMEs. In the fourth place, the use of our proposal for pseudospectral QOC combined with machine learning techniques stands out as a promising tool capable of provide quantitative information regarding the interpretation of the mechanism of control for the system at hand.

The modular approach to the molecular dynamics on excited states using TvNLs offers a systematic procedure that can be tailored to run using the computational resources that are available, making the proposed methodology particularly promising for the study of the on-the-fly molecular dynamics. Even more, the promise of be capable of decomposing com-

plex molecular processes in simpler sub-processes by populating specific Franck-Condon and/or diabatic active regions is very appealing because will provide further insights regarding the processes that are dominant along involved molecular events.

The use of Padé approximants in the propagation of Slater determinant is promising in order to attempt QOC at the electronic level. But, in virtue of the Brillouin theorem sector of the excitations space having even and odd number of excitations are decoupled,therefore the Padé approximants to the propagator should be computed at a level of theory capable of cover a wider sector of the space of excitations. However, the achievements of this work on this regard, constitutes a solid proof on that the proposed methodology is suitable to perform on-the-fly QOC.

PERSPECTIVES

Our goals in the future can be summarized as follows:

- Perform on-the-fly QOC in order to maximize the life-time of the excited state in ethylene.
- Implement in *HELIOS* the multiconfigurational self-consistent-field response theory method.
- Use the Padé approximant in order to do nuclear-electronic propagations on-the-fly.
- Apply the methodologies developed in the thesis to the control of photoisomerization.
- On-the-fly QOC of photo-transducers
- Development of data-bases of quantum gates for information processing using heteronuclear diatomics
- Development of databases for quantum algorithms
- Nuclear-orbital molecular-orbital dynamics using tvNLs

ACADEMIC PRODUCTS ALONG THE DOCTORAL STUDIES

Article *J. Mol. Mod. 19 (4), 1677-1683*(2013)

Article *Mol. Phys. 112 (3-4), 408-415*(2014)

Article *J. Chem. Phys. 143 (12), 124108*(2015)

Article *J. Chem. Phys. 145 (3), 031101*(2016)

Software HELIOS: Split-Operator+GA-QOC(1D,2D) $\approx$ 3200 lines of C++ code

Software HELIOS: tvNL + pulse (Arbitrary dimensionality) $\approx$ 3000 lines of C++ code

Software HELIOS: tvNL+pulse on-the-fly(Arbitrary dimensionality) $\approx$ 2500 lines of C++ code

Software HELIOS: SCF + CIS(D)+real-time propagator (Gradients are pending) $\approx$ 7500 lines of C++ code

Software HELIOS for GPU: SCF + CIS(D) (Gradients are pending) $\approx$ 4500 lines of CUDA-C code

Appendix A

Annexes

ELECTRONIC INTEGRALS.

Overlap Integrals (OIs)

Following the reference [16] For a unnormalized Cartesian gaussian function (CGF) defined as:

$$\chi_a(\mathbf{r};\alpha,\mathbf{A},l,m,n) = (x-A_x)^l(y-A_y)^m(z-A_z)^n e^{-\alpha\|\mathbf{r}-\mathbf{A}\|^2} \tag{A.1}$$

where $\mathbf{A}$ is is the coordinate of the nuclei to which this CGF belongs, α is the orbital exponent (OE), and the angular momentum of the CGF is defined as $\lambda = l+m+n$. The product of two CGF satisfies the gaussian product theorem (GPT), it applies to the case $\lambda = 0$, and guarantees that the result is another CGF multiplied by prefactor and with shifted center:

$$K_{\mathbf{AB}} = \exp\left(-\frac{\alpha\beta}{\alpha+\beta}\|\mathbf{A}-\mathbf{B}\|^2\right) \tag{A.2}$$

$$\mathbf{P} = \frac{\alpha\mathbf{A}\beta\mathbf{B}}{\alpha+\beta} \tag{A.3}$$

$$\chi_a(\mathbf{r};\alpha,\mathbf{A},\mathbf{n}=0)\chi_b(\mathbf{r};\beta,\mathbf{B},\mathbf{m}=0) = K_{\mathbf{AB}} e^{-(\alpha+\beta)\|\mathbf{r}-\mathbf{P}\|^2} \tag{A.4}$$

A criteria that is often used to speed up the computation of molecular integrals consist in neglect those integrals for which the prefactor, eq. (A.2), is bellow a threshold, most of the modern codes to compute molecular integrals uses $1.0e^{-12}$ as threshold.

The computation of the overlap integral reduces to compute integrals of the form:

$$\int_{-\infty}^{\infty} \exp\left(-\gamma t^2\right) = \sqrt{\frac{\pi}{\gamma}} \tag{A.5}$$

for each cartesian component. In the case of higher angular, the integrand will involve powers of the cartesian component of the integration variable as:

$$(x - A_x)^{l_1}(x - B_x)^{l_2} \tag{A.6}$$

that must be factorized as polynomials of the integration variables times constant factors in a sum of term whose integrals can be computed as:

$$\int_{-\infty}^{\infty} t^{2n} \exp\left(-\gamma t^2\right) = \frac{(2n-1)!!}{2^{n+1}} \sqrt{\frac{\pi}{\gamma^{2n+1}}}. \tag{A.7}$$

This is achieved as follows: In vectorial notation the cartesian factors can be shifted respect to the center resulting from apply the GPT:

$$\vec{r}_A = \vec{r} - \vec{A} = (\vec{r} - \vec{P}) + (\vec{P} - \vec{A}) = \vec{r}_P - \vec{P}A \tag{A.8}$$

and in the particular case of the component along the x-direction:

$$f_j(l, m, a, b) = \sum_{max(0,j-m)}^{min(j,l)} \binom{l}{k} \binom{m}{j-k} a^{l-k} b^{m+k-j} \tag{A.9}$$

$$x_A^{l_1} x_B^{l_2} = (x - \vec{P}A_x)^{l_1}(x - \vec{P}B_x)^{l_2} = \sum_{j=0}^{l_1+l_2} f_j(l_1, l_2, \vec{P}A_x, \vec{P}B_x) x_P^j. \tag{A.10}$$

Therefore,defining $\gamma = \alpha+\beta$, the integrand of the overlap between $\chi_1(\mathbf{r}; \alpha, \mathbf{A}, l_1, m_1, n_1)$ and $\chi_2(\mathbf{r}; \alpha, \mathbf{B}, l_2, m_2, n_2)$ can be expanded as:

$$\begin{aligned} \chi_1\chi_2 = \exp&\left(-\frac{\alpha\beta}{\gamma} \left\|\mathbf{A} - \mathbf{B}\right\|^2\right) \\ &\times \sum_{i=0}^{l_1+l_2} f_i(l_1, l_2, \vec{P}A_x, \vec{P}B_x) x_P^i \exp\left(-\gamma x_P^2\right) \\ &\times \sum_{j=0}^{m_1+m_2} f_j(m_1, m_2, \vec{P}A_y, \vec{P}B_y) y_P^j \exp\left(-\gamma y_P^2\right) \\ &\times \sum_{k=0}^{n_1+n_2} f_k(n_1, n_2, \vec{P}A_z, \vec{P}B_z) z_P^k \exp\left(-\gamma z_P^2\right). \end{aligned} \tag{A.11}$$

In such a way that the integral can be factorized as the product of its cartesian components:

$$\int \chi_1\chi_2 dxdydz = \exp\left(-\frac{\alpha\beta}{\gamma}\left\|\mathbf{A}-\mathbf{B}\right\|^2\right) S_x S_y S_z. \tag{A.12}$$

Again, in the particular case of the x-direction:

$$S_x = \sum_{i=0}^{l_1+l_2} f_i(l_1, l_2, \vec{P}A_x, \vec{P}B_x) \int_{-\infty}^{\infty} x_P^i \exp\left(-\gamma x_P^2\right) dx \tag{A.13}$$

And by symmetry arguments the non-zero contributions to this integral must have even powers in x_P. Now we are in position of use the result in eq. (A.7) to get the final result for the overlap integral:

$$\begin{aligned}
S_x =& \sqrt{\frac{\pi}{\gamma}} \sum_{i=0}^{(l_1+l_2)/2} f_{2i}(l_1, l_2, \vec{P}A_x, \vec{P}B_x) \frac{(2i-1)!!}{(2\gamma)^i} \qquad \text{(A.14)}\\
S_y =& \sqrt{\frac{\pi}{\gamma}} \sum_{j=0}^{(m_1+m_2)/2} f_{2j}(m_1, m_2, \vec{P}A_y, \vec{P}B_y) \frac{(2j-1)!!}{(2\gamma)^j}\\
S_z =& \sqrt{\frac{\pi}{\gamma}} \sum_{k=0}^{(n_1+n_2)/2} f_{2k}(n_1, n_2, \vec{P}A_z, \vec{P}B_z) \frac{(2k-1)!!}{(2\gamma)^k}\\
\langle 1|2\rangle = S_{12} =& \int \chi_1\chi_2 dxdydz = \exp\left(-\frac{\alpha\beta}{\gamma}\left\|\mathbf{A}-\mathbf{B}\right\|^2\right) S_x S_y S_z.
\end{aligned}$$

That is the expression used in the HELIOS code to compute the overlap integrals.

Kinetic Energy Integrals (KEIs)

The evaluation of the kinetic energy integrals is expedited by the fact that the derivative of a CGF is another CGF:

$$\frac{\partial}{\partial x}\chi(\mathbf{r};\alpha,\mathbf{A},l,m,n) = l\chi(\mathbf{r};\alpha,\mathbf{A},l-1,m,n) - 2\alpha\chi(\mathbf{r};\alpha,\mathbf{A},l+1,m,n) \tag{A.15}$$

$$\frac{\partial}{\partial y}\chi(\mathbf{r};\alpha,\mathbf{A},l,m,n) = m\chi(\mathbf{r};\alpha,\mathbf{A},l,m-1,n) - 2\alpha\chi(\mathbf{r};\alpha,\mathbf{A},l,m+1,n) \tag{A.16}$$

$$\frac{\partial}{\partial z}\chi(\mathbf{r};\alpha,\mathbf{A},l,m,n) = n\chi(\mathbf{r};\alpha,\mathbf{A},l,m,n-1) - 2\alpha\chi(\mathbf{r};\alpha,\mathbf{A},l,m,n+1). \tag{A.17}$$

applying twice this set of formulas, it can be shown that the action of the kinetic operator in an arbitrary CGF is:

$$\begin{aligned}-\frac{1}{2}\nabla^2\chi(\mathbf{r};\alpha,\mathbf{A},l,m,n) &= \alpha(2\lambda+3)\chi(\mathbf{r};\alpha,\mathbf{A},l,m,n) \\ &\quad -2\alpha^2\left(\chi(\mathbf{r};\alpha,\mathbf{A},l+2,m,n)\right. \\ &\quad +\chi(\mathbf{r};\alpha,\mathbf{A},l,m+2,n) \\ &\quad \left.+\chi(\mathbf{r};\alpha,\mathbf{A},l,m,n+2)\right) \\ &\quad +\frac{1}{2}\left(l(l-1)\chi(\mathbf{r};\alpha,\mathbf{A},l-2,m,n)\right. \\ &\quad +m(m-1)\chi(\mathbf{r};\alpha,\mathbf{A},l,m-2,n) \\ &\quad \left.+n(n-1)\chi(\mathbf{r};\alpha,\mathbf{A},l,m,n-2)\right).\end{aligned} \tag{A.18}$$

Therefore, The computation of this matrix element is reduced to compute a sum of overlaps in eq. (A.15):

$$\left\langle 1\right|\hat{T}_e\left|2\right\rangle = t_{12} = \int \chi_1(-\frac{1}{2}\nabla^2\chi_2)dxdydz. \tag{A.19}$$

Nuclear Attraction Integrals (NAIs)

The amount of algebraic work to compute the electronic integrals is lessen, in part, by employ use the gaussian product rule, eq. (A.11). At some point in this computation we will have to employ the Fourier identity for $1/r$:

$$\frac{1}{r} = \frac{1}{2\pi}\int_{-\infty}^{\infty}\frac{\vec{dk}}{|\vec{k}|^2}\exp\left(i\vec{k}\cdot\vec{r}\right). \tag{A.20}$$

therefore to prevent confusions we will switch the old dummy indexes, i, j, k; to l, m, n in eq. (A.11):

$$\begin{aligned}\int \chi_1 \frac{1}{r_C} \chi_2 dxdydz = \exp\left(-\frac{\alpha\beta}{\gamma}\left\|\mathbf{A}-\mathbf{B}\right\|^2\right) \\ \times \sum_{l=0}^{l_1+l_2} f_l(l_1, l_2, \vec{P}A_x, \vec{P}B_x) \\ \times \sum_{m=0}^{m_1+m_2} f_m(m_1, m_2, \vec{P}A_y, \vec{P}B_y) \\ \times \sum_{n=0}^{n_1+n_2} f_n(n_1, n_2, \vec{P}A_z, \vec{P}B_z) \\ \times \int x_P^l y_P^m z_P^n \frac{1}{r_C} \exp\left(-\gamma r_P^2\right).\end{aligned} \tag{A.21}$$

Expanding again around the center:

$$\vec{r}_C = \vec{r} - \vec{C} = (\vec{r} - \vec{P}) + (\vec{P} - \vec{C}) = \vec{r}_P + \vec{P}C, \tag{A.22}$$

and using the Fourier integral identity for $1/r_C$, in eq. (A.20):

$$\frac{1}{r_C} = \frac{1}{2\pi^2} \int \frac{\vec{dk}}{k^2} \exp\left(i\vec{k}\cdot\vec{P}C\right) \exp\left(-\vec{k}\cdot\vec{r}_P\right). \tag{A.23}$$

The nuclear Attraction integral becomes in:

$$\begin{aligned}\int \chi_1 \frac{1}{r_C} \chi_2 dxdydz = \exp\left(-\frac{\alpha\beta}{\gamma}\left\|\mathbf{A}-\mathbf{B}\right\|^2\right) \frac{1}{2\pi^2} \\ \times \sum_{l=0}^{l_1+l_2} f_l(l_1, l_2, \vec{P}A_x, \vec{P}B_x) \\ \times \sum_{m=0}^{m_1+m_2} f_m(m_1, m_2, \vec{P}A_y, \vec{P}B_y) \\ \times \sum_{n=0}^{n_1+n_2} f_n(n_1, n_2, \vec{P}A_z, \vec{P}B_z) \\ \times \int \left(k^{-2} \exp\left(i\vec{k}\cdot\vec{P}C\right) V_l^x V_m^y V_n^z\right) \vec{dk}\end{aligned} \tag{A.24}$$

As we did in the case of the overlap integral, I will do the computation in detail for the cartesian factor in the x-direction:

$$V_l^x = \int x_P^l \exp\left(-\gamma x_P^2 + ik_x x_P\right) dx_P, \tag{A.25}$$

that can be computed using the gaussian integral identity:

$$\begin{aligned}\int_{-\infty}^{\infty} \exp\left(-at^2 + ibt\right) dt =& i^n n! \sqrt{\frac{\pi}{a}} \left(\frac{1}{2\sqrt{a}}\right)^n \exp\left(-\frac{ab^2}{4}\right) \\ & \sum_{j=0}^{\lceil n/2 \rceil} \frac{(-1)^j (2b\sqrt{a})^{n-2j}}{j!(n-2j)!}.\end{aligned} \tag{A.26}$$

Using this formula to compute V_l^x we get the partial result:

$$\begin{aligned}V_l^x =& i^l l! \sqrt{\frac{\pi}{\gamma}} \left(\frac{1}{4\gamma}\right)^{l/2} \exp\left(-\frac{k_x^2}{4\gamma}\right) \\ & \sum_{r=0}^{\lceil l/2 \rceil} \frac{(-1)^r \left(2\sqrt{\frac{1}{4\gamma}} k_x\right)^{l-2r}}{r!(l-2r)!},\end{aligned} \tag{A.27}$$

one more integral is left, the integral over $\vec{k}$ introduced by the Fourier integral identity for the Coulomb potential.

Multiplying the three cartesian factors, introducing two new indexes $\{s, t\}$ and collecting out constant factors:

$$V_l^x V_m^y V_n^z \propto \exp\left(-\frac{k^2}{4\gamma}\right) k_x^{l-2r} k_y^{m-2s} k_z^{n-2t}. \tag{A.28}$$

We will deal with the integral in $\vec{dk}$ of eq. (A.24) here:

$$\int k^{-2} k_x^{l-2r} k_y^{m-2s} k_z^{n-2t} \exp\left(-\frac{k^2}{4\gamma}\right) \exp\left(i\vec{k} \cdot \vec{P}C\right) \vec{dk}. \tag{A.29}$$

The Use of the identity:

$$\exp\left(\epsilon k^2\right) = 2\epsilon k^2 \int_0^1 u^{-3} \exp\left(-\epsilon \frac{k^2}{u^2}\right) du. \tag{A.30}$$

Allows us to rewrite our integral as:

$$\begin{aligned}\int k^{-2}k_x^{l-2r}k_y^{m-2s}k_z^{n-2t}\exp\left(-\frac{k^2}{4\gamma}\right)\exp\left(i\vec{k}\cdot\vec{P}C\right)\vec{dk} = \frac{2}{\gamma}\int_0^1\frac{du}{u^3} \\ \times\int_{-\infty}^{\infty}dk_x k_x^{l-2r}\exp\left(\frac{k_x^2}{4\gamma u^2}+i\vec{P}C_x k_x\right) \\ \times\int_{-\infty}^{\infty}dk_y k_y^{m-2s}\exp\left(\frac{k_y^2}{4\gamma u^2}+i\vec{P}C_y k_y\right) \\ \times\int_{-\infty}^{\infty}dk_z k_z^{n-2t}\exp\left(\frac{k_z^2}{4\gamma u^2}+i\vec{P}C_z k_z\right)\end{aligned} \tag{A.31}$$

After tackle the integrals in k using the identity in eq. (A.26), the remaining integrals in u are of the form:

$$\begin{aligned}\int_0^1 u^{2\nu}\exp\left(-\gamma|\vec{P}C|^2u^2\right)du =& F_\nu(\gamma|\vec{P}C|^2u^2) \\ \nu =& l+m+n-2(r+s+t)-(i+j+k) \\ & 0\leqslant i\leqslant(l-2r)/2 \\ & 0\leqslant j\leqslant(m-2s)/2 \\ & 0\leqslant k\leqslant(n-2t)/2\end{aligned} \tag{A.32}$$

introducing the shorthand notation for the constants:

$$A_{l,r,i}(l_1,l_2,\vec{A}_x,\vec{B}_x,\vec{C}_x,\gamma) = (-1)^l f_l(l_1,l_2,\vec{P}A_x,\vec{P}B_x)\frac{(-1)^i l!\vec{P}C_x^{l-2r-2i}\left(\frac{1}{4\gamma}\right)^{r+i}}{r!i!(l-2r-2i)!} \tag{A.33}$$

We can write the final result for the nuclear attraction integral:

$$\begin{aligned}\left\langle 1\left|\frac{1}{r_C}\right|2\right\rangle &= \int \chi_1 \frac{1}{r_C}\chi_2 dxdydz \\ &= \frac{2\pi}{\gamma}\exp\left(-\frac{\alpha\beta}{\gamma}\left\|\mathbf{A}-\mathbf{B}\right\|^2\right) \\ &\times \sum_{l=0}^{l_1+l_2}\sum_{r=0}^{\lceil l/2\rceil}\sum_{i=0}^{\lceil (l-2r)/2\rceil} A_{l,r,i}(l_1,l_2,\vec{A}_x,\vec{B}_x,\vec{C}_x,\gamma) \\ &\times \sum_{m=0}^{m_1+m_2}\sum_{s=0}^{\lceil m/2\rceil}\sum_{j=0}^{\lceil (m-2s)/2\rceil} A_{m,s,j}(m_1,m_2,\vec{A}_y,\vec{B}_y,\vec{C}_y,\gamma) \\ &\times \sum_{n=0}^{n_1+n_2}\sum_{t=0}^{\lceil n/2\rceil}\sum_{k=0}^{\lceil (n-2t)/2\rceil} A_{n,t,k}(n_1,n_2,\vec{A}_z,\vec{B}_z,\vec{C}_z,\gamma) \\ &F_{l+m+n-2(r+s+t)-(i+j+k)}(\gamma|\vec{P}C|^2).\end{aligned} \tag{A.34}$$

With this equation we completed the one electron matrix element of the Hartree-Fock matrices or the so called *h-core*:

$$h_{12} = \left\langle 1\left|\hat{h}\right|2\right\rangle = \left\langle 1\left|\hat{T}_e\right|2\right\rangle + \left\langle 1\left|\frac{1}{r_C}\right|2\right\rangle. \tag{A.35}$$

Electron-Repulsion Integrals (ERIs)

This are integrals over densities of pairs of electrons, therefore the integration occurs in a six-dimensional space in the more general case. Accounting symmetry considerations, and defining $m = N(N+1)/2$ the number of unique repulsion integrals is $m(m+1)/2$ been N the size of the basis.

The computation is long, but most of the features of the technique where introduced in the previous section, so let us start. Expanding again around centers for each pair of electrons:

$$\vec{r}_{A1} = \vec{r}_1 - \vec{A} = (\vec{r}_1 - \vec{P}) + (\vec{P} - \vec{A}) = \vec{r}_{A1} + \vec{P}A, \tag{A.36}$$

$$\vec{r}_{C2} = \vec{r}_2 - \vec{C} = (\vec{r}_2 - \vec{Q}) + (\vec{Q} - \vec{C}) = \vec{r}_{C2} + \vec{Q}C, \tag{A.37}$$

The integral that we are computing is:

$$\begin{aligned}G = &\int \chi_1(\vec{A},\alpha_1,l_1,m_1,n_1)(\vec{r}_{A1})\chi_2(\vec{B},\alpha_2,l_2,m_2,n_2)(\vec{r}_{B1}) \\ &\times\frac{1}{r_{12}}\chi_3(\vec{C},\alpha_3,l_3,m_3,n_3)(\vec{r}_{C2})\chi_4(\vec{D},\alpha_4,l_4,m_4,n_4)(\vec{r}_{D2})\end{aligned} \tag{A.38}$$

applying the GPT, eq. (A.4), to each density of pairs:

$$\begin{aligned}\chi_1\chi_2 \propto \exp\left(-\alpha_1 r_{A1}^2\right)\exp\left(-\alpha_2 r_{B1}^2\right) =& \exp\left(\frac{\alpha_1\alpha_2|\vec{A}B|}{\alpha_1+\alpha_2}\right)\exp\left(\gamma_1 r_{P1}^2\right)\\ =& K_1\exp\left(\gamma_1 r_{P1}^2\right)\\ \chi_3\chi_4 \propto \exp\left(-\alpha_3 r_{C2}^2\right)\exp\left(-\alpha_4 r_{D2}^2\right) =& \exp\left(\frac{\alpha_3\alpha_4|\vec{C}D|}{\alpha_3+\alpha_4}\right)\exp\left(\gamma_2 r_{Q2}^2\right)\\ =& K_2\exp\left(\gamma_2 r_{Q2}^2\right)\end{aligned} \tag{A.39}$$

and expanding the cartesian products using eq. (A.10), we get:

$$\begin{aligned}G =& K_1K_2\sum_{l=0}^{l_1+l_2}\sum_{m=0}^{m_1+m_2}\sum_{n=0}^{n_1+n_2} f_l(l_1,l_2,\vec{P}A_x,\vec{P}B_x)\\ &\times f_m(m_1,m_2,\vec{P}A_y,\vec{P}B_y)f_n(n_1,n_2,\vec{P}A_z,\vec{P}B_z)\\ &\times\sum_{l'=0}^{l_3+l_4}\sum_{m'=0}^{m_3+m_4}\sum_{n'=0}^{n_3+n_4} f_{l'}(l_3,l_4,\vec{Q}C_x,\vec{Q}D_x)\\ &\times f_{m'}(m_3,m_4,\vec{Q}C_y,\vec{Q}D_y)f_{n'}(n_3,n_4,\vec{Q}C_z,\vec{Q}D_z)\\ &\times\int\int x_{P1}^l y_{P1}^m z_{P1}^n x_{Q2}^{l'} y_{Q2}^{m'} z_{Q2}^{n'}\frac{1}{r_{12}}\exp\left(-\gamma_1 r_{P1}^2-\gamma_2 r_{Q2}^2\right)dV_1dV_2.\end{aligned} \tag{A.40}$$

shifting the electronic variables as:

$$\begin{aligned}\vec{r}_{12}=\vec{r}_1-\vec{r}_2 =& (\vec{r}_1-\vec{P})-(\vec{r}_2-\vec{Q}) = r_{P1}-r_{Q2}+\vec{p}\\ \vec{p} =& \vec{P}-\vec{Q}\end{aligned} \tag{A.41}$$

combining it with the Fourier identity, eq. (A.20):

$$\frac{1}{r}_{12} = \frac{1}{2\pi^2}\int\frac{d\vec{k}}{k^2}\exp\left(i\vec{r}_{P1}\cdot\vec{k}\right)\exp\left(i\vec{r}_{Q2}\cdot\vec{k}\right)\exp\left(i\vec{p}\cdot\vec{k}\right); \tag{A.42}$$

after the definition of the prefactor

$$\Omega = \frac{2\pi^2}{\gamma_1\gamma_2}\sqrt{\frac{\pi}{\gamma_1+\gamma_2}}\exp\left(-\frac{\alpha_1\alpha_2\mathbf{A}B^2}{\gamma_1}-\frac{\alpha_3\alpha_4\mathbf{C}D^2}{\gamma_2}\right) \tag{A.43}$$

and the factors:

$$\theta(l,l_1,l_2,a,b,r,\gamma) = f_l(l_1,l_2,a,b)\frac{l!\gamma^{r-l}}{r!(2r)!}, \tag{A.44}$$

and

$$\begin{aligned} &B_{l,l',r_1,r_2,i}(l_1,l_2,\mathbf{A}_x,\mathbf{B}_x,\mathbf{P}_x,\gamma_1;l_3,l_4,\mathbf{C}_x,\mathbf{D}_x,\mathbf{Q}_x,\gamma_2) \\ =&(-1)^{l'}\theta(l,l_1,l_2,\mathbf{P}A_x,\mathbf{P}B_x,r,\gamma_1)\theta(l',l_3,l_4,\mathbf{Q}C_x,\mathbf{Q}D_x,r',\gamma_2) \\ &\frac{(-1)^i(2\delta^{r+r'}(l+l'-2r-2r')!\delta^i\mathbf{p}_x^{l+l'-2(r+r'+i)})}{(4\delta)^{l+l'}i!(l+l'-2(r+r'+i))!}. \end{aligned} \tag{A.45}$$

The repulsion integral can be written as:

$$\left\langle 12(1)\left|\frac{1}{r_{12}}\right|34(2)\right\rangle = G \tag{A.46}$$

$$G = \Omega \sum_{l=0}^{l_1+l_2}\sum_{r=0}^{\lceil l/2\rceil}\sum_{i=0}^{\lceil (l-2r)/2\rceil}\sum_{l'=0}^{l_3+l_4}\sum_{r'=0}^{\lceil l'/2\rceil}$$

$$B_{l,l',r_1,r_2,i}(l_1,l_2,\mathbf{A}_x,\mathbf{B}_x,\mathbf{P}_x,\gamma_1;l_3,l_4,\mathbf{C}_x,\mathbf{D}_x,\mathbf{Q}_x,\gamma_2)$$

$$\times \sum_{m=0}^{m_1+m_2}\sum_{s=0}^{\lceil m/2\rceil}\sum_{j=0}^{\lceil (m-2s)/2\rceil}\sum_{m'=0}^{m_3+m_4}\sum_{s'=0}^{\lceil m'/2\rceil}$$

$$B_{m,m',s_1,s_2,j}(m_1,m_2,\mathbf{A}_y,\mathbf{B}_y,\mathbf{P}_y,\gamma_1;m_3,m_4,\mathbf{C}_y,\mathbf{D}_y,\mathbf{Q}_y,\gamma_2)$$

$$\times \sum_{n=0}^{n_1+n_2}\sum_{t=0}^{\lceil n/2\rceil}\sum_{k=0}^{\lceil (n-2t)/2\rceil}\sum_{n'=0}^{n_3+n_4}\sum_{t'=0}^{\lceil n'/2\rceil}$$

$$B_{n,n',t_1,t_2,k}(n_1,n_2,\mathbf{A}_z,\mathbf{B}_z,\mathbf{P}_z,\gamma_1;n_3,n_4,\mathbf{C}_z,\mathbf{D}_z,\mathbf{Q}_z,\gamma_2)$$

$$\times F_\nu\left(\frac{\mathbf{p}^2}{4\delta}\right).$$

been:

$$\delta = \frac{1}{4\gamma_1}+\frac{1}{4\gamma_2} \tag{A.47}$$

$$\nu = l+l'+m+m'+n+n'-2(r+r'+s+s'+t+t')-(i+j+k). \tag{A.48}$$

The integral tha is left,

$$F_\nu(x) = \int_0^1 t^{2\nu}\exp\left(-xt^2\right)dt \tag{A.49}$$

In a short hand notation, introducing the new variable $x = \frac{\mathbf{p}^2}{4\delta}$, the ERI

exposses itself in a very simple way:

$$G = \sum_{\nu=0}^{L} C_\nu(x) F_\nu(x) \tag{A.50}$$

with L depending on the angular moment of the quartet. This formula means that the ERI is the integral of a su of polynomial in even powers of x:

$$G = \sum_{\nu} \int_0^1 C_\nu t^{2\nu} \exp\left(-xt^2\right) dt \tag{A.51}$$

that can be computed exactly as a quadrature, it is, as a weighted sum of $L/2+1$ evaluation of the corresponding polynomial in the corresponding roots of the quadrature There are various sets of roots and weights in the market to do this, but the so called Rys polynomials have shown to be the set of choise to tho this computation with outstanding accuray and is the opion I chosen to compute the ERIs in the HELIOS code. Even more, to speed up the computations I used an interpolation table for the root and weights allowing to compute integrals until angular moment 7 it is the ERI $\left\langle 77(1)\right| \frac{1}{r_{12}} \left|77(2)\right\rangle$

Second Quantization formalism

In second quantization for quantum mechanics the wave function is expressed in terms of creation and annihilation operators acting on the vacuum state and the antisymmetry of the wave function follows from the anti-commutation algebra of this operators. As an useful example, consider that the Slater determinant, eq. (2.126), in representation of second quantization is expressed as follows:

$$|\mathbf{k}\rangle = |k_1, k_2, \ldots, k_M\rangle\,, \qquad k_P = \begin{cases} 1 & \text{if } \phi_P \text{ is occupied.} \\ 0 & \text{if } \phi_P \text{ is empty.} \end{cases} \tag{A.52}$$

Introducing a abstract linear vector space, the Fock space, formed by the collection of all the possible occupation number (ON) vectors(Slater determinants), $|\mathbf{k}\rangle$. For a collection of orthonormal spin-orbitals the inner product of two ON vectors $|\mathbf{k}\rangle$ and $|\mathbf{m}\rangle$ is:

$$\langle \mathbf{k}|\mathbf{m}\rangle = \delta_{\mathbf{km}} = \prod_{P=1}^{M} \delta_{k_P, m_P}, \tag{A.53}$$

If the orbitals are in canonical order the correspondence between a given Slater determinant and a ON vector is unique. The former property allows that for a given molecule, we can express in this vectorial space: the ground and excited states of the molecule, the neutral and all the meaningful ionized states, or all the possible configurations produced by its fragmentation.

Unlike the Slater determinants the ON vectors does not have spatial structure, this is introduced via multiplicative factors as will be shown later. The scalar product in the ON vectorial space is defined as follows. given two ON vectors in the same Fock space,

$$|\mathbf{c}\rangle = \sum_k c_{\mathbf{k}} |\mathbf{k}\rangle \tag{A.54}$$

$$|\mathbf{d}\rangle = \sum_k d_{\mathbf{k}} |\mathbf{k}\rangle \tag{A.55}$$

$$\tag{A.56}$$

Their scalar(inner) product is given by:

$$\langle \mathbf{c}|\mathbf{d}\rangle = \sum_{\mathbf{km}} c^\star_{\mathbf{k}} \langle \mathbf{k}|\mathbf{m}\rangle d_{\mathbf{m}} = \sum_{\mathbf{k}} c^\star_{\mathbf{k}} d_{\mathbf{k}}. \tag{A.57}$$

As a consequence, the resolution of the identity for the Fock space can be written as:

$$\mathbb{1} = \sum_{\mathbf{k}} |\mathbf{k}\rangle \langle \mathbf{k}| \tag{A.58}$$

Using the standard notation of quantum chemistry, for a molecular system composed by N electrons using as basis set, a set of M spin-orbitals, the set of ON vectors, eq. (A.52), generates a 2^M-dimensional Fock space, $F(M)$, that can be decomposed into direct sums of subspaces $F(M,N)$ with $0 \leq N \leq M$:

$$F(M) = F(M,0) \oplus F(M,1) \oplus \cdots F(M,M) \tag{A.59}$$

where $F(M,N)$ represents all the ON vectors obtained by distributing N electrons on M spin-orbitals. $F(M,0)$ is the vacuum state, $|vac\rangle$, of course. The exact wave function of the molecule can be expressed as a linear combination in s Fock space of dimension $\begin{pmatrix} M \\ N \end{pmatrix}$.

In the second quantization formulation all the physically meaningful states and operators can be constructed in terms of creation and anihilation operators, and all the expectation values can be given in terms of the basic commutation rules. Given a molecule, exist as many pairs of this operators as spin-orbitals in the basis set, *i.e.* M. The M fermionic creation operators are defined as: [1]

$$\hat{a}_P^\dagger \left|k_1, k_2, \ldots, 0_P, \ldots, k_M\right\rangle = \Gamma_P^{\mathbf{k}} \left|k_1, k_2, \ldots, 1_P, \ldots, k_M\right\rangle \tag{A.60}$$

$$\hat{a}_P^\dagger \left|k_1, k_2, \ldots, 1_P, \ldots, k_M\right\rangle = 0 \tag{A.61}$$

where the phase factor $\Gamma_P^{\mathbf{k}}$ is -1 if there is a odd number of electrons in the spin-orbitals before the spin-orbital P, and is is $+1$ if this number is even, in general:

$$\Gamma_P^{\mathbf{k}} = \prod_{Q=1}^{P-1} (-1)^{k_Q}. \tag{A.62}$$

To avoid refers explicitly to the unoccupied orbitals, we will express the ON vector as a string of creation operators acting on the vacuum state, in canonical order:

$$\left|\mathbf{k}\right\rangle = \left[\prod_{P=1}^{M} \left(\hat{a}_P^\dagger\right)^{k_P}\right] \left|vac\right\rangle. \tag{A.63}$$

Given two operators $\hat{a}_P^\dagger$ and $\hat{a}_Q^\dagger$ with $Q > P$ in canonical order, using the definitions in eqs. (A.60) and (A.61), it is easy to show that:

$$\begin{aligned}
\left[\hat{a}_P^\dagger, \hat{a}_Q^\dagger\right]_+ \left|\mathbf{k}\right\rangle &= \left[\hat{a}_P^\dagger, \hat{a}_Q^\dagger\right]_+ \left|\ldots, k_P, \ldots, k_Q, \ldots\right\rangle \\
&= \hat{a}_P^\dagger \hat{a}_Q^\dagger \left|\ldots, k_P, \ldots, k_Q, \ldots\right\rangle + \hat{a}_Q^\dagger \hat{a}_P^\dagger \left|\ldots, k_P, \ldots, k_Q, \ldots\right\rangle \\
&= \hat{a}_P^\dagger \delta_{k_Q 0} \Gamma_Q^{\mathbf{k}} \left|\ldots, k_P, \ldots, 1_Q, \ldots\right\rangle + \hat{a}_Q^\dagger \delta_{k_P 0} \Gamma_P^{\mathbf{k}} \left|\ldots, 1_P, \ldots, k_Q, \ldots\right\rangle \\
&= \delta_{k_P 0} \delta_{k_Q 0} \Gamma_P^{\mathbf{k}} \Gamma_Q^{\mathbf{k}} \left|\ldots, 1_P, \ldots, 1_Q, \ldots\right\rangle + \delta_{k_P 0} \delta_{k_Q 0} \Gamma_P^{\mathbf{k}} (-\Gamma_Q^{\mathbf{k}}) \left|\ldots, 1_P, \ldots, 1_Q, \ldots\right\rangle \\
&= \left(\delta_{k_P 0} \delta_{k_Q 0} \Gamma_P^{\mathbf{k}} \Gamma_Q^{\mathbf{k}} - \delta_{k_P 0} \delta_{k_Q 0} \Gamma_P^{\mathbf{k}} \Gamma_Q^{\mathbf{k}}\right) \left|\ldots, 1_P, \ldots, 1_Q, \ldots\right\rangle \\
\left[\hat{a}_P^\dagger, \hat{a}_Q^\dagger\right]_+ &= 0,
\end{aligned} \tag{A.64}$$

[1] The basic ON vector for the pair of bosonic creation and anihilation operators, eqs. (2.50) and (2.51), can be constructed replacing the determinant by the permanent in eq. (2.126).

where the $(-\Gamma_Q^{\mathbf{k}})$ in the second term, is due to the fact that the operator $\hat{a}_Q^\dagger$ in the second term must jump one orbital to act on the $|\mathbf{k}\rangle$ state when canonical ordering is imposed. The commutation relation in eq. (A.64) holds for any pair of creation operators in canonical order.

The hermitian adjoint operators of the creation operators, $\hat{a}_P$ are called anihilation operators and their definition and properties can be inferred starting from those of the creation operators, thus from eq. (A.64) we get:

$$\begin{aligned}\left(\left[\hat{a}_P^\dagger, \hat{a}_Q^\dagger\right]_+\right)^\dagger &= (0)^\dagger \\ \left[\hat{a}_P, \hat{a}_Q\right]_+ &= 0\end{aligned} \tag{A.65}$$

The resolution of the identity in the Fock space, eq. (A.58), combined with the definition of the creation operator on an ON vector, eqs. (A.60) and (A.61), let us infer the action of the anihilation operator on a ON vector $|\mathbf{k}\rangle$:

$$\begin{aligned}\hat{a}_P |\mathbf{k}\rangle &= \sum_{\mathbf{m}} |\mathbf{m}\rangle \langle \mathbf{m}| \hat{a}_P |\mathbf{k}\rangle \\ \langle \mathbf{m}| \hat{a}_P |\mathbf{k}\rangle &= \left\langle \mathbf{k} \right| \hat{a}_P^\dagger \left| \mathbf{m} \right\rangle^\star = \begin{cases} \delta_{k_P 1} \Gamma_P^{\mathbf{k}} & \text{if } m_Q = k_Q - \delta_{QP}. \\ 0 & \text{if otherwise.} \end{cases} \\ \hat{a}_P |\mathbf{k}\rangle &= \delta_{k_P 1} \Gamma_P^{\mathbf{k}} |k_1, \ldots, 0_P, \ldots, k_M\rangle .\end{aligned} \tag{A.66}$$

In words, the operator $\hat{a}_P$ changes $k_P = 1$ to $k_P = 0$ if the spin orbital is occupied and produces 0 otherwise, Therefore is is called an anihilation operator. Regarding the anti-commutation relations between creation and anihilation operators:

$$\begin{aligned}\left[\hat{a}_P^\dagger, \hat{a}_P\right]_+ |\mathbf{k}\rangle &= \hat{a}_P^\dagger \hat{a}_P |\mathbf{k}\rangle + \hat{a}_P \hat{a}_P^\dagger |\mathbf{k}\rangle \\ &= (\delta_{k_P 1} + \delta_{k_P 0}) |\mathbf{k}\rangle \\ \left[\hat{a}_P^\dagger, \hat{a}_P\right]_+ &= 1.\end{aligned} \tag{A.67}$$

In the general case of spin orbitals in canonical order:

$$\left[\hat{a}_P^\dagger, \hat{a}_Q\right]_+ = \delta_{PQ}, \tag{A.68}$$

for arbitrary P and Q. The summary of the anti-commutation relations the

creation and anihilation operators obey can be summarized as follows:

$$\left[\hat{a}_P^\dagger, \hat{a}_P^\dagger\right]_+ = 0 \tag{A.69}$$

$$\left[\hat{a}_P, \hat{a}_P\right]_+ = 0 \tag{A.70}$$

$$\left[\hat{a}_P^\dagger, \hat{a}_P\right]_+ = \delta_{PQ}. \tag{A.71}$$

$$\tag{A.72}$$

Creation and anihilation operators couples subspaces with different number of particles of the Fock space, eq. (A.59), but strings of creation and anihilation operators can be constructed to couple ON vectors that belong to subspaces that preserves the number of particles. The simplest example of this kind of operators is the occupation number operator:

$$\hat{\mathbf{N}}_P = \hat{a}_P^\dagger \hat{a}_P, , \tag{A.73}$$

$$\hat{\mathbf{N}}_P \left|\mathbf{k}\right\rangle = \hat{a}_P^\dagger \hat{a}_P \left|\mathbf{k}\right\rangle = \delta_{k_P 1} (\Gamma_P^{\mathbf{k}})^2 \left|\mathbf{k}\right\rangle = k_P \left|\mathbf{k}\right\rangle, \tag{A.74}$$

This operator is hermitian, idempotent, and two different occupation number operators commutes:

$$\left[\hat{\mathbf{N}}_P, \hat{\mathbf{N}}_Q\right] = 0. \tag{A.75}$$

Using the anti-commutation relations in eqs. (A.69) to (A.71) it is possible to infer the following results for the commutators of the occupation number operator and the creation and anihilation operators:

$$\left[\hat{N}_P, \hat{a}_Q^\dagger\right] = \delta_{PQ} \hat{a}_Q^\dagger \tag{A.76}$$

$$\left[\hat{N}_P, \hat{a}_Q\right] = -\delta_{PQ} \hat{a}_Q. \tag{A.77}$$

Given a string of creation and anihilation operators, $\hat{X} = \hat{a}_P^\dagger \hat{a}_Q \hat{a}_P \hat{a}_R^\dagger \hat{a}_S$, The former commutation relations can be used to infer that:

$$\left[\hat{N}_P, \hat{X}\right] = N_P^X \hat{X}. \tag{A.78}$$

where N_P^X is the difference between the number of times that $\hat{a}_P^\dagger$ occurs in the string, and the numbers of times that occurs $\hat{a}_P$.

The particle-number operator is defined as:

$$\hat{N} = \sum_{P=1}^{M} \hat{N}_P \tag{A.79}$$

$$\hat{N} \left|\mathbf{k}\right\rangle = \sum_{P=1}^{M} k_P \left|\mathbf{k}\right\rangle = N \left|\mathbf{k}\right\rangle, \tag{A.80}$$

and owns the following property, if $\hat{X}$ is an arbitrary string of creation and anihilation operators:

$$\left[\hat{N}, \hat{X}\right] = N^X \hat{X}, \tag{A.81}$$

where N^X is the excess(or defect) of creation respect to anihilation operators on the string. Therefore the particle-number operator commutes with any string, $\hat{T}$, accomplished by equal number of creation and anihilation operators and such strings are called number-conserving strings.

Another important example of number-conserving string are the excitation operators among which the most elementary one is:

$$\hat{X}_Q^P = \hat{a}_P^\dagger \hat{a}_Q \tag{A.82}$$

$$\hat{a}_P^\dagger \hat{a}_Q \left|\mathbf{k}\right\rangle = \hat{a}_P^\dagger \hat{a}_Q \left|k_1, \ldots, 1_Q, \ldots, 0_P, \ldots, k_m\right\rangle \tag{A.83}$$

$$= \Gamma_P^{\mathbf{k}} \delta_{k_Q 1} \Gamma_Q^{\mathbf{k}} \left|k_1, \ldots, 0_Q, \ldots, k_P, \ldots, k_m\right\rangle \tag{A.84}$$

$$= \delta_{k_p 0} \delta_{k_Q 1} \Gamma_P^{\mathbf{k}} \Gamma_Q^{\mathbf{k}} \epsilon_{PQ} \left|k_1, \ldots, 0_Q, \ldots, 1, \ldots, k_m\right\rangle \tag{A.85}$$

$$\epsilon_{PQ} = \begin{cases} 1 & \text{if } P \leq Q. \\ -1 & \text{if } P > Q. \end{cases} \tag{A.86}$$

In words, this operator excites one electron from the spin orbital Q to the spin orbital P keeping constant the number of electrons in the molecule. Thus any ON vector within the subspace $F(M, n)$ can be obtained from any other ON vector within the same subspace by applying a sequence of excitation operators[2]. Higher powers of the operator $\hat{X}_Q^P$ correspond to doubles($\hat{X}_Q^P \hat{X}_R^S$), triples($\hat{X}_Q^P \hat{X}_R^S \hat{X}_T^U$), quadruples($\hat{X}_Q^P \hat{X}_R^S \hat{X}_T^U \hat{V}_T^W$) excitations.

We will derive here the for that takes the molecular Hamiltonian in second quantization.

[2]From a geometric perspective this operation can be understood as a sequence of rotations

INTEGRALS FOR THE PSEUDOSPECTRAL METHOD

Matrix Elements Used in the Pseudospectral Method

Generalized set of Integrals Using Klauder Coherent States

Klauder coherent state in 1D

$$G[Q\alpha\_, P\alpha\_, \gamma\_] = \text{Exp}\left[i \frac{P\alpha}{h} (q - Q\alpha) + i P\alpha Q\alpha - \frac{\gamma}{2} (q - Q\alpha)^2\right]$$

$$e^{\frac{i P\alpha (q-Q\alpha)}{h} + i P\alpha Q\alpha - \frac{1}{2}(q-Q\alpha)^2 \gamma}$$

Overlap Integral

$$\text{Assuming}\left[\text{Re}[\gamma\alpha + \gamma\beta] > 0, \left(\frac{\gamma\alpha}{\pi}\right)^{1/4} \left(\frac{\gamma\beta}{\pi}\right)^{1/4} \int_{-\infty}^{\infty} G[Q\alpha, -P\alpha, \gamma\alpha] G[Q\beta, P\beta, \gamma\beta] dq\right]$$

$$\frac{\sqrt{2}\ e^{-\frac{P\alpha^2 + P\beta^2 + h^2 (Q\alpha - Q\beta)^2 \gamma\alpha \gamma\beta - 2 i h P\beta (Q\alpha \gamma\alpha + Q\beta ((-1+h)\gamma\alpha + h\gamma\beta)) + 2 i P\alpha (i P\beta + h ((-Q\alpha + Q\beta)\gamma\beta + h Q\alpha (\gamma\alpha + \gamma\beta)))}{2 h^2 (\gamma\alpha + \gamma\beta)}} \gamma\alpha^{1/4} \gamma\beta^{1/4}}{\sqrt{\gamma\alpha + \gamma\beta}}$$

$$-\frac{1}{2 h^2 (\gamma\alpha + \gamma\beta)} \left(P\alpha^2 + P\beta^2 + h^2 (Q\alpha - Q\beta)^2 \gamma\alpha \gamma\beta - 2 i h P\beta (Q\alpha \gamma\alpha + Q\beta ((-1+h)\gamma\alpha + h\gamma\beta)) + 2 i P\alpha (i P\beta + h ((-Q\alpha + Q\beta)\gamma\beta + h Q\alpha (\gamma\alpha + \gamma\beta)))\right) /. \{(Q\alpha - Q\beta) \to \Delta Q, (-Q\alpha + Q\beta) \to -\Delta Q\}$$

$$-\left(\Delta P^2 - 2 i h P\beta (Q\alpha \gamma\alpha + Q\beta ((-1+h)\gamma\alpha + h\gamma\beta)) + h^2 \gamma\alpha \gamma\beta \Delta Q^2 + 2 i P\alpha ((h Q\alpha (\gamma\alpha + \gamma\beta) - \gamma\beta \Delta Q))\right) / \left(2 h^2 (\gamma\alpha + \gamma\beta)\right)$$

After factorizing in a symmetric way, and generalize to higher dimensions:

P = $\gamma\beta$.Mp.Pα - $\gamma\alpha$.Mp.Pβ.

plus the phase -$\frac{i}{h}$(Pα Qα – PβQβ)

Potential energy Integral

```
Assuming[Re[γα + γβ] > 0,
 (γα/π)^(1/4) (γβ/π)^(1/4) ∫_-∞^∞ G[Qα, -Pα, γα] (q - (γα Qα + γβ Qβ)/(γα + γβ)) G[Qβ, Pβ, γβ] dq]
```

$$-\frac{1}{h\,(\gamma\alpha+\gamma\beta)^{3/2}}$$

$$i\sqrt{2}\; e^{-\frac{P\alpha^2+P\beta^2+h^2\,(Q\alpha-Q\beta)^2\,\gamma\alpha\,\gamma\beta-2\,i\,h\,P\beta\,(Q\alpha\,\gamma\alpha+Q\beta\,((-1+h)\,\gamma\alpha+h\,\gamma\beta))+2\,i\,P\alpha\,(i\,P\beta+h\,((-Q\alpha+Q\beta)\,\gamma\beta+h\,Q\alpha\,(\gamma\alpha+\gamma\beta)))}{2\,h^2\,(\gamma\alpha+\gamma\beta)}}\,(P\alpha-P\beta)\,\gamma\alpha^{1/4}\,\gamma\beta^{1/4}$$

Obtaining that $\rho = -\frac{i}{\hbar}(\gamma\alpha+\gamma\beta)^{-1}\,\Delta P$.

```
Assuming[Re[γα + γβ] > 0,
 (γα/π)^(1/4) (γβ/π)^(1/4) ∫_-∞^∞ G[Qα, -Pα, γα] (q - (γα Qα + γβ Qβ)/(γα + γβ))^2 G[Qβ, Pβ, γβ] dq]
```

$$\frac{1}{h^2\,(\gamma\alpha+\gamma\beta)^{5/2}}\sqrt{2}\; e^{-\frac{P\alpha^2+P\beta^2+h^2\,(Q\alpha-Q\beta)^2\,\gamma\alpha\,\gamma\beta-2\,i\,h\,P\beta\,(Q\alpha\,\gamma\alpha+Q\beta\,((-1+h)\,\gamma\alpha+h\,\gamma\beta))+2\,i\,P\alpha\,(i\,P\beta+h\,((-Q\alpha+Q\beta)\,\gamma\beta+h\,Q\alpha\,(\gamma\alpha+\gamma\beta)))}{2\,h^2\,(\gamma\alpha+\gamma\beta)}}$$

$$\gamma\alpha^{1/4}\,\gamma\beta^{1/4}\,\left(-P\alpha^2+2\,P\alpha\,P\beta-P\beta^2+h^2\,(\gamma\alpha+\gamma\beta)\right)$$

Wignerg Transform

```
G[Qα, -Pα, γα] /. {q → q + s/2}
```

$$e^{-i\,P\alpha\,Q\alpha-\frac{i\,P\alpha\left(q-Q\alpha+\frac{s}{2}\right)}{h}-\frac{1}{2}\left(q-Q\alpha+\frac{s}{2}\right)^2\gamma\alpha}$$

```
G[Qβ, Pβ, γβ] /. {q → q - s/2}
```

$$e^{i\,P\beta\,Q\beta+\frac{i\,P\beta\left(q-Q\beta-\frac{s}{2}\right)}{h}-\frac{1}{2}\left(q-Q\beta-\frac{s}{2}\right)^2\gamma\beta}$$

```
Assuming[Re[γα + γβ] > 0,
 (γα/π)^(1/4) (γβ/π)^(1/4)/(2 π h) ∫_-∞^∞ e^(-i Pα Qα - (i Pα (q - Qα + s/2))/h - 1/2 (q - Qα + s/2)^2 γα) e^(i Pβ Qβ + (i Pβ (q - Qβ - s/2))/h - 1/2 (q - Qβ - s/2)^2 γβ) Exp[i/h Π s] ds]
```

$$\frac{1}{h\,\pi\,\sqrt{\gamma\alpha+\gamma\beta}}\sqrt{2}\; e^{-\frac{P\alpha^2+P\beta^2+4\,h^2\,q^2\,\gamma\alpha\,\gamma\beta-4\,h^2\,q\,Q\alpha\,\gamma\alpha\,\gamma\beta+h^2\,Q\alpha^2\,\gamma\alpha\,\gamma\beta-4\,h^2\,q\,Q\beta\,\gamma\alpha\,\gamma\beta+2\,h^2\,Q\alpha\,Q\beta\,\gamma\alpha\,\gamma\beta+h^2\,Q\beta^2\,\gamma\alpha\,\gamma\beta-2\,i\,P\beta\left(h\,(2\,q-Q\alpha-Q\beta)\,\gamma\alpha+h^2\,Q\beta\,(\gamma\alpha+\gamma\beta)-2\,i\,\Pi\right)+2\,i\,P\alpha\left(-i\,P\beta+h\,(2\,q-Q\alpha-Q\beta)\,\gamma\beta+h^2\,Q\alpha\,(\gamma\alpha\right.}}{2\,h^2\,(\gamma\alpha+\gamma\beta)}}$$

$$\gamma\alpha^{1/4}\,\gamma\beta^{1/4}$$

This integrals is enough to compute the wigner transform of a swarm of coherent states in arbitrary dimensionality

Dynamical Couplings

```
D[G[Qβ[t], Pβ[t], γβ ], t]
```

$$e^{\frac{i\,P\beta[t]\,(q-Q\beta[t])}{h}-\frac{1}{2}\gamma\beta\,(q-Q\beta[t])^2+i\,P\beta[t]\,Q\beta[t]}\left(\frac{i\,(q-Q\beta[t])\,P\beta'[t]}{h}+i\,Q\beta[t]\,P\beta'[t]+i\,P\beta[t]\,Q\beta'[t]-\frac{i\,P\beta[t]\,Q\beta'[t]}{h}+\gamma\beta\,(q-Q\beta[t])\,Q\beta'[t]\right)$$

```
% /. {Qβ[t] → Qβ, Pβ[t] → Pβ}
```

$$e^{\frac{i\,P\beta\,(q-Q\beta)}{h}+i\,P\beta\,Q\beta-\frac{1}{2}(q-Q\beta)^2\,\gamma\beta}\left(\frac{i\,(q-Q\beta)\,P\beta'[t]}{h}+i\,Q\beta\,P\beta'[t]+i\,P\beta\,Q\beta'[t]-\frac{i\,P\beta\,Q\beta'[t]}{h}+(q-Q\beta)\,\gamma\beta\,Q\beta'[t]\right)$$

```
Assuming[Re[γα + γβ] > 0, ∫_-∞^∞ ((i (q - Qβ) dPβ)/h + i Qβ dPβ + i Pβ dQβ - (i Pβ dQβ)/h + (q - Qβ) γβ dQβ)
    G[Qα, -Pα, γα ] G[Qβ, Pβ, γβ ] (γα/π)^(1/4) (γβ/π)^(1/4) dq]
```

$$\frac{1}{h^2\,(\gamma\alpha+\gamma\beta)^{3/2}}\,i\,\sqrt{2}\;e^{\frac{(-i\,P\alpha+i\,P\beta+h\,Q\alpha\,\gamma\alpha+h\,Q\beta\,\gamma\beta)^2}{\gamma\alpha+\gamma\beta}-h\,\left(2\,i\,(-1+h)\,P\alpha\,Q\alpha-2\,i\,(-1+h)\,P\beta\,Q\beta+h\,\left(Q\alpha^2\,\gamma\alpha+Q\beta^2\,\gamma\beta\right)\right)}{2\,h^2}}$$

$$\gamma\alpha^{1/4}\,\gamma\beta^{1/4}\,(dQ\beta\,h\,(-(P\alpha+i\,h\,(Q\alpha-Q\beta)\,\gamma\alpha)\,\gamma\beta+P\beta\,((-1+h)\,\gamma\alpha+h\,\gamma\beta))+dP\beta\,(-i\,P\alpha+i\,P\beta+h\,(Q\alpha\,\gamma\alpha+Q\beta\,((-1+h)\,\gamma\alpha+h\,\gamma\beta))))$$

```
(dQβ h (-(Pα + i h (Qα - Qβ) γα) γβ + Pβ ((-1 + h) γα + h γβ)) +
    dPβ (-i Pα + i Pβ + h (Qα γα + Qβ ((-1 + h) γα + h γβ)))) /. {(Qα - Qβ) → ΔQ}
```

$$dP\beta\,(-i\,P\alpha+i\,P\beta+h\,(Q\alpha\,\gamma\alpha+Q\beta\,((-1+h)\,\gamma\alpha+h\,\gamma\beta)))+dQ\beta\,h\,(P\beta\,((-1+h)\,\gamma\alpha+h\,\gamma\beta)+\gamma\beta\,(-P\alpha-i\,h\,\gamma\alpha\,\Delta Q))$$

```
% // Expand
```

$$-i\,dP\beta\,P\alpha+i\,dP\beta\,P\beta-dQ\beta\,h\,P\beta\,\gamma\alpha+dQ\beta\,h^2\,P\beta\,\gamma\alpha+dP\beta\,h\,Q\alpha\,\gamma\alpha-dP\beta\,h\,Q\beta\,\gamma\alpha+dP\beta\,h^2\,Q\beta\,\gamma\alpha-dQ\beta\,h\,P\alpha\,\gamma\beta+dQ\beta\,h^2\,P\beta\,\gamma\beta+dP\beta\,h^2\,Q\beta\,\gamma\beta-i\,dQ\beta\,h^2\,\gamma\alpha\,\gamma\beta\,\Delta Q$$

```
Collect[%, h^2]
```

$$-i\,dP\beta\,P\alpha+i\,dP\beta\,P\beta+h\,(-dQ\beta\,P\beta\,\gamma\alpha+dP\beta\,Q\alpha\,\gamma\alpha-dP\beta\,Q\beta\,\gamma\alpha-dQ\beta\,P\alpha\,\gamma\beta)+h^2\,(dQ\beta\,P\beta\,\gamma\alpha+dP\beta\,Q\beta\,\gamma\alpha+dQ\beta\,P\beta\,\gamma\beta+dP\beta\,Q\beta\,\gamma\beta-i\,dQ\beta\,\gamma\alpha\,\gamma\beta\,\Delta Q)$$

$$\left(i\,\sqrt{2}\;\gamma\alpha^{1/4}\,\gamma\beta^{1/4}\,(dQ\beta\,h\,(-(P\alpha+i\,h\,(Q\alpha-Q\beta)\,\gamma\alpha)\,\gamma\beta+P\beta\,((-1+h)\,\gamma\alpha+h\,\gamma\beta))+dP\beta\,(-i\,P\alpha+i\,P\beta+h\,(Q\alpha\,\gamma\alpha+Q\beta\,((-1+h)\,\gamma\alpha+h\,\gamma\beta))))\right)\Big/\left(h^2\,(\gamma\alpha+\gamma\beta)^{3/2}\right)\Big/\frac{\sqrt{2}\;\gamma\alpha^{1/4}\,\gamma\beta^{1/4}}{\sqrt{\gamma\alpha+\gamma\beta}}$$

Factorizing the overlap we get :

```
(i (dQβ h ((-Pα - i h (Qα - Qβ) γα) γβ + Pβ ((-1 + h) γα + h γβ)) +
      dPβ (-i Pα + i Pβ + h (Qα γα + Qβ ((-1 + h) γα + h γβ))))) / (h^2 (γα + γβ))
```

```
(i (dQβ h ((-Pα - i h (Qα - Qβ) γα) γβ + Pβ ((-1 + h) γα + h γβ)) +
      dPβ (-i Pα + i Pβ + h (Qα γα + Qβ ((-1 + h) γα + h γβ))))) / (h^2 (γα + γβ))
```

```
1/h^2 i (dQβ h ((-Pα - i h (Qα - Qβ) γα) γβ + Pβ ((-1 + h) γα + h γβ)) +
      dPβ (-i Pα + i Pβ + h (Qα γα + Qβ ((-1 + h) γα + h γβ)))) // ExpandAll
```

$$\frac{dP\beta\, P\alpha}{h^2} - \frac{dP\beta\, P\beta}{h^2} + i\, dQ\beta\, P\beta\, \gamma\alpha - \frac{i\, dQ\beta\, P\beta\, \gamma\alpha}{h} + \frac{i\, dP\beta\, Q\alpha\, \gamma\alpha}{h} + i\, dP\beta\, Q\beta\, \gamma\alpha - \frac{i\, dP\beta\, Q\beta\, \gamma\alpha}{h} - \frac{i\, dQ\beta\, P\alpha\, \gamma\beta}{h} + i\, dQ\beta\, P\beta\, \gamma\beta + i\, dP\beta\, Q\beta\, \gamma\beta + dQ\beta\, Q\alpha\, \gamma\alpha\, \gamma\beta - dQ\beta\, Q\beta\, \gamma\alpha\, \gamma\beta$$

```
Collect[%, {dQβ, dPβ}]
```

$$dP\beta \left(\frac{P\alpha}{h^2} - \frac{P\beta}{h^2} + \frac{i\, Q\alpha\, \gamma\alpha}{h} + i\, Q\beta\, \gamma\alpha - \frac{i\, Q\beta\, \gamma\alpha}{h} + i\, Q\beta\, \gamma\beta\right) + dQ\beta \left(i\, P\beta\, \gamma\alpha - \frac{i\, P\beta\, \gamma\alpha}{h} - \frac{i\, P\alpha\, \gamma\beta}{h} + i\, P\beta\, \gamma\beta + Q\alpha\, \gamma\alpha\, \gamma\beta - Q\beta\, \gamma\alpha\, \gamma\beta\right)$$

The final expression for the dynamical coupling is:

$$\left(dP\beta \left(\frac{1}{\gamma\alpha+\gamma\beta}\right) \left(\frac{1}{h^2}(P\alpha - P\beta) + \frac{i}{h}\gamma\alpha\,(Q\alpha - Q\beta) + i\,(\gamma\alpha + \gamma\beta)\, Q\beta\right) + dQ\beta \left(\frac{1}{\gamma\alpha+\gamma\beta}\right) \left(i\,(\gamma\alpha + \gamma\beta)\, P\beta - \frac{i}{h}(\gamma\alpha\, P\beta - \gamma\beta\, P\alpha) + (Q\alpha - Q\beta)\,\gamma\alpha\,\gamma\beta\right)\right) S_{\alpha\beta}$$

Observables

Average Position

```
Assuming[Re[γ] > 0, ∫_-∞^∞ G[Qα, -Pα, γ] q G[Qβ, Pβ, γ] dq]
```

```
1 / (2 h γ) e^(1/4 ((2 i (Pα+Pβ) (Qα-Qβ))/h - (Pα-Pβ)^2/(h^2 γ) - (Qα-Qβ)^2 γ)) (-i Pα + i Pβ + h (Qα + Qβ) γ) /
   e^(1/4 ((2 i (Pα+Pβ) (Qα-Qβ))/h - (Pα-Pβ)^2/(h^2 γ) - (Qα-Qβ)^2 γ)) // Simplify
```

$$\frac{-i\, P\alpha + i\, P\beta + h\,(Q\alpha + Q\beta)\,\gamma}{2\, h\, \gamma}$$

Average Momentum

```
Assuming[Re[γ] > 0, ∫_-∞^∞ G[Qα, -Pα, γ] D[G[Qβ, Pβ, γ], Qβ] dq]
```

$$\frac{1}{2\,h}\,e^{-\frac{P\alpha^2+P\beta^2-2\,i\,h\,P\beta\,(Q\alpha-Q\beta)\,\gamma+h^2\,(Q\alpha-Q\beta)^2\,\gamma^2-2\,P\alpha\,(P\beta+i\,h\,(Q\alpha-Q\beta)\,\gamma)}{4\,h^2\,\gamma}}\,(-i\,P\alpha-i\,P\beta+h\,(Q\alpha-Q\beta)\,\gamma)$$

```
% / e^(1/4 (2 i (Pα+Pβ) (Qα-Qβ)/h - (Pα-Pβ)^2/(h^2 γ) - (Qα-Qβ)^2 γ)) // FullSimplify
```

$$\frac{-i\,(P\alpha+P\beta)+h\,(Q\alpha-Q\beta)\,\gamma}{2\,h}$$

Exact integral for the Morse potential

```
Assuming[Re[γ] > 0 && Re[β] > 0,
 ∫_-∞^∞ G[Qα, -Pα, γ] d (1 - Exp[-β (q - Qβ - qe)])^2 G[Qβ, Pβ, γ] dq]
```

$$d\,e^{-\frac{P\alpha^2+P\beta^2-2\,P\alpha\,(P\beta+i\,h\,(Q\alpha-Q\beta)\,\gamma)+2\,i\,h\,P\beta\,(2\,\beta-Q\alpha\,\gamma+Q\beta\,\gamma)+h^2\,\gamma\,(4\,Q\alpha\,\beta+Q\alpha^2\,\gamma-2\,Q\alpha\,Q\beta\,\gamma+Q\beta^2\,\gamma)}{4\,h^2\,\gamma}}\left(e^{\beta\left(Q\alpha+\frac{i\,P\beta}{h\,\gamma}\right)}+e^{\frac{\beta\,(i\,P\alpha+h\,(\beta+2\,qe\,\gamma+Q\beta\,\gamma))}{h\,\gamma}}-2\,e^{\frac{\beta\,(2\,i\,P\alpha+2\,i\,P\beta+h\,(\beta+2\,(2\,qe+Q\alpha+Q\beta)\,\gamma))}{4\,h\,\gamma}}\right)$$

```
d e^(-(Pα^2+Pβ^2-2 Pα (Pβ+i h (Qα-Qβ) γ)+2 i h Pβ (2 β-Qα γ+Qβ γ)+h^2 γ (4 Qα β+Qα^2 γ-2 Qα Qβ γ+Qβ^2 γ))/(4 h^2 γ)) /
 e^(1/4 (2 i (Pα+Pβ) (Qα-Qβ)/h - (Pα-Pβ)^2/(h^2 γ) - (Qα-Qβ)^2 γ)) //
 FullSimplify
```

$$d\,e^{-\beta\left(Q\alpha+\frac{i\,P\beta}{h\,\gamma}\right)}$$

```
1/2 (d e^(-β (Qα + i Pβ/(h γ))) (e^(β (Qα + i Pβ/(h γ))) + e^((β (i Pα + h (β + 2 qe γ + Qβ γ)))/(h γ)) - 2 e^((β (2 i Pα + 2 i Pβ + h (β + 2 (2 qe + Qα + Qβ) γ)))/(4 h γ))) +
     d e^(-β (Qβ + i Pβ/(h γ))) (e^(β (Qβ + i Pβ/(h γ))) + e^((β (i Pα + h (β + 2 qe γ + Qα γ)))/(h γ)) - 2 e^((β (2 i Pα + 2 i Pβ + h (β + 2 (2 qe + Qα + Qβ) γ)))/(4 h γ)))) // FullSimplify
```

$$\frac{1}{2}\,d\,e^{-\beta\left(Q\alpha+Q\beta+\frac{2\,i\,P\beta}{h\,\gamma}\right)}\left(2\,e^{\beta\left(Q\alpha+Q\beta+\frac{2\,i\,P\beta}{h\,\gamma}\right)}+e^{\frac{\beta\,(i\,P\alpha+i\,P\beta+h\,\beta+2\,h\,(qe+Q\alpha)\,\gamma)}{h\,\gamma}}+e^{\frac{\beta\,(i\,P\alpha+i\,P\beta+h\,\beta+2\,h\,(qe+Q\beta)\,\gamma)}{h\,\gamma}}-2\,e^{\frac{\beta\,(2\,i\,P\alpha+6\,i\,P\beta+h\,\beta+2\,h\,(2\,qe+3\,Q\alpha+Q\beta)\,\gamma)}{4\,h\,\gamma}}-2\,e^{\frac{\beta\,(2\,i\,P\alpha+6\,i\,P\beta+h\,\beta+2\,h\,(2\,qe+Q\alpha+3\,Q\beta)\,\gamma)}{4\,h\,\gamma}}\right)$$

List of Figures

List of Tables

Bibliography

[1] Daniel Gottesman, Eric Rains Calderbank, Peter Shor, NJA Sloane, et al. A transition from the information age to the quantum information age. 3

[2] R. L. Fork,B. I. Greene and C. V. Shank. Generation of optical pulses shorter than 0.1 psec by colliding pulse mode locking. *Appl. Phys. Lett.*, 38(9):671, 1981. 4

[3] C. V. Shank,R. L. Fork, R. Yen, R. H. Stolen and W. J. Tomlinson. Compression of femtosecond optical pulses. *Appl. Phys. Lett.*, 40(9):761, 1982. 4

[4] J. G. Fujimoto, A. M. Weiner and E. P. Ippen. Generation and measurement of optical pulses as short as 16 fs. *Appl. Phys. Lett.*, 44(9):832, 1984. 4

[5] J. M. Halbout and D. Grischkowsky. 12-fs ultrashort optical pulse compression at a high repetition rate. *Appl. Phys. Lett.*, 45(12):1281, 1984. 4

[6] W. H. Knox, R. L. Fork, M. C. Downer, R. H. Stolen, C. V. Shank and J. A. Valdmanis. Optical pulse compression to 8 fs at a 5-khz repetition rate. *Appl. Phys. Lett.*, 46:1120, 1985. 4

[7] R. L. Fork, C. H. Brito-Cruz, P. C. Becker and C. V. Shank. Compression of optical pulses to six femtoseconds by using cubic phase compensation. *Opt. Lett.*, 12(7):483, 1987. 4

[8] M. T. Asaki, C. P. Huang, D. Garvey, J. Zhou, H. C. Kapteyn and M. M. Murnane. Generation of 11-fs pulses from a self-mode-locked ti: sapphire laser. *Opt. Lett.*, 18(12):977, 1993. 4

[9] J. Zhou, I. P. Christov, G. Taft, C. P. Huang, M. M. Murnane, and H. C. Kapteyn. Pulse evolution in a broad-bandwidth ti: sapphire laser. *Opt. Lett.*, 19(15):1149, 1994. 4

[10] A. Stingl,R. Szipöcs, M. Lenzner, C. H. Spielmann, and F. Krausz. Sub-10-fs mirror-dispersion-controlled ti: sapphire laser. *Opt. Lett.*, 20(6):602, 1995. 4

[11] A. Shirakawa, I. Sakane, T. Kobayashi. Pulse-front-matched optical parametric amplification for sub-10-fs pulse generation tunable in the visible and near infrared. *Opt. Lett.*, 23(16):1292, 1998. 4

[12] L. Xu,G. Tempea, C. H. Spielmann, F. Krausz, A. Stingl, K. Ferencz and S. Takano. Continuous-wave mode-locked ti: sapphire laser focusable to $5 \times 10^{13}(w/cm^2)$. *Opt. Lett.*, 23(10):789, 1998. 4

[13] U. Morgner, F. X. Kärtner, S. H. Cho, Y. Chen, H. A. Haus, J. G. Fujimoto, E. P. Ippen, V. Scheuer, G. Angelow and T. Tschudi. Sub-two-cycle pulses from a kerr-lens mode-locked ti: sapphire laser. *Opt. Lett.*, 24(6):411, 1999. 4

[14] A. M. Weiner. Femtosecond pulse shaping using spatial light modulators. *Rev. Sci. Instrum.*, 71(5):1929, 2000. 4

[15] A. Szabo and N. S. Ostlund. *Modern quantum chemistry: introduction to advanced electronic structure theory*. Dover, New York, 2012. 5, 10, 13, 89, 91

[16] D. B. Cook. *Handbook of computational quantum chemistry*. Dover, New York, 2012. 5, 13, 42, 105

[17] T. Helgaker, P. Jorgensen and J. Olsen. *Molecular electronic-structure theory*. John Wiley & Sons, 2014. 5, 10, 13

[18] D. Feller. The use of systematic sequences of wave functions for estimating the complete basis set, full configuration interaction limit in water. *J. Chem. Phys.*, 98(9):7059, 1993. 5

[19] S. Wilson, and G. H. F. Diercksen. *Methods in computational molecular physics*, volume 293. Springer Science & Business Media, Berlin, 2013. 6

[20] R. P. Feynman. Space-time approach to quantum electrodynamics. *Phys. Rev.*, 76(6):769, 1949. 6

[21] K. Yamanouchi. *Lectures on ultrafast intense laser science*. Springer, Berlin, 2010. 6

[22] L. S. Cederbaum. The multistate vibronic coupling problem. *J. Chem. Phys*, 78(9):5714, 1983. 7, 46

[23] W. Domcke and G. Stock. Theory of ultrafast nonadiabatic excited-state processes and their spectroscopic detection in real time. *Advances in Chemical Physics, Volume 100*, pages 1–169, 1997. 7, 10, 46

[24] A. Raab, G. A. Worth, H. D. Meyer and L. S. Cederbaum. Molecular dynamics of pyrazine after excitation to the s_2 electronic state using a realistic 24-mode model hamiltonian. *J. Chem. Phys.*, 110(2):936, 1999. 7

[25] D. J. Tannor and S. A. Rice. Control of selectivity of chemical reaction via control of wave packet evolution. *J. Chem. Phys.*, 83(10):5013, 1985. 7

[26] P. Brumer and M. Shapiro. Control of unimolecular reactions using coherent light. *Chem. Phys. Lett.*, 126(6):541, 1986. 7

[27] D. J. Tannor, R. Kosloff and S. A. Rice. Coherent pulse sequence induced control of selectivity of reactions: Exact quantum mechanical calculations. *J. Chem. Phys.*, 85(10):5805, 1986. 7

[28] R. Kosloff, S. A. Rice, P. Gaspard, S. Tersigni and D. J. Tannor. Wavepacket dancing: Achieving chemical selectivity by shaping light pulses. *Chem. Phys.*, 139(1):201, 1989. 7

[29] S. J. Glaser, U. Boscain, T. Calarco, C. P. Koch, W. Köckenberger, R. Kosloff, I. Kuprov, B. Luy, S. Schirmer and *et.al* T. Schulte-Herbrüggen. Training schrödinger's cat: quantum optimal control. *arXiv preprint arXiv:1508.00442*, 2015. 8, 9, 45, 53, 56

[30] W. S. Warren, H. Rabitz and M. Dahleh. Coherent control of quantum dynamics: the dream is alive. *Science*, 259(5101):1581, 1993. 8

[31] R. E. Kalman, P. L. Falb and M. A. Arbib. *Topics in mathematical system theory*, volume 33. McGraw-Hill, New York, 1969. 8

[32] A. E. Bryson. *Applied optimal control: optimization, estimation and control*. CRC Press, 1975. 8

[33] L. S. Pontryagin. *Mathematical theory of optimal processes*. Gordon and Breach, New York, 1986. 8

[34] P. Gross, D. Neuhauser and H. Rabitz. Optimal control of curve-crossing systems. *J. Chem. Phys.*, 96(4):2834, 1992. 8

[35] T. Szakács, B. Amstrup, P. Gross, R. Kosloff, H. Rabitz and A. Lörincz. Locking a molecular bond: A case study of CsI. *Phys. Rev. A.*, 50(3):2540, 1994. 8, 53

[36] W. Zhu, J. Botina and H. Rabitz. Rapidly convergent iteration methods for quantum optimal control of population. *J. Chem. Phys.*, 108(5):1953, 1998. 8, 9

[37] P. de Fouquieres, S. G. Schirmer, S. J. Glaser, and I. Kuprov. Second order gradient ascent pulse engineering. *J. Magn Reson.*, 212(2):412, 2011. 8

[38] U. Sander, S. J. Glaser, P. de Fouquieres, A. Gruslys, S. Schirmer, S. Machnes and T. Schulte-Herbrüggen. Comparing, optimizing, and benchmarking quantum-control algorithms in a unifying programming framework. *Phys. Rev. A.*, 84(2):022305, 2011. 8

[39] G. Ciaramella, A. Borzì, G. Dirr, and D. Wachsmuth. Newton methods for the optimal control of closed quantum spin systems. *SIAM J. Sci. Comput.*, 37(1):A319, 2015. 8

[40] V. Krotov. *Global methods in optimal control theory*, volume 195. Dover, New York, 1995. 8

[41] Y. Maday and G. Turinici. New formulations of monotonically convergent quantum control algorithms. *J. Chem. Phys.*, 118(18):8191, 2003. 8

[42] D. M. Reich, M. Ndong, and C. P. Koch. Monotonically convergent optimization in quantum control using krotov's method. *J. Chem. Phys.*, 136(10):104103, 2012. 8

[43] J. Werschnik and E. K. U. Gross. Quantum optimal control theory. *J. Phys. B.*, 40(18):R175, 2007. 9

[44] E. Deumens, A. Diz, H. Taylor and Y. Öhrn. Time-dependent dynamics of electrons and nuclei. *J. Chem. Phys.*, 96(9):6820, 1992. 9

[45] R. Longo, E. Deumens and Y. Öhrn. H++ h, he, and h2 scattering using a new time-dependent method for electron nuclear dynamics. *J. Chem. Phys.*, 99(6):4554, 1993. 9

[46] E. J. Heller. Frozen gaussians: A very simple semiclassical approximation. *J. Chem. Phys.*, 75(6):2923, 1981. 9

[47] T. J. Martínez and R. D. Levine. Non-adiabatic molecular dynamics: Split-operator multiple spawning with applications to photodissociation. *J. Chem. Soc. Faraday Trans.*, 93(5):941, 1997. 9

[48] M. D. Hack, A. M. Wensmann, D. G. Truhlar, M. Ben-Nun, and T. J. Martínez. Comparison of full multiple spawning, trajectory surface hopping, and converged quantum mechanics for electronically nonadiabatic dynamics. *J. Chem. Phys.*, 115(3):1172, 2001. 9

[49] M. Ben-Nun, J. Quenneville and T. J. Martínez. Ab initio multiple spawning: Photochemistry from first principles quantum molecular dynamics. *J. Phys Chem. A*, 104(22):5161, 2000. 9, 46, 72

[50] B. G. Levine, J. D. Coe, A. M. Virshup and T. J. Martinez. Implementation of ab initio multiple spawning in the molpro quantum chemistry package. *Chem. Phys.*, 347(1):3, 2008. 9, 77

[51] D. R. Yarkony. Conical intersections: Diabolical and often misunderstood. *Acc. Chem. Res.*, 31(8):511, 1998. 10

[52] Conical Intersections. Electronic structure, dynamics and spectroscopy. *Advanced Series inPhysical Chemistry*, 15, 2004. 10

[53] M. Baer. *Beyond Born-Oppenheimer: electronic nonadiabatic coupling terms and conical intersections*. John Wiley & Sons, New Jersey, 2006. 10

[54] B. Lasorne, G. A. Worth and M. A. Robb. Excited-state dynamics. *Wiley Interdisciplinary Reviews: Computational Molecular Science*, 1(3):460, 2011. 10

[55] K. L. Bak, P. Jo, H. Jo, J. Olsen and T. Helgaker. First-order nonadiabatic coupling matrix elements from multiconfigurational self-consistent-field response theory. *J. Chem. Phys*, 97(10):7573, 1992. 10, 86

[56] W. L. Goffe, G. D. Ferrier and J. Rogers. Global optimization of statistical functions with simulated annealing. *J. Econometrics*, 60(1):65, 1994. 11

[57] D. J. Tannor. *Introduction to quantum mechanics: a time-dependent perspective*. University Science Books, Sausalito, CA, 2007. 13

[58] Shaul Mukamel. Principles of nonlinear spectroscopy, 1995. 13

[59] F. Jensen. *Introduction to computational chemistry*. John Wiley & Sons, New York, 2013. 13, 40, 95

[60] Y. Weissman. Semiclassical approximation in the coherent states representation. *J. Chem. Phys.*, 76(8):4067, 1982. 21

[61] F. Scheck. *Mechanics: from Newton's laws to deterministic chaos*. Springer Science & Business Media, Berlin, 2010. 23, 85

[62] J. H. Van Vleck. The Correspondence Principle in the Statistical Interpretation of Quantum Mechanics. *Proc. Nat. Acad. Sci.*, 14:178, 1928. 23

[63] G. Campolieti and P. Brumer. Semiclassical Propagation: Phase Indices and the Initial-Value Formalism. *Phys. Rev. A*, 50:997, 1994. 26

[64] and D. E. Manolopoulos M. L. Brewer, J. S. Hulme. Semiclassical dynamics in up to 15 coupled vibrational degrees of freedom. *J. Chem. Phys.*, 106(12):4832, 1997. 30, 31

[65] Gili Hochman and Kenneth G Kay. Semiclassical corrections to the herman-kluk propagator. *Phys. Rev. A*, 73(6):064102, 2006. 31

[66] M. F. Herman. Improving the accuracy of semiclassical wavepacket propagation using integral conditioning techniques. *Chem. Phys. Lett.*, 275(5):445, 1997. 31

[67] K. G. Kay. Semiclassical propagation for multidimensional systems by an initial value method. *J. Chem. Phys.*, 101(3):2250, 1994. 33

[68] A. R. Walton and D. E. Manolopoulos. A new semiclassical initial value method for franck-condon spectra. *J. Mol. Phys.*, 87(4):961, 1996. 34

[69] M. Weissbluth. *Atoms and molecules*. Academic Press,New York, 2012. 40

[70] S. F. Boys. Electronic wave functions I. a general method of calculation for the stationary states of any molecular system. In *Proc. R. Soc. London Ser. A Math. Phys. Eng. Sci.*, volume 200, page 542. The Royal Society, 1950. 40

[71] H. Taketa, S. Huzinaga, and K. O-Ohata. Gaussian-expansion methods for molecular integrals. *J. Phys. Soc. of Jap.*, 21(11):2313, 1966. 42

[72] J. B. Foresman, M. Head-Gordon, J. A. Pople and M. J. Frisch. Toward a systematic molecular orbital theory for excited states. *J. Chem. Phys.*, 96(1):135, 1992. 42

[73] N. L. Doltsinis and D. Marx. First principles molecular dynamics involving excited states and nonadiabatic transitions. *J. Theor. Comput. Chem.*, 1(02):319, 2002. 46

[74] G. Stock, C. Woywod, W. Domcke, T. Swinney and B. S. Hudson. Resonance raman spectroscopy of the s_1 and s_2 states of pyrazine: Experiment and first principles calculation of spectra. *J. Chem. Phys.*, 103(16):6851, 1995. 46, 80

[75] S. Hahn and G. Stock. Quantum-mechanical modeling of the femtosecond isomerization in rhodopsin. *J. Phys. Chem. B*, 104(6):1146, 2000. 46, 58, 59, 128

[76] J. Alvarellos and H. Metiu. The evolution of the wave function in a curve crossing problem computed by a fast fourier transform method. *J. Chem. Phys.*, 88(8):4957, 1988. 47, 97

[77] C. D. Sherrill. Derivation of the configuration interaction singles (cis) method for various single determinant references and extensions to include selected double substitutions (xcis), 1996. 48

[78] C. David Sherrill. An introduction to configuration interaction theory, 1995. 48

[79] R. D. Guerrero, C. A. Arango and A. Reyes. Optimal control of wavepackets: a semiclassical approach. *Mol. Phys.*, 112(3-4):408, 2014. 50

[80] S. Ruhman and R. Kosloff. Application of chirped ultrashort pulses for generating large-amplitude ground-state vibrational coherence: a computer simulation. *J. Opt. Soc. Am. B.*, 7(8):1748, 1990. 53

[81] H. Zhang, K. L. Han, G. Z. He and N. Q. Lou. Wavepacket-shaping by a frequency-chirping technique. *Chem. Phys. Lett.*, 289(5):494, 1998. 53

[82] J. L. Carini, J. A. Pechkis, C. E. Rogers III, P. L. Gould, S. Kallush and R. Kosloff. Quantum dynamical calculations of ultracold collisions induced by nonlinearly chirped light. *Phys. Rev. A.*, 85(1):013424, 2012. 53

[83] Y. Huang, W. Zhang, G. R. Wang, T. Xie and S. L. Cong. Formation of $^{85}Rb_2$ ultracold molecules via photoassociation by two-color laser fields modulating the gaussian amplitude. *Phys. Rev. A.*, 86(4):043420, 2012. 53

[84] S. Amaran, R. Kosloff, M. Tomza, W. Skomorowski, F. Pawłowski, R. Moszynski, L. Rybak, L. Levin, Z. Amitay, J. Martin Berglund, D. M. Reich and C. P. Koch. Femtosecond two-photon photoassociation of hot magnesium atoms: A quantum dynamical study using thermal random phase wavefunctions. *J. Chem. Phys.*, 139(16):164124, 2013. 53

[85] J. L. Carini, J. A. Pechkis, C. E. Rogers III, P. L. Gould, S. Kallush, and R. Kosloff. Production of ultracold molecules with chirped nanosecond pulses: Evidence for coherent effects. *Phys. Rev. A.*, 87(1):011401, 2013. 53

[86] Y. Huang, T, Xie, G. R. Wang, W, Zhang and S. L. Cong. Creation of ultracold Cs_2 molecules via two-step photoassociation with gaussian and chirped pulses. *Las. Phys.*, 24(4):046001, 2014. 53

[87] Zoubin Ghahramani. *Unsupervised learning*. Springer Berlin Heidelberg, 2004. 55

[88] R. D. Guerrero, C. A. Arango and A. Reyes. Analytical optimal pulse shapes obtained with the aid of genetic algorithms. *J. Chem. Phys.*, 143(12):124108, 2015. 55, 57, 59, 60, 97

[89] D. Mustafi and K. Palczewski. Topology of class AG protein-coupled receptors: insights gained from crystal structures of rhodopsins, adrenergic and adenosine receptors. *Mol. Pharm.*, 75(1):1, 2009. 56

[90] S. Rinaldi, F. Melaccio, S. Gozem, F. Fanelli and M. Olivucci. Comparison of the isomerization mechanisms of human melanopsin and

invertebrate and vertebrate rhodopsins. *Proc. Natl. Acad. Sci. U. S. A.*, 111(5):1714, 2014. 56

[91] R. W. Schoenlein, J. Y. Bigot, M. T. Portella and C. V. Shank. Generation of blue-green 10 fs pulses using an excimer pumped dye amplifier. *Appl. Phys. Lett.*, 58(8):801, 1991. 56

[92] R. W. Schoenlein, L. A. Peteanu, Q. Wang, R. A. Mathies, and C. V. Shank. Femtosecond dynamics of cis-trans isomerization in a visual pigment analog: isorhodopsin. *J. Phys. Chem.*, 97(46):12087, 1993. 56

[93] K. Palczewski. G Protein-Coupled Receptor Rhodopsin. *Annu. Rev. Biochem.*, 75:743–767, 2006. 56

[94] R. A. Mathies, C. H. Brito Cruz, W. T. Pollard, and C. V. Shank. Direct Observation of the Femtosecond Excited-State cis-trans Isomerization in Bacteriorhodopsin. *Science*, 240:777–779, 1988. 56

[95] Q. Wang, R. W. Schoenlein, L. A. Pateanu, R. A. Mathies, and C. V. Shank. Vibrational Coherent Photochemistry in the Femtosecond Primary Event of Vision. *Science*, 266:422–424, 1994. 56

[96] P. Kukura, D. W. McCamant, S. Yoon, D. B. Wandschneider, and R. A. Mathies. Structural Observation of the Primary Isomerization in Vision with Femtosecond-Stimulated Raman. *Science*, 310:1006–1009, 2005. 56

[97] V. I. Prokhorenko, A. M. Nagy, S. A. Waschuk, L. S. Brown, R. R. Birge, and R. J. D. Miller. Coherent control of Retinal Isomerization in Bacteriorhodopsin. *Science*, 313:1257–1261, 2006. 57

[98] V. I. Prokhorenko, A. M. Nagy, L. S. Brown, and R. J. D. Miller. On the mechanism of weak-field coherent control of retinal isomerization in bacteriorhodopsin. *Chem. Phys.*, 341:296–309, 2007. 57

[99] C. A. Arango M. Spanner and P. Brumer. Communication: Conditions for one-photon coherent phase control in isolated and open quantum systems. *J. Chem. Phys.*, 133(15):–, 2010. 57

[100] G. Katz, M. A. Ratner and R. Kosloff. Control by decoherence: weak field control of an excited state objective. *New J. Phys.*, 12(1):015003, 2010. 57

[101] C. A. Arango and Paul Brumer. Communication: One-photon phase control of cis-trans isomerization in retinal. *J. Chem Phys.*, 138(7):–, 2013. 57

[102] L. A. Pachon and P. Brumer. Mechanisms in environmentally assisted one-photon phase control. *J. Chem. Phys.*, 139(16):–, 2013. 57

[103] L. Yu L. A. Pachon and P. Brumer. Coherent one-photon phase control in closed and open quantum systems: A general master equation approach. *Faraday Discuss.*, 163:485–495, 2013. 57

[104] M. H. Beck , A. Jäckle, G. A. Worth and H.D. Meyer. The multiconfiguration time-dependent hartree (mctdh) method: A highly efficient algorithm for propagating wavepackets. *REP*, 324:1–105, 1999. 57

[105] D. Geppert and R. de Vivie-Riedle. Control strategies for reactive processes involving vibrationally hot product states. *J Photoch. Photobio. A.*, 180(3):282, 2006. 57

[106] M. Abe, Y. Ohtsuki, Y. Fujimura and W. Domcke. Optimal control of ultrafast cis-trans photoisomerization of retinal in rhodopsin via a conical intersection. *J. Chem. Phys.*, 123(14):144508, 2005. 57

[107] A. C. Florean, D. Cardoza, J. L. White, J. K. Lanyi, R. J. Sension and P. H. Bucksbaum. Control of retinal isomerization in bacteriorhodopsin in the high-intensity regime. *Proc. Natl. Acad. Sci. U. S. A.*, 106(27):10896, 2009. 57

[108] M. Shapiro and P. Brumer. Coherent control of molecular dynamics. *Rep. Prog. Phys.*, 66(6):859, 2003. 57

[109] T. V. Tscherbul, P., and Brumer. Excitation of biomolecules with incoherent light: Quantum yield for the photoisomerization of model retinal. *The J. Phys. Chem. A*, 118(17):3100, 2014. 57

[110] F. Grossmann, L. Feng, G. Schmidt, T. Kunert and R. Schmidt. Optimal control of a molecular cis-trans isomerization model. *Europhys. Lett.*, 60(2):201, 2002. 59

[111] T. J. Martinez, M. Ben-Nun and R. D. Levine. Multi-electronic-state molecular dynamics: A wave function approach with applications. *J. Phys. Chem.*, 100(19):7884, 1996. 68

[112] C. Sanderson. Armadillo: An open source c++ linear algebra library for fast prototyping and computationally intensive experiments. 2010. 69

[113] A. K. Roy. Accurate ro-vibrational spectroscopy of diatomic molecules in a morse oscillator potential. *Results Phys.*, 3:103, 2013. 70

[114] K. G. Kay. The matrix singularity problem in the time-dependent variational method. *Chem. Phys.*, 137(1):165, 1989. 77

[115] W. Siebrand and M. Z. Zgierski. The dushinsky effect in resonance raman spectroscopy. *Chem. Phys. Lett.*, 62(1):3, 1979. 80

[116] H. B. Schlegel. Optimization of equilibrium geometries and transition structures. *J. Comp. Chem.*, 3(2):214, 1982. 84

[117] A. Amadei, A. B. Linssen and H. J. Berendsen. Essential dynamics of proteins. *Proteins: Struct., Funct., Bioinf.*, (17):412, 1994. 85

[118] M. W. Schmidt, K. K. Baldridge, J. A. Boatz, S. T. Elbert, M. S. Gordon, J. H. Jensen, S. Koseki, N. Matsunaga, K. A. Nguyen and S. Su. General atomic and molecular electronic structure system. *J. Comp. Chem.*, 14(11):1347–1363, 1993. 86

[119] V. Moler and C. Van Loan. Nineteen dubious ways to compute the exponential of a matrix. *SIAM review*, 20(4):801, 1978. 95